Development of a Mass Spectrometric Method based on Hydrogen-Deuterium Exchange (HDX-MS) for the Determination of Epitope Regions of Glycoproteins in High Throughput

Dissertation

der Mathematisch-Naturwissenschaftlichen Fakultät

der Eberhard Karls Universität Tübingen

zur Erlangung des Grades eines

Doktors der Naturwissenschaften

(Dr. rer. nat.)

vorgelegt von

Marius Johannes Gramlich

aus Weinheim

Tübingen

2022

Gedruckt mit Genehmigung der Mathematisch-Naturwissenschaftlichen Fakultät der Eberhard Karls Universität Tübingen.

Tag der mündlichen Qualifikation:	24.01.2023
Dekan:	Prof. Dr. Thilo Stehle
1. Berichterstatter:	Prof. Dr. Thilo Stehle
2. Berichterstatter:	Prof. Dr. Dirk Schwarzer

Supervisor at the Eberhard Karls University, Tübingen

Prof. Dr. Thilo Stehle

Supervisor at the University of Applied Sciences
Albstadt Sigmaringen, Sigmaringen

Prof. Dr. Dieter Stoll

Supervisor at the Natural and Medical Sciences Institute
at the University of Tübingen

Dr. Anne Zeck

Published work

Parts of this work have been published:

M. Gramlich, S. Maier, P. D. Kaiser, B. Traenkle, T. R. Wagner, J. Voglmeir, D. Stoll, U. Rothbauer and A. Zeck: *A Novel PNGase Rc for Improved Protein N-Deglycosylation in Bioanalytics and Hydrogen-Deuterium Exchange Coupled With Mass Spectrometry Epitope Mapping under Challenging Conditions*. Anal. Chem. (2022). DOI: 10.1021/acs.analchem.2c01748

M. Gramlich, H. C. W. Hays, S. Crichton; P. D. Kaiser, A. Heine, N. Schneiderhan-Marra, U. Rothbauer, D. Stoll, S. Maier and A. Zeck: *HDX-MS for Epitope Characterization of a Therapeutic ANTIBODY Candidate on the Calcium-Binding Protein Annexin-A1*, Antibodies, **10,** (2021). DOI: 10.3390/antib10010011

T. R. Wagner, E. Ostertag, P. D. Kaiser, **M. Gramlich**, N. Ruetalo, D. Junker, J. Haering, B. Traenkle, M. Becker, A. Dulovic, H. Schweizer, S. Nueske, A. Scholz, A. Zeck, K. Schenke-Layland, A. Nelde, M. Strengert, J. S. Walz, G. Zocher, T. Stehle, M. Schindler, N. Schneiderhan-Marra and U. Rothbauer: *NeutrobodyPlex - monitoring SARS-CoV-2 neutralizing immune responses using nanobodies*, EMBO Rep., **22**, (2021). DOI: 10.15252/embr.202052325

M. Gramlich, S. Maier, P. D. Kaiser, D. Stoll, J. Voglmeir, U. Rothbauer and A. Zeck: *Application of a novel PNGase for peptide N-deglycosylation at acidic pH within the HDX-MS workflow for epitope mapping* [Poster Presentation], International Conference On Hydrogen Deuterium Exchange Mass Spectrometry, London, (24-26 April 2022).

M. Gramlich, S. Maier, P. D. Kaiser, D. Stoll, J. Voglmeir, U. Rothbauer and A. Zeck: *A novel PNGase Rc to improve protein N-deglycosylation for mass spectrometric protein characterization* [Poster Presentation], Analytica conference, Munich, (21-23 June 2022).

Published work that is not part of this thesis:

B. Traenkle, P. D. Kaiser, S. Pezzana, J. Richardson, **M. Gramlich**, T. R. Wagner, D. Seyfried, M. Weldle, M. Holz, Y. Parfyonova, S. Nueske, A. M. Scholz, A. Zeck, M. Jakobi, N. Schneiderhan-Marra, M. Schaller, A. Maurer, C. Gouttefangeas, M. Kneilling, B. J. Pichler, D. Sonanini and U. Rothbauer: *Single-domain antibodies for targeting, detection, and in vivo imaging of human CD4⁺ cells,* Front. Immunol., **12**, (2021). DOI: 10.3389/fimmu.2021.799910

R. Guo, G. Comamala, H. Yang, **M. Gramlich,** Y. Du, T. Wang, A. Zeck, K. D. Rand, L. Liu and J. Voglmeir: *Discovery of Highly Active Recombinant PNGase H+ Variants Through the Rational Exploration of Unstudied Acidobacterial Genomes.* Front. Bioeng. Biotechnol., **8**, (2020). DOI: 10.3389/fbioe.2020.00741.

Acknowledgements

First of all, I would like to thank Dr. Anne Zeck for accepting me as a master's student and subsequently giving me the opportunity to write my dissertation, as well as for her continuous support and trust over the past years. Furthermore, I would like to express my special thanks to Prof. Dr. Thilo Stehle and Prof. Dr. Dieter Stoll for supervising the dissertation and providing valuable feedback during the doctoral phase. Furthermore, I would like to thank Prof. Dr. Dirk Schwarzer, who provided the second opinion for my dissertation.

A special thank goes also to Dr. Oliver Pötz and Prof. Dr. Christoph Borchers enabling a short research trip at the UVic-Genome BC Proteomics Centre at the University of Victoria in Canada. In this context, I would like to thank Dr. Jason Sherpa, my supervisor during the early HDX-MS experiments in Canada, and the Boehringer Ingelheim Foundation for Basic Research in Medicine for granting me the travel and research opportunity.

Furthermore, I would like to thank the research group of Prof. Dr. Ulrich Rothbauer especially, himself, Dr. Philipp D. Kaiser, Dr. Björn Tränkle and Teresa R. Wagner for the close collaboration in solving interesting scientific questions, their support, and for providing the molecule studied here. Writing of, I am grateful for the collaboration with Prof. Dr. Josef Voglmeir the Nanjing Agricultural University in China resulting in the discovery of the novel PNGase Rc used within the present work.

I particularly would like to thank my work colleagues: Sandra Maier for the supervision during the master thesis and the introduction to mass spectrometric analysis methods, Robin Kretz and Felix Ruoff for the continuous exchange of knowledge, brainstorming, and the regular support during troubleshooting and the friendly working atmosphere. I am grateful for all other colleagues for the pleasant working atmosphere, especially my colleagues, Anne Heine, Madeleine Fandrich, Simon Fink, Jens Gruber, Anja Tausch, Cornelia Sommersdorf, Dr. Helen Hammer; Dr. Wael Naboulsi; Dr. Andreas Steinhilber, Dr. Hannes Planatscher and Dr. Viktoria Anselm.

I would also like to thank my family for mental support, as well as my friends for the motivation, encouragement, and energy during this time.

Content

List of Figures

List of Tables

List of Abbreviations

Ab	Antibody
Af	Ammonium formate
Ag	Antigen
ANXA1	Annexin A1
APS	Ammonium persulfate
BLI	Biolayer interferometry
CD	Cluster of Differentiation
CID	Collision induced dissociation
Cryo-EM	Cryo-electron microscopy
DTT	Dithiothreitol
E.coli	*Escherichia coli*
E:S	Enzyme-to-Substrate ratio
EDTA	Ethylenediaminetetraacetic acid
EIC	Extracted Ion Chromatogram
ELISA	Enzyme-linked immunosorbent assay
FA	Formic acid
FDR	False discovery rate
FPOP	Fast photochemical oxidation of proteins
GdmCl	Guanidine hydrochloride
GGBRC	Glycomics and Glycan Bioengineering Research Center
GlcNAc	N-Acetylglucosamine
HCD	Higher-energy collisional dissociation
HDX	Hydrogen-deuterium exchange
HEPES	4-(2-hydroxyethyl)-1-piperazineethanesulfonic acid
(U) HPLC	(Ultra) High performance liquid chromatography
HRP	Horseradish peroxidase
HX	Hydrogen exchange
IAA	Iodoacetamide (IAA)
IgG	Immunoglobulin G
IPTG	Isopropyl-β-D-thiogalactopyranoside
LC	Liquid chromatography
LC-MS	Liquid chromatography coupled to mass spectrometry
mAb	Monoclonal antibody
MeCN	Acetonitrile
MS	Mass spectrometer

Nb	Nanobody
ON	Overnight
ORF	Open reading fame
PBS	Phosphate buffered saline
PDB	Protein data bank
PNGase	Peptide-N-Glycosidase (peptide-N4-(N-acetyl-β-glucosaminyl)asparagine amidase)
PPI	Protein-Protein-Interaction
PTM	Post-translational modification
RBD	Receptor-binding Domain
RNase B	Ribonuclease B
RT	Room temperature
SAIDE	Semi-Automated Interface for HD exchange
SARS-CoV-2	Severe acute respiratory syndrome coronavirus type 2
SD	Standard deviation
SDS	Sodium dodecyl sulfate
SDS-PAGE	Sodium dodecyl sulfate polyacrylamide gel electrophoresis
SIRPα	Signal-regulatory protein alpha
SPR	Surface plasmon-Resonance
TCEP	Tris(2-carboxyethyl)phosphin
TEMED	Tetramethylethylenediamine
TFA	Trifluoroacetic acid
TIC	Total ion current chromatogram

1 Abstract

The vast majority of biological processes such as cell-cell communication, immune response, reaction catalysis and the protein transport are driven by protein-protein interactions (PPIs). Elucidation of PPIs, which when altered are associated with various pathophysiological processes, opened an emerging era of protein analysis. The knowledge of the PPIs interfaces is crucial to obtain deeper insights into the PPIs mode of action and how to modulate them. In particular, PPIs between antibodies and antigens are of great interest for diagnostic and therapeutic applications in the biopharmaceutical industry and scientific research. In addition to high-resolution techniques such as nuclear magnetic resonance spectroscopy (NMR), X-ray crystallography and cryo-electron microscopy (cryo-EM), hydrogen-deuterium exchange coupled to mass spectrometry (HDX-MS) has evolved to a powerful analysis method for the elucidation of PPI interfaces. Without introducing structural modifications, HDX-MS can be used to elucidate protein dynamics and protein-ligand interaction sites of proteins of almost unlimited size, with high tolerance against impurities, low sample consumption and reasonable resolution and throughput. In addition, HDX data reflect the native in-solution protein conformation. However, HDX-MS remains challenging for the analysis of proteins encompassing multiple post-translational modifications such as disulphide bonds and N-glycosylations.

In the context of the present work, a setup and workflow for HDX-MS bottom-up analyses was established. A prerequisite for reliable and efficient HDX analyses is the precise control of the pH, temperature and timing, which was facilitated by a tailor made Semi-Automated Interface for HD exchange (SAIDE). The SAIDE enables flexible use of a HPLC-MS instrumentation for various analyses, efficient use of the laboratory space while displaying a cost efficient approach compared to fully automated, commercial HDX systems.

With this setup, a protocol for HDX analyses was developed and optimised, which addressed critical generic HDX parameters such as efficient proteolysis and good reproducibility while keeping the back exchange as low as possible. Compared to dissolved pepsin, the proteolysis efficiency could be increased using pepsin immobilized on beads. This enabled a tenfold reduction in digestion time while achieving a higher number of peptides, run-to-run recovery, a lower HDX variance, and lower average peptide length. These optimisations were performed as part of an HDX study designed to elucidate the binding region of a clinical mAb drug candidate targeting Annexin-A1 in a calcium dependent manner.

Subsequently, the HDX-MS protocol was improved in terms of sample throughput and adapted to another protein target, the receptor-binding domain (RBD) of SARS-CoV-2. The high reproducibility of the established protocol enabled its application in an HDX screening

workflow using a lower number of deuteration time points. Epitopes of seven nanobodies were characterized within a time period of roughly four weeks. The HDX-MS screening approach was used to support evidence based identification of two lead candidates potent in their viral neutralization.

Subsequent endeavours aimed to adapt the established screening approach to proteins encompassing multiple post-translational modification (PTMs). While extracellular proteins display attractive drug targets or are themselves used as biopharmaceuticals, nearly each of them encompass multiple PTMs such as N-glycosylated and disulphide bonds. Originated in their heterogeneity, N-glycosylations remain challenging for structural analysis such as HDX-MS. Here, a novel peptide N-glycanase from *Rudaea cellulosilytica* (Rc) was characterized that exhibits broad substrate specificity and high activity for deglycosylation of natively folded proteins. Thus, the enzyme was used to facilitate MS based top-down protein analytics and offers the opportunity for N-deglycosylation of peptides in several minutes. Moreover, following heterologous expression the enzyme can be obtained from *E. coli* with high yield sufficient purity. Due to its acidic pH optimum, the PNGase Rc was successfully used under challenging HDX-MS quenching conditions (0 °C; pH 2.5) in presence of commonly applied concentrations of reducing and denaturing agents Tris(2-carboxyethyl)phosphine (TCEP), urea and guanidinium chloride (GdmCl). As a proof-of-principle the PNGase Rc was integrated into the established HDX epitope screening workflow (post-proteolysis) resulting in the elucidation of four nanobody epitopes targeting the multiple N-glycosylated extracellular domain of the signal-regulatory protein alpha (SIRPα). The additional deglycosylation increased sequence coverage and redundancy and also enabled the detection of epitopes in proximity of N-glycosylation sites.

2 Zusammenfassung

Die allermeisten biologischen Prozesse, wie die Zell-Zell Kommunikation, Immunantwort, Reaktionskatalyse und der Proteintransport wird durch Protein-Protein Interaktionen (PPIs) gesteuert. Die Aufklärung von PPIs, welche, wenn sie verändert werden mit verschiedenen pathophysiologischen Prozessen assoziiert sind, eröffnete eine neue Ära der Proteinanalyse. Die Kenntnis der Schnittstellen von PPIs ist entscheidend, um tiefere Einblicke in die Wirkungsweise von PPIs und deren Modulation zu erhalten. Insbesondere PPIs zwischen Antikörpern und Antigenen sind für diagnostische und therapeutische Anwendungen in der biopharmazeutischen Industrie und der wissenschaftlichen Forschung von großem Interesse. Neben den hochauflösenden Techniken wie Kernspinresonanzspektroskopie (NMR), Röntgenkristallographie und Kryo-Elektronenmikroskopie (Kryo-EM) hat sich der Wasserstoff-Deuterium Austausch verbunden mit Massenspektrometrie (HDX-MS) zu einer leistungsfähigen Analysemethode entwickelt, um diese Interaktionsflächen aufzuklären. Ohne strukturelle Modifikationen einzubringen, lassen sich mittels HDX-MS Proteindynamiken und Protein-Ligand-Interaktionsstellen von Proteinen mit nahezu unlimitierter Größe, mit hoher Toleranz gegenüber Verunreinigungen, geringem Probenverbrauch mit angemessener Auflösung und angemessenem Durchsatz bestimmen. Darüber hinaus spiegeln HDX-Daten die native Proteinkonformation in Lösung wider. HDX-MS bleibt jedoch eine Herausforderung für die Analyse von Proteinen, die mehrere posttranslationale Modifikationen wie Disulfidbindungen und N-Glykosylierungen aufweisen.

Im Rahmen der vorliegenden Arbeit wurde ein HDX-MS Setup und Arbeitsablauf etabliert. Eine Voraussetzung für zuverlässige und effiziente HDX-Analysen ist die präzise Kontrolle des pH-Werts, der Temperatur und des Timings, was durch eine maßgeschneiderte halbautomatische Schnittstelle für den HD-Austausch (SAIDE) erreicht wurde. Das SAIDE ermöglicht eine flexible Nutzung von ein und derselben HPLC-MS-Instrumentierung für verschiedene Analysen, eine effiziente Nutzung des vorhandenen Laborplatzes und stellt gleichzeitig einen kosteneffizienten Ansatz im Vergleich zu vollautomatischen, kommerziellen HDX-Systemen dar.

Mit diesem Setup wurde ein Protokoll für HDX-Analysen erstellt und optimiert, um kritische, generische HDX-Parameter wie die effiziente Proteolyse und Reproduzierbarkeit zu adressieren und gleichzeitig den Rückaustausch so gering wie möglich zu halten. Verglichen mit Pepsin frei in Lösung konnte die Effizienz der Proteolyse durch Verwendung von immobilisiertem Pepsin erhöht werden. Dies ermöglichte eine zehnfache Reduktion der Proteolysezeit mit gleichzeitiger Erreichung einer höheren Peptidanzahl, Wiederfindbarkeit von Lauf zu Lauf, einer geringeren HDX-Varianz und einer geringeren durchschnittlichen Peptidlänge. Diese Optimierungen wurden im Rahmen einer HDX-Studie durchgeführt, die

darauf ausgelegt war die Bindungsregion eines klinischen mAb-Arzneimittelkandidaten aufzuklären, der Annexin-A1 auf eine kalziumabhängige Weise bindet.
Anschließend wurde das HDX-MS-Protokoll in Bezug auf den Probendurchsatz verbessert und an ein weiteres Zielprotein, die Rezeptorbindungsdomäne (RBD) von SARS-CoV-2, angepasst. Die hohe Reproduzierbarkeit des etablierten Protokolls ermöglichte die Anwendung in einem HDX-Screening-Workflow unter Verwendung einer geringeren Anzahl von Deuterierungszeitpunkten. Dies ermöglichte das Screening eines Pools von sieben potenziellen Nanobodies-Epitopen innerhalb eines Zeitraums von etwa vier Wochen. Der HDX-MS-Screening-Ansatz wurde verwendet, um die evidenzbasierte Identifizierung von zwei Hauptkandidaten zu unterstützen, die in ihrer viralen Neutralisierung wirksam sind.
Anschließende Bemühungen zielten darauf ab, den etablierten Screening-Ansatz auf Proteine mit mehreren posttranslationalen Modifikationen (PTMs) anzupassen. Während extrazelluläre Proteine attraktive Arzneimittelziele darstellen oder selbst als Biopharmazeutika verwendet werden, tragen fast alle von ihnen mehrere PTMs wie N-Glykosylierungen und Disulfidbrücken. Aufgrund ihrer Heterogenität bleiben N-Glykosylierungen eine Herausforderung für Strukturanalysen wie HDX-MS. In dieser Arbeit wurde eine neuartige Peptid-N-Glykanase aus *Rudaea cellulosilytica* (Rc) charakterisiert, die eine breite Substratspezifität und eine hohe Aktivität zur Deglykosylierung nativ gefalteter Proteine aufweist. Somit wurde das Enzym verwendet, um MS-basierte Top-down-Proteinanalytik zu erleichtern und bietet die Möglichkeit für N-Deglykosylierung von Peptiden in wenigen Minuten. Darüber hinaus kann das Enzym nach heterologer Expression aus *E. coli* mit hoher Ausbeute und ausreichender Reinheit erhalten werden. Aufgrund des pH-Optimums im sauren Bereich wurde die PNGase Rc erfolgreich unter anspruchsvollen HDX-MS supprimierenden Bedingungen (0 °C; pH 2,5), in Gegenwart von üblicherweise verwendeten Konzentrationen von Reduktions- und Denaturierungsmitteln Tris(2-carboxyethyl)phosphin (TCEP) Harnstoff und Guanidiniumchlorid (GdmCl), verwendet. Als Grundsatzbeweis wurde die PNGase Rc in den etablierten HDX-Epitop-Screening-Workflow (post-proteolytisch) integriert, was zur Aufklärung von vier Nanokörperepitopen führte, die auf die mehrfach N-glykosylierte extrazelluläre Domäne des signalregulierenden Proteins alpha (SIRPα) abzielen. Durch die zusätzliche Deglykosylierung wurde die Sequenzabdeckung, Redundanz erhöht und es zusätzlich ermöglicht Epitope in Nachbarschaft einer Glykosylierungsstelle zu detektieren.

3 Introduction

3.1 Protein-Protein Interaction

3.1.1 Principles

The probably first protein-protein interaction (PPI) to be reported was the interaction of trypsin and antitrypsin in 1906 by Hedin [1]. Since then, a myriad of PPIs were discovered and today, they are known to be essential for the cellular machinery and the control of most of the biological processes such as intercellular communication, immune response, reaction catalysis, transport or viral entry [2, 3]. Furthermore, interaction of specialized proteins mediate the basic life processes of DNA replication, transcription and translation [2]. These interactions represent a large and complex network of cellular pathways, named "interactome" [4].
Interactions are mediated by complementary regions on the proteins surface that usually comprises a protein-protein interaction interface of around 1500–3000 $Å^2$ [5]. Furthermore, the interface show a chemical complementarity resulting in polar, hydrophobic and charged interaction forces. In general, proteins interact with each other if the Gibbs free energy of the complex is lower than that of the un-complexed binding partners and as this interaction is dependent on the concentration of the binding partners, the interaction between all proteins is physically possible [6]. The formation of a protein complex, consisting of protein A and B, can be explained by a four state model (Equation 1) [7]. Upon protein association both interaction partner form a so called encounter complex (AB*), a complex mostly stabilized by long-ranging electrostatic interactions. The encounter complex can turned into an intermediate complex (AB**) by interface desolvation, the formation of short-range interactions and eventually structural rearrangements than leading to the final complex AB [8].

$$A + B \rightleftarrows AB* \rightleftarrows AB** \rightleftarrows AB \qquad \text{Equation 1 [7]}$$

PPIs can be classified in many different ways including the classification according to the composition of the complex or its binding strength [3]. Whereas homo-oligomeric complexes consist of identical proteins, the interaction between different proteins is classified as hetero-oligomeric. The binding strength and therefore the stability and lifetime of a protein complex might determine the classification into transient and permanent, obligate and non-obligate PPIs [9]. In obligate interactions, also referred to as quaternary structures, the proteins exist only in complex and are permanently bound to each other, while most of the non-obligate PPIs are transient [10]. In order to describe the lifetime of a complex in a one-to-one stoichiometry equilibrium one can either use the expression with the law of mass action or as a kinetic

process of association and dissociation. The binding affinity can be expressed using the equilibrium dissociation constant (K_D) which equals the molar concentration (M, mol/L), where the interfaces are half saturated. It is equivalent to the ratio between the reaction rate constant of the complex dissociation ($k_{off;}$ s^{-1}) and association (k_{on}, $M^{-1}s^{-1}$).

$$A + B \rightleftarrows AB \qquad \text{Equation 2}$$

$$K_D = \frac{[A][B]}{[AB]} = \frac{k_{off}}{k_{on}} \qquad \text{Equation 3}$$

Transient interaction partners associate and dissociate temporarily with different lifetimes and thus binding affinities. These can range from very weak interactions with lifetimes of milliseconds and affinities in high micromolar to millimolar range up to tight complexes with half-lifes of days and picomolar affinities [6].

Within a PPI interface, amino acid residues contribute differently to the binding free energy and most of the binding affinity can be attributed to small fraction, the so called “hot spot” residues [11]. The contribution of individual residues can be determined by a systematic amino acid mutagenesis to alanine [12]. An amino acid is considered as hot spot residue if the mutation leads to an increase of binding-free energy of ≥2 kcal/mol [6]. Protein structures are flexible in solution and can undergo various conformational changes. These structural changes can be referred to as molecular “breathing” motions [13]. Hence, the complex formation can induce a structural rearrangement either within the binding interface (“induced fitting”) or allosterically at a specific site, hampering computational docking experiments [14].

As described above PPIs are significantly involved in physiological and pathological processes such as cell proliferation, apoptosis, differentiation and invasion. Thus, altered PPIs are associated with many diseases including cancer, infectious, and neurodegenerative diseases [15-17]. Knowing the interaction partner as well as the interaction site can be crucial for understanding the mode of action of a certain protein. Furthermore, the PPI interface itself shows great potential as drug target for new therapeutic modulators such as small molecules, peptides or proteins [15, 16, 18].

3.1.2 Antibody – Antigen Interactions

One of the largest classes of therapeutic proteins whose mechanism of action relies on protein-protein interactions is the immunoglobuline G (IgG) class of monoclonal antibodies (mAbs). Since the first therapeutic mAb reached the market in the mid-1980s, more than 80 mAbs have been approved by the European Medicine Agency (EMA) by the end of 2019 [19]. Thus, the market for therapeutic mAbs has grown and reached nearly 115 billion US$ in 2018 and is expected to reach 300 billion US$ in 2025 [20].

The general structure of a human IgG is assembled by two light chains and two heavy chains (Figure 1). These structure can be further classified into two regions, the binding-mediating region (Fab), and the constant region (Fc), which are connected by a proline-rich hinge region (Figure 1). The Fab regions contain the variable domains of the heavy and light chain that mediate the protein-protein interaction with the target protein. Interaction interfaces of Abs, the paratopes, mainly consists of three flexible hypervariable loops of each chain referred to as complementary determined regions (CDR) but may additionally include frame work regions [21, 22]. The interaction of the antibody is mediated through specific binding to the antigens (Ag) interaction region, the epitope.

In 1993, Hamers-Casterman *et al.* discovered heavy chain-only antibodies in sera of Camelidae (Figure 1) [23]. The equivalent Fab fragment is referred to as variable domain of the heavy chain of heavy chain-only antibodies (VHH) or nanobody (Nb) [24]. Although Nbs bear only three CDR regions they can bind their target molecules with high affinity with a K_D in the low nanomolar or even picomolar range. Moreover, the interaction strength is often dominated by the CDR3 region whose sequence homology and length also can be used to cluster individual Nbs into families [25]. Nbs have proven to be valuable tools in biomedical research, diagnostics and therapy. The small size of ~15 kDa, which is one-tenth of the size of an antibody offers chemical stability and solubility as well as fast tissue penetration [24, 26]. Therefore, Nbs have great potential to be used for in vivo and immunohistochemical imaging [26].

The nature of the interface region on the antigen can be classified in continuous (linear) and discontinues (conformational) epitope regions. Continuous epitopes consist of amino acid stretches that are in close proximity in the polypeptide chain, whereas discontinuous epitopes are comprised by amino acid residues that are only proximate in the folded, native structure of the protein [27]. However, most (90%) of native epitopes are discontinues [28]. The characterization of the Ab:Ag interaction site, the so-called epitope mapping aids the development and discovery of novel antibodies for therapeutic and diagnostic use [29-31].

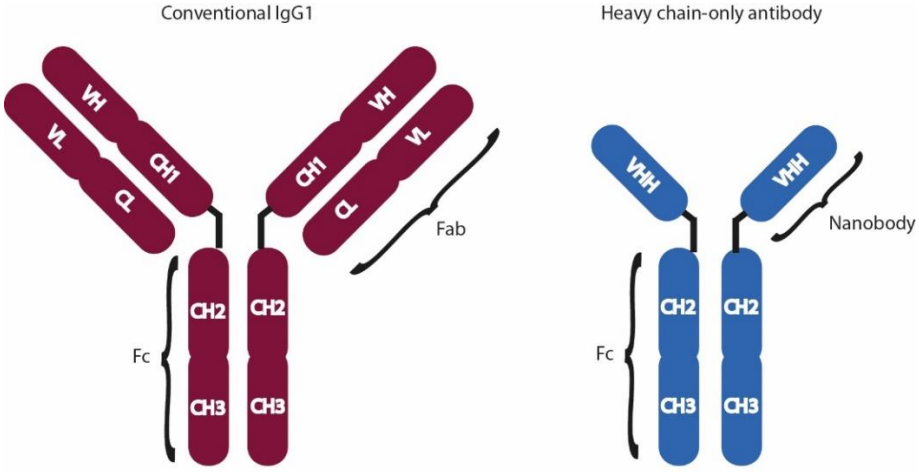

Figure 1: Schematic representation of a human IgG1 antibody (left) and a heavy chain-only antibody derived from Camelidae (right) [26]. *The human IgG1 antibody consists of two heavy chains and two light chains, which contain a binding-mediating domain (Fab) and a constant region (Fc). Fabs and Fcs further consist of variable domains (V domains) of the light (VL) and heavy chains (VH) as well as constant domains of light (CL) and heavy (CH1-3) chains. The heavy chain-only antibodies lack the light chain and CH1 domains. The variable binding region (VHH), also known as nanobody mediates the binding.*

3.1.3 Methods for Determination of Antibody-Antigen Binding Interfaces

Numerous techniques have been developed for the elucidation of PPI interfaces in general and antibody-antigen epitope mapping in particular including biophysical and biochemical approaches [31-33]. They can be classified into immunochemical and structural analysis methods [30]. The immunochemical analysis of PPIs consists of methods such as displaying techniques including yeast surface display [34], enzyme-linked immune sorbent assay (ELISA) [35] and biosensor techniques including surface plasmon resonance (SPR) [36] and biolayer interferometry (BLI) [37], amongst others.

As one of various displaying techniques, the eukaryotic nature of yeast surface display offers to study PPIs of larger and more complex proteins with additional posttranslational modification [38]. Using these techniques the protein of interest is expressed on the surface of the yeast cells and ligands can be screened allowing the identification of PPIs in high throughput. The expression of different genetically modified antigen domains allows an application for antibody epitope screening including conformational and linear binding interfaces. Thus, this technique was used for epitope mapping and the identification via fluorescent tag-conjugated Abs in combination with flow cytometry enabled both, quantitative and qualitative analyses [39, 40]. However, protein glycosylation profiles in yeast cells differ from those of mammalian cells, that might alter the structure and the Ab:Ag interactions. Beside displaying techniques, ELISA has been used for elucidation of Ab:Ag binding sites [41, 42]. While this technique is inexpensive, requires only non-specialised equipment and

provides the ability of high sample throughput, it suffers in the detection of weak transient interactions due to required washing steps [32]. Immunoassays and optical methods such as SPR and BLI are used to roughly map epitopes to individual antigen domains or antigen surface areas. For this purpose, the displacement or simultaneous binding of different antibodies to an antigen or antigen domain is tested. This procedure is called "epitope binning" [43]. To further narrow down the epitope, the binding of antibodies to overlapping peptides, each consisting of 10-20 amino acids of the antigen, can be tested. These so-called "peptide arrays" can be used well for linear epitopes consisting of a sequence of several amino acids [30, 31]. Additionally, SPR and BLI, which differ in their throughput and sensitivity provides the opportunity of label free quantification of the PPI [44]. In combination with site directed mutagenesis, both techniques can be used to determine interface hot spot residues. While, immunochemical approaches can provide detailed qualitative and quantitative characterization of the PPI they yield little information about exact amino acids forming discontinues epitopes on the antigens. Thus, these techniques are frequently combined with other, structural epitope mapping techniques [45-47].

The most powerful structural epitope mapping techniques regarding the resolution are X-ray crystallography [48], nuclear magnetic resonance (NMR) spectroscopy [49] and cryo-electron microscopy (cryo-EM) [50]. These approaches provide detailed information of the exact epitope location up to single amino acid resolution. However, they remain technically challenging and bear individual limitations. While X-ray crystallography can be considered as the gold standard for the analysis of PPIs it is limited to the solid state proteins which have to be crystallized prior to the analysis. Protein crystallization might be a challenging, time consuming task or even fail [30, 31]. Furthermore, X-ray crystallography and the cryo-EM analysis are susceptible against the intrinsic nature of proteins and a desired level of monodispersity may be not reached [31, 51]. Moreover, major disadvantages of cryo-EM are the high costs for the instrumentation and maintenance as well as the need for tremendous computational resources [50]. In contrast, NMR spectroscopy can be used to probe the protein-protein interaction in native (solution) state, but is generally limited to smaller proteins (<30 kDa) [30].

Mass spectrometric (MS) approaches based on crosslinking and protein footprinting techniques provides valuable alternatives for the elucidation of protein-protein interaction sites. These techniques can be applied to almost infinitely large proteins under native conditions, they show high tolerance against impurities and low sample consumption (Figure 2) [30].

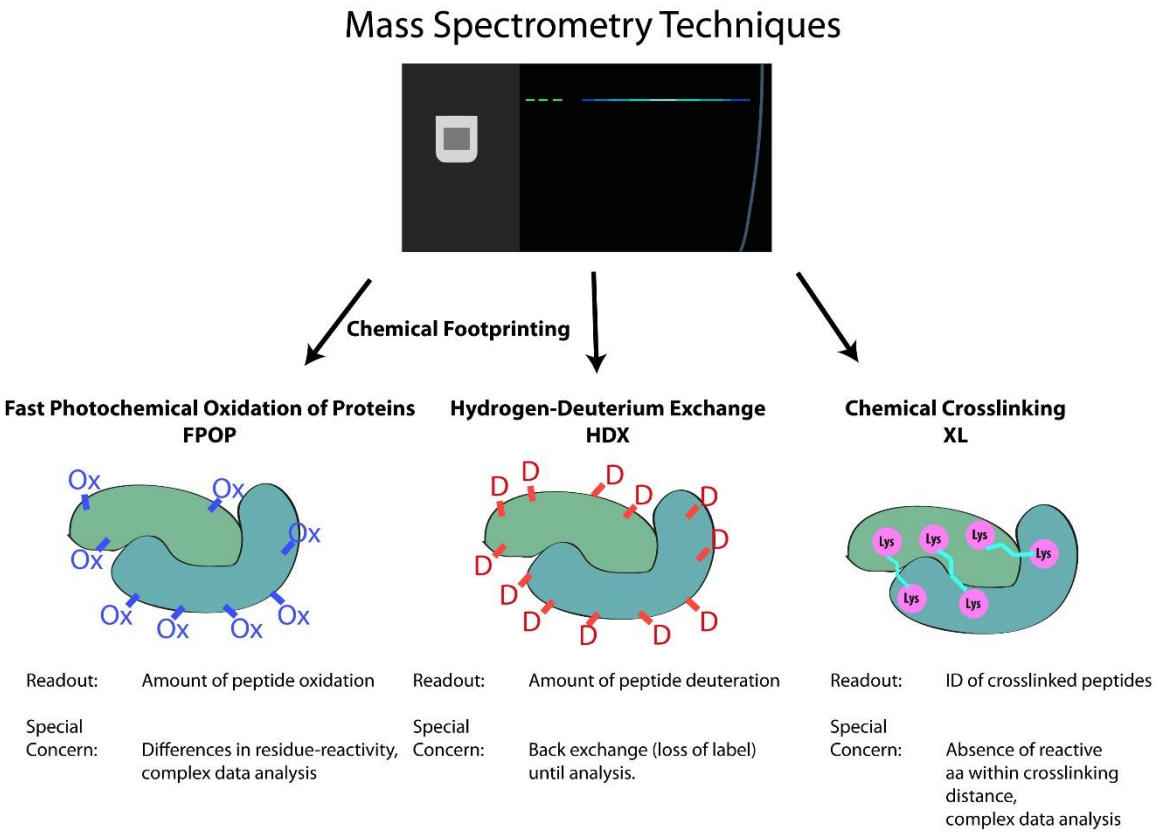

Figure 2: MS based methods for epitope mapping.

Chemical crosslinking uses various chemical entities differing in their length that covalently link amino acids in particular proximity [52]. Coupled to mass spectrometry chemical crosslinking (XL-MS) has been shown to be effective in characterizing of PPIs [53, 54]. A major drawback is that the technique relies on the availability of defined chemical linker and reactive amino acids, mostly lysine [52]. Furthermore, linkages bears the risk to introduce nonspecific interactions, which on the other hand might stabilize weak transient interactions facilitating the elucidation of epitopes of even low affinity PPIs. Moreover, the data analysis remains challenging due to the low abundance of the cross-linked peptides and the complexity of the obtained fragment ion spectra [55]. The footprinting approaches are based on the analysis of mass shifts generated by chemical modifications on amino acid side chains or backbone amides detected by MS. Due to the reduction of solvent accessibilities, PPIs might shield individual amino acids selectively from modification within the PPI interface or by subsequent structural changes. These footprinting techniques include, hydroxyl-radical protein footprinting (HRPF) and hydrogen-deuterium exchange (HDX). In the widely used HRPF technique, fast photochemical oxidation of proteins (FPOP), hydroxyl radicals are generated by photolysis of hydrogen peroxide [56]. FPOP monitors the percentage of labelling of side chain residues by reactive oxygen species mostly at aromatic and sulphur containing amino acid residues [56]. In contrast, in HDX-MS the exchange of hydrogen by its heavier isotope deuterium of backbone

amides is monitored (see also 3.2). While in HDX-MS the labelling is based on hydrogen bonding and the solvent accessible surface area (SASA), FPOP emphasize the latter [57]. Both techniques can provide comprehensive information of the PPI interface and the structural dynamic of a protein. However, HDX-MS can be used to probe each amino acid residue (except proline) across the entire protein with no disruption of the proteins native structure [57]. The main disadvantage of HDX-MS analysis is the reversibility of the labelling and the associated demands on the analysis, which has to take place in a short time at very low temperatures and pH in order to obtain high-resolution results (see 3.2).

In summary, epitope mapping methods differ in their complexity in terms of optimization required, sample throughput and the resolution obtained for the epitope residues (Figure 3). Often, an orthogonal combination of multiple techniques is applied for elucidation of the interaction interface and structural dynamic of the protein.

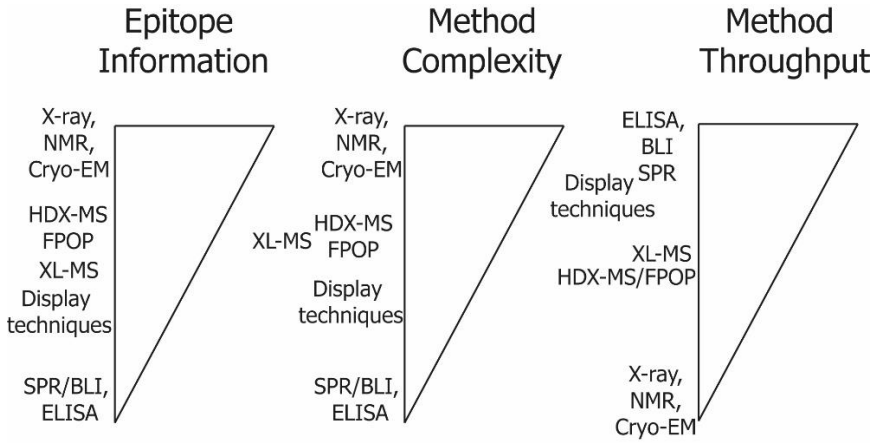

Figure 3: Schematic overview of different epitope mapping techniques based on the extend of epitope information, method complexity and throughput.

3.2 Hydrogen-deuterium Exchange Mass Spectrometry (HDX-MS)

3.2.1 History

The deuterium exchange of hydrogen atoms on proteins was first described in 1954 by the pioneer work of Kai U. Linderstrøm Lang and co-workers of the Carlsberg laboratories (Copenhagen) [58]. They used analytical ultracentrifugation for the separation and detection of the deuterated proteins. While limited to the measurement of the global deuterium uptake of the protein, their work and following approaches laid the foundations for the H/D exchange theory known today. In 1963, S. W. Englander [59] started to use tritium instead of deuterium and coupled the analysis to gel filtration allowing the determination of the radioactive

hydrogen-tritium exchange by liquid scintillation counting. This analysis method of HX was extensively used until the 1980s [60].

Then H/D exchange was coupled to NMR spectroscopy, which provided the first amino acid resolution method using HDX. However, this method was limited to small proteins [60]. Rosa and Richards [61] and Englander *et al.* [62] described a peptic proteolytic fragmentation under HDX quenching conditions, which was combined with a HPLC separation at 0 °C by Zhang and Smith in 1993 [63]. They also used an excess of deuterium to circumvent the radioactive tritium. The detection by liquid scintillation analysis was replaced by the use of a mass spectrometer to detect time-dependent deuterium uptake at peptide level. This removed the size limitation of the analysis by NMR spectroscopy, reduced the required amount of sample and allowed the detection of local hydrogen-deuterium exchange of proteins, leading to a dramatic growth in the field of HDX analyses.

3.2.2 Principle of HDX

3.2.2.1 Chemical Basis of HDX

A hydrogen atom bound to an electronegative heteroatom such as oxygen, nitrogen and sulphur is classified as labile and thus “exchangeable”. Proteins comprise multiple labile hydrogens in the amino acid backbone and side chains (Figure 4). These are in continuous exchange with the protons of the surrounding medium [64]. If the latter consists mainly of deuterium atoms, these are incorporated instead of hydrogen leading to a mass increase by 1.008 Da per isotopic exchange, which can then be detected by mass spectrometry [65]. The incorporation of deuterium in the amino acids side chains and the N-terminal amid bound hydrogen show short half-life ($t_{1/2}$ = ~0.01-1 ms). Thus, only the deuterium within the backbone ($t_{1/2}$= 5 s – 60 days) can be detected within the time frame of a HPLC-MS analysis which makes HDX-MS a direct measure of deuterium exchange in the backbone amides [66, 67].

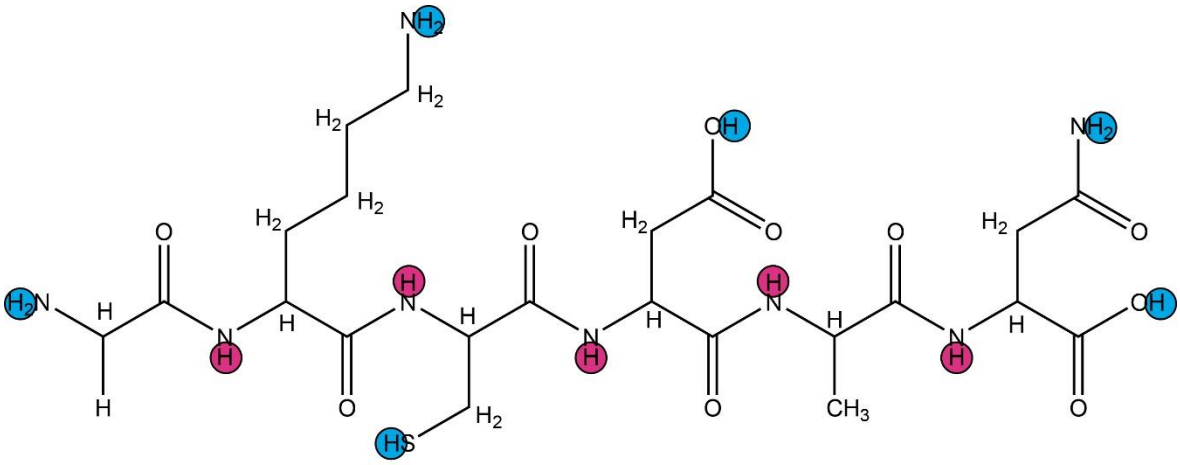

Gly-Lys-Cys-Asp-Ala-Asn

Figure 4: Exchangeable hydrogens shown on a chemical structure of a peptide. *Exchangeable (labile) hydrogens of backbone amides and side chains are coloured in pink and blue, respectively. Only the exchange of the backbone hydrogens shows a sufficiently long half-life to be amendable to HDX-HPLC-MS analysis.*

3.2.2.2 pH Dependency and Exchange Kinetics of HDX

HDX is mediated through base, acid or water catalysed reactions, whereby the catalysis by water is negligible and therefore often neglected (Equation 4) [66]. The exchange rate k_{ch} for an unstructured peptide in solution expressed for the given three intrinsic catalysis rate coefficients is:

$$k_{ch} = k_{acid}^{int}[H_3O^+] + k_{base}^{int}[OH^-] + k_{water}^{int}[H_2O] \qquad \text{Equation 4 [66]}$$

where the base-catalysed reaction rate (k_{base}^{int}) becomes dominant at physiological pH and exceeds the acid-based reaction rate (k_{acid}^{int}) that dominates at pH values below pH 3. The minimum exchange rate can be observed at pH of 2.5-3.0, leading to a decrease of the backbone hydrogen exchange (HX) by approximately four orders of magnitude compared to the exchange at pH 7 [64]. The base catalysis occurs through a nucleophilic attack of an OD^- ion, which abstracts the amide proton that is subsequently reprotonated by an abstraction of a proton from water (Figure 5a). The acid-catalysed HDX can occur through two mechanisms the N and O-protonation summarized in Figure 5b and c.

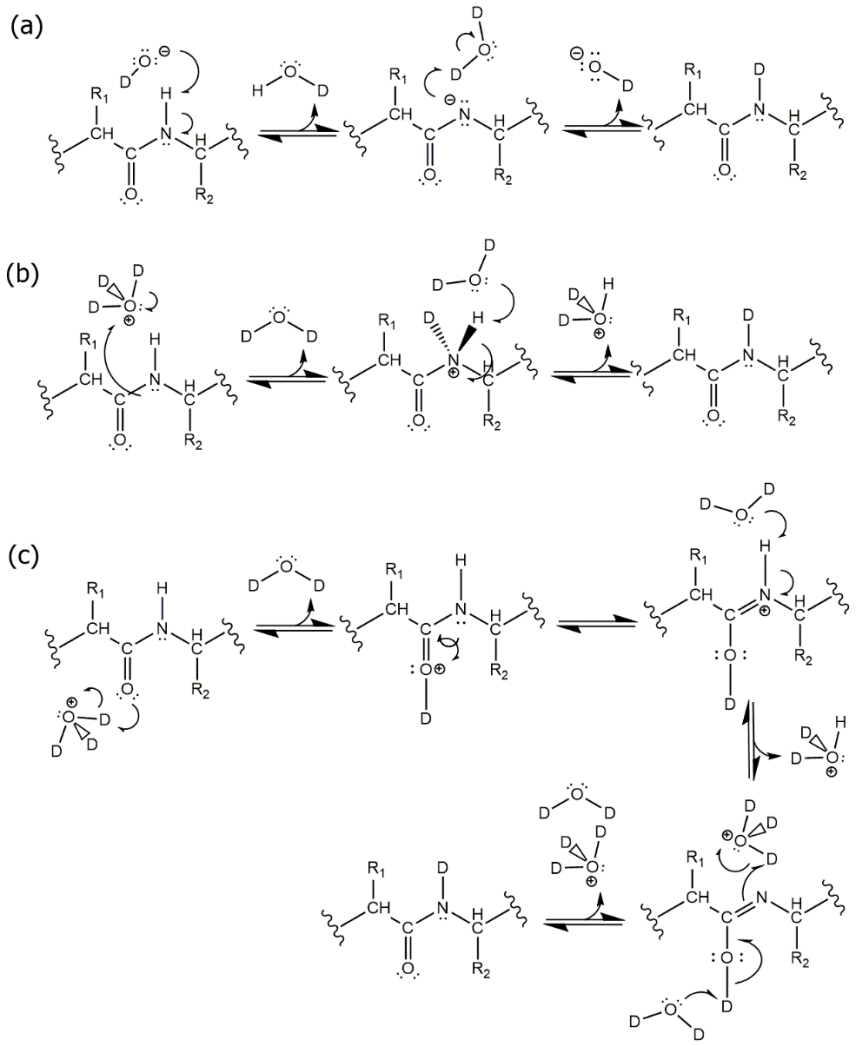

Figure 5: Chemical reaction of the base- and acid-catalysed HDX of backbone amides drawn according to [64]. *(a) Base catalysis, acid catalysis through protonation of (b) nitrogen or (c) oxygen.*

3.2.2.3 Temperature Dependency of HDX

The exchange rate k_{ch} is further dependent on the temperature in such a way that a reduction of 22 °C leads to a reduction of k_{ch} by ~10 fold [60]. This is primarily due to the ionization rate of water K_w and therefore the concentration of OH^- ions present during labelling [64]. The relationship between k_{ch} and the temperature is exponential and can be expressed for an unstructured peptide using Equation 5 [66]:

$$k_{ch}(T) = k_{ch}(293)\exp\left(-\frac{E_a}{R}\left[\frac{1}{T}-\frac{1}{293}\right]\right) \qquad \text{Equation 5 [66]}$$

where $k_{ch}(293)$ is a reference rate of the rate constants for acid, water and base catalysis at 293 K (~20 °C); E_a is the activation energy of the catalysis of the exchange and R is the universal gas constant [66].

3.2.2.4 Structure Dependency of HDX

The equations above describe the temperature and pH dependency of the HD exchange of unstructured peptides. The exchange is further dependent on the side chains from neighbouring amino acid residues that can lead to inductive and steric effects [66].
However, these equations do not apply to a structured protein, in which the higher-order structure largely contributes to the HX rates, potentially leading to an enormous decrease of theoretical HDX half-life times from seconds up to even months or years [68]. The HX rate of amino acids in natively folded proteins is dependent on their solvent accessibility and on their engagement in intramolecular hydrogen bonds [69]. Thus, an amino acid is usually considered as exchange-incompetent if it is sterically inaccessible or hydrogen-bonded (NH_{close}). The dynamic protein motion (molecular "breathing"), already described by the Linderstrøm-Lang laboratory [13], leads to local and global unfolding events, where backbone amides can become HX competent (NH_{open}) and exchangeable (Equation 6) [70].

$$NH_{close} \underset{k_{cl}}{\overset{k_{op}}{\rightleftarrows}} NH_{open} \xrightarrow[D_2O]{k_{ch}} ND_{open} \underset{k_{op}}{\overset{k_{cl}}{\rightleftarrows}} ND_{close} \qquad \text{Equation 6 [70]}$$

Thus, the transient exchange-competent intervals of an amino acid residue are based on the opening (k_{op}) and closing (k_{cl}) rates, which compete with the HX rate (k_{ch}), resulting in two different kinetic scenarios: if the HDX occurs faster than the reclosure ($k_{ch} \gg k_{cl}$), it attains an asymptotic behaviour and dependents only on the opening of the structure and $k_{op}=k_{HDX}$. This scenario is referred to as EX1 kinetic or so-called "monomolecular" exchange. It occurs at high pH (base-catalysed high k_{ch}) or low protein stability where k_{cl} is low [70]. EX1 kinetics often result in varying degrees of bimodal isotopic distribution, since two subpopulations of isotopic pattern are co-existing, the fully deuterium exchanged as well as the non-exchanged.
However, for most of the residues within a natively folded protein, reclosing of the structure occurs faster than the HX rate ($k_{cl} \gg k_{ch}$). Therefore, multiple openings of the structure have to occur before an HX event takes place. This is referred to as EX2 kinetic or so-called "bimolecular" exchange and can be expressed in a steady-state equilibrium using the following equation (Equation 7) [71]:

$$k_{HDX} = k_{ch}\frac{k_{op}}{k_{cl}} = K_{op}k_{ch}$$ Equation 7 [71]

where k_{HDX} is the exchange rate of for a given amino acid residue and K_{op} (k_{op}/k_{cl}) is the equilibrium opening constant. Therefore, a structural protection factor can be calculated in free Gibbs energy by:

$$\Delta G_{op} = -RTln(K_{op}) = -RTln\left(\frac{k_{op}}{k_{cl}}\right) = -RTln\left(\frac{k_{HDX}}{k_{ch}}\right)$$ Equation 8 [71]

with the differential Gibbs free energy for HX (ΔG_{HDX}) dependent on the temperature (T) and the universal gas constant R. For differential HDX experiments, a second states might result in changes in structural stability free energy and thus in HDX of back bone amides. The equation can be rearranged to:

$$\Delta\Delta G_{op} = -RT\Delta ln(K_{op}) = -RTln\left(\frac{k_{HDX,1}}{k_{HDX,2}}\right)$$ Equation 9 [71]

where $k_{HDX,1}$ represents the exchange rate of state one and $k_{HDX,2}$ the of state two [71].

3.2.3 Application of HDX

A protection from the HDX in the protein backbone also occurs upon a PPI which might lead to a stabilized structure and a reduction of the surface accessibility for the solvent [30]. Thus, beside the analysis of protein dynamics, HDX-MS is a powerful tool for the analysis of PPIs.
A typical HDX-MS analysis workflow for the elucidation of the PPI such as an antibody and antigen is the bottom-up approach (Figure 6). It can be divided into six steps, namely the (1) equilibration (complex formation), (2) the deuterium exchange, (3) quenching, (4) protein digestion, (5) chromatographic separation and (6) determination of the incorporated deuterium by mass spectrometry. For the epitope mapping approach these steps are performed for the antigen alone and in complex with the antibody and changes of the HDX upon complexation are monitored [30, 67].

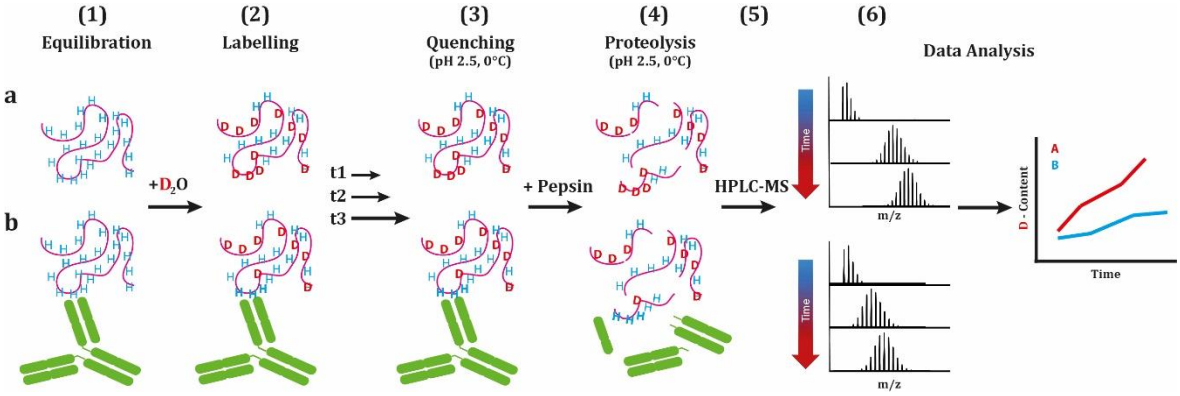

Figure 6: Scheme of a typical bottom-up approach of an HDX-MS epitope mapping experiment using continuous deuterium labelling. *After equilibration with (a) or without antibody (b) in H_2O, the deuterium exchange is initiated by diluting the complex in an excess of D_2O. At defined times, the exchange is quenched by lowering the pH and the temperature, and the proteins are digested by an acidic protease (e.g. pepsin). The mass shift of the resulting peptides is analysed via HPLC-MS. Protection of the deuterium uptake due to the introduction of the binding partner is then used to elucidate the epitope region.*

(1) Prior to HDX analysis, the interaction partner are incubated for complex formation at physiological conditions. For epitope mapping most of the ligand molecule should be in complex ensuring a uniformly deuterated molecule population. Otherwise, differently deuterated molecule populations arise, each of which showing different exchange kinetics. This can lead to a false EX1 exchange signatures, reflected by bimodal spectra, which subsequently complicate data interpretation [64]. The relative amounts of complexed Ab and Ag in a monovalent binding manner can be calculated considering the binding stoichiometry of the antibody-antigen complex [72] (Equation 10, Equation 11)

$$Ag{:}\,Ab = \frac{(K_d + Ag_t + Ab_t) - \sqrt{(K_d + Ag_t + Ab_t)^2 - 4[(Ab_t)(Ag_t)]}}{2} \qquad \text{Equation 10 [72]}$$

$$\%Ab_{bound} = \frac{Ag{:}\,Ab}{Ab_t} \qquad \%Ag_{bound} = \frac{Ab{:}\,Ag}{Ag_t} \qquad \text{Equation 11 [72]}$$

where Ag:Ab represents the concentration of the antibody-antigen complex. Ab_t and Ag_t are the total quantities of the antibody and antigen, respectively [72].

(2) Deuteration is initiated by dilution with an excess of D_2O. The subsequent change in reaction volume should be considered for the calculation of the percentage of bound Ag.

(3) After different incubation time periods, hydrogen-deuterium exchange is quenched by lowering the pH and temperature to pH 2.5 and 0 °C, respectively. Under these conditions, the average half-life of deuterium in the backbone amides is between 30 and 120 min, representing sufficient time for the subsequent analysis by HPLC-MS [73]. However, the sensitivity of an HDX experiment correlates with the back-exchange. Therefore, the back exchange must be

controlled for the experimental setup and protocol used [74]. Recently, some groups applied sub-zero quenching to further reduce back exchange during analysis [75, 76].

(4) To sub-localize HDX differences to defined parts of the protein, a proteolysis with an acidic proteases such as pepsin, protease type XIII from *Aspergillus saitoi*, protease type XVIII from *Rhizhopus* species or nepenthesin can be applied [77-79]. Of these proteases, pepsin is most commonly used in HDX-MS and exhibits a promiscuous cleavage specificity [67]. This leads to overlapping peptides of various length that can be used to increase site specific resolution [79]. The proteolysis conditions of the protein of interest have to be optimized aiming high sequence coverage, with high redundancy, while keeping the back exchange as low as possible. Additionally, the proteolysis is typically aided by high concentrations of denaturing and reducing agents (see 3.2.4).

(5) The obtained peptides are separated via a cooled HPLC and analysed by mass spectrometry. Peptide identification by tandem MS such as collision-induced dissociation (CID-MS/MS) is only applied to the non-deuterated samples resulting in a peptide list (peptide pool). This list includes at least the retention time, the charge state and sequence of the identified peptides, which then is used for the assessment of the isotopic patterns during the HDX-MS analysis [67, 74]. Application of CID fragmentation to deuterated peptides induces H/D migration throughout the backbone which also is referred to as scrambling [80]. Multiple charge states of a peptide can increase the confidence of the determined HDX since they show the same HDX kinetics [67, 74].

(6) The average deuterium incorporation is determined using the centroid mass shift of the peptide isotopic pattern and compared to a non-deuterated peptide pattern and various states (e.g. bound vs unbound state). The result can be plotted using uptake plots representing the basis of each HDX analysis (Figure 6) [67, 74]. The centroid of the isotopic envelope is calculated as follows:

$$\langle m \rangle_{centroid} = z\left(\frac{\sum_{i=1}^{n}(m/z)_i * I_i}{\sum_{i=1}^{n} I_i} - m_{H^+}\right) \qquad \text{Equation 12 [67]}$$

where z is the charge state of the peptide with the determined m/z value and the intensity (I) of an isotopic peak and the mass of the attached H^+ ion, m_{H^+} [67].

3.2.4 PTMs, Challenges for HDX-MS Analysis

Within the last decades HDX-MS has become a powerful tool for the analysation of protein dynamics and molecular interactions of proteins. However, the analysis of large, multi-protein complexes, disordered proteins, membrane proteins, highly N-glycosylated or disulphide-bonded proteins still represent challenges for HDX-MS analysis [81]. Extracellular proteins and protein domains typically contain multiple posttranslational modifications (PTMs) such as glycosylation and disulphide bonds that ensure proper folding, solubility and stabilization of their native conformation to maintain their biological function [82-85].

3.2.4.1 N-Glycosylation

Glycosylation is one of the most prevalent PTM and is involved in many physiological and pathophysiological processes such as cell-cell interactions, receptor activation, tumour growth, metastasis and viral immune evasion [85-87]. Most of the secreted proteins or extracellular protein domains are glycosylated. Glycosylation mediates and alters protein-protein interactions and ensures proper folding and stability [83-85]. Furthermore, glycosylation increases the hydrophilicity and acidity and thus the solubility, which explains the high prevalence of this modification in plasma proteins. The negative charge of sialic acid and sterical hindrance of glycans also provides a greater resistance to proteolysis [85] and shields the proteins from unwanted interaction with other proteins. Dependent on the linkage site to the amino acid residue, this PTM can be divided in two groups: the O- and N-linked glycosylations. O-linked glycans are attached to the hydroxyl oxygen of threonine and serine residues [84]. N-linked glycans are attached to the nitrogen of asparagine side chains through an N-glycosidic bond. Moreover, N-linked glycosylation is only mediated at the consensus sequence motif of Asn-X-Ser/Thr, with X representing any residue except proline. Although the core of the N-glycan structure is highly preserved, the decoration is dependent on the glycosidase and glycosyltransferase pool of an organism or cell type [83, 88]. The N-glycans can be furthermore divided into three main types the high mannose, complex and hybrid type (Figure 7a). This complexity in N-glycan structure at a specific site (microheterogeneity) in combination with a varying extent of occupation within protein subpopulations (macro-heterogeneity) results in a highly heterogeneous and variable PTM group (Figure 7b) [89].

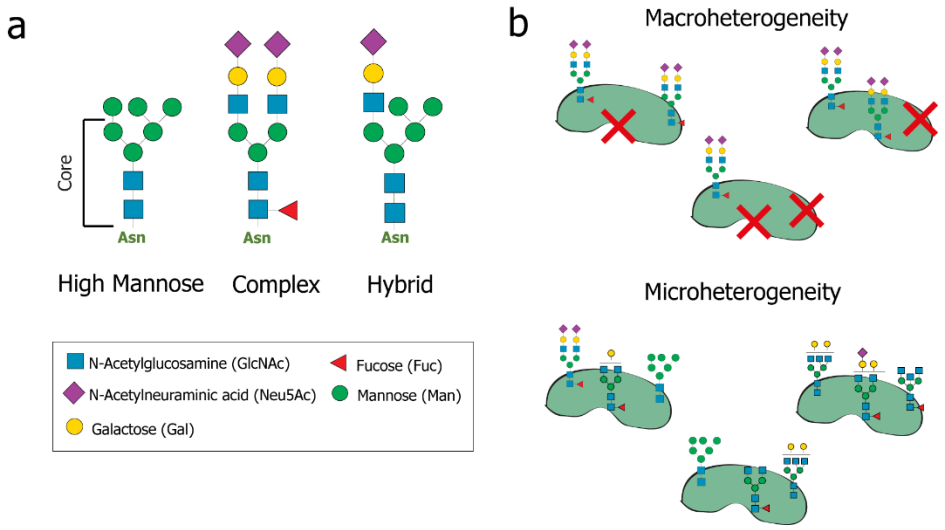

Figure 7: Types of N-glycans (a) and types of N-glycan heterogeneity (b).

The structural analysis of complex glycosylated proteins poses challenges for many structural techniques such as X-ray crystallography, NMR spectroscopy and HDX-MS. HDX-MS shows sensitivity and tolerance to sample complexity and thus has been shown to have notable potential for the analysis of glycosylated proteins [90, 91]. However, N-glycans pose challenges as they impede peptide identification due to signal distribution across multiple glycopeptide species with unknown N-glycan content and promiscuous cleaved peptide sequence [81, 92, 93]. Furthermore, peptide identification using conventional fragmentation techniques such as collision induced dissociation (CID) yield little information of the peptide backbone since the weaker glyosidic bonds will preferentially fragment [94]. Thus, bottom-up HDX-MS analysis often lacks sequence coverage adjacent to N-glycosylation site.

Another obstacle is the fact that the N-glycan pentasaccharide core contains two acetamido groups, which can exchange deuterium and retain it under quench conditions. Furthermore, the N-linked glycosidic bond formed between the asparagine side chain and the glycan attached might be protected from deuterium exchange leading to misinterpretation of HDX results [95]. Detailed integrity, conformation and interaction analysis of such proteins is important, as glycoproteins are often drug targets or are themselves used as biopharmaceuticals [89, 96].

Peptide-N(4)-(N-acetyl-β-glucosaminyl)asparagine amidases (PNGases) have been shown to be valuable tools releasing the N-glycans and subsequently facilitating the analysis of N-deglycosylated proteins [89, 97, 98]. PNGases are endoglycosidases and hydrolyse the amide bond between the innermost N-Acetylglucosamine (GlcNAc) and asparagine side chain with subsequent release of the N-glycan and the asparagine residue converted into an aspartic acid (Figure 8). Two types of PNGases are widely used [89] for N-glycan hydrolysis: one from *Flavobacterium meningosepticum* called PNGase F [99] and one isolated from *Prunus dulcis*

(almond; PNGase A) [100]. The acidic PNGase A is itself a glycoprotein heterodimer of a 54.2 and 21.2 kDa subunit, containing 12 potential N-glycosylation sites, with an optimal activity at pH 5 [98]. In contrast, PNGase F is a monomer of 35 kDa with a pH range between pH 6.0 and 9.3. PNGase A shows a broader spectrum of N-glycan release regarding the fucosylation of the innermost GlcNAc residue (α-1,3 and α-1,6) compared to the PNGase F that only releases N-glycan moieties with a-1,6 fucosylation [98]. However, in contrast to PNGase F, PNGase A shows limited efficiency in N-glycan release from natively folded, intact proteins requiring proteolytic cleavage prior to PNGase treatment [101]. While PNGase F can be recombinantly expressed using *Escherichia coli* (*E.coli*), PNGase A has not yet been expressed recombinant using a prokaryotic organism. Thus, PNGase F is commercially available in high amount and purity which is one major reason for the widespread use of this enzyme in protein analyses [89, 98, 102].

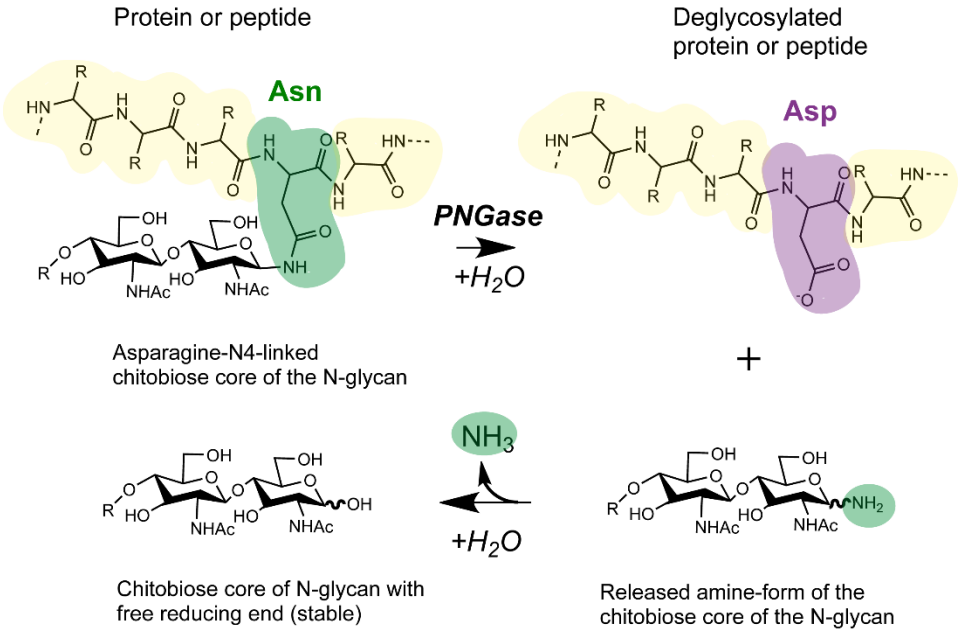

Figure 8: Scheme of enzymatic deglycosylation by PNGases adapted from Wang et al. [103].

However, this enzyme has its pH working range at physiological conditions and shows no activity at a pH below 4.0 [99]. This limits the implementation into the HDX workflow to deglycosylation prior to complex formation (pre-HDX). Cleaving the protein glycosylation prior to complex formation brings the risk to alter the three-dimensional conformation of the protein and therefore its binding to interaction partners [75, 90]. Furthermore, some interactions are influenced by the N-glycosylation that prevent the detection of the native antibody-antigen binding behaviour [91, 104]. As alternative, the acidic PNGase A was successfully applied in post-HDX deglycosylation, although it showed only residual enzyme activity at pH 2.5 [65, 105]. Besides the commercially available enzymes, a set of novel acidic

PNGase enzymes has been discovered by Guo *et al*. [102]. One enzyme variant has been probed for application in an on-line HDX workflow with electrochemical reduction [106]. However, this approach needs additional, cost-intensive equipment and expertise and the availability of used N-glycanase is still limited.

3.2.4.2 Disulphide Bonds

Disulphide bonds pose an additional challenge for HDX-MS as their presence hampers proteolysis and leads to a lack of sequence coverage especially in proximity to cysteine residues. Chemical reduction of disulphide bonds is commonly accomplished using tris-(2-caboxyethyl)phosphine (TCEP), but is inefficient at low temperatures, pH and short reaction times required for HDX experiments. Thus, TCEP is used in high concentrations and the proteolysis is also aided by chaotropic agents such as urea or guanidine hydrochloride (GdmCl) [67, 107-109].

3.2.5 Case Study Antigen Molecules

3.2.5.1 Annexin-A1

Background information on annexin A1 (ANXA1) regarding the herein described case study were recently been published by Gramlich *et al.* [110]. In brief, ANXA1 belongs to the family of annexins, which are phospholipid-binding proteins that interacting in a calcium-dependent manner. ANXA1 has a molecular weight of 38 kDa and consists of a 41 amino acid N-terminal region and a C-terminal core region. ANXA1's core is comprised by four homologous repeat domains (I - IV) of which each consists of five α-helices [111]. The C-terminal core structure is tightly compressed and forms a slightly curved disc that harbours 12 calcium-binding sites on the convex surface [112]. Calcium occupation leads to a conformational change exposing the flexible N-terminal domain from the core repeat III. Thus, two ANXA1 proteins can form a dimer or can interact with a bilayer through the exposed N-terminal repeat [111]. This N-terminal domain is highly variable between the individual members of the annexin family [113]. The function of annexin A1 is mediated either by complex formation with the formyl peptide receptor or by binding to the phospholipid bilayer of the cell membrane [114]. ANXA1 has been shown to play a role in a variety of diseases such as cardiology, immunology, neurology, endocrinology and oncology [114-116]. However, its function to alter the innate and adaptive immune system is one of its most important properties [114, 117]. In addition to the well-documented role of ANXA1 in neutrophil and monocyte function of the innate immune system, it has also been shown to modulate the signalling strength of the T cell receptor and consequently the T cell differentiation and activation [118, 119]. This makes ANXA1 an

attractive drug target for the treatment of diseases that originate from the dysregulation of the T-cell activation, such as rheumatoid arthritis or multiple sclerosis [120, 121]. In this case study, the binding interface of a therapeutic, humanized antibody candidate that binds to ANXA1 in calcium-dependent manner was elucidated. The investigated humanized mAb was generated from a murine antibody that has been shown to specifically inhibit T-cell activation without any adverse cytotoxic effects [120]. [110]

3.2.5.2 Receptor-Binding Domain (RBD) of SARS-CoV-2

The coronavirus disease 2019 (COVID-19) pandemic caused by the severe acute respiratory syndrome coronavirus 2 (SARS-CoV-2) was first recorded in patients in Wuhan in China at the end of 2019 [122]. As of June 2022, the pandemic has caused the death of more than 6 million people worldwide (source: WHO, https://covid19.who.int/, accessed June 20, 2022) and is further associated with dramatic socioeconomic challenges [123].

The infection by the virus is mediated through a trimeric spike glycoprotein (S-protein) on the surface of the virus. Each monomer of the homotrimeric S-protein consists of two subunits (S1 & S2). The fusion with the cell membrane is initiated by the binding of the receptor-binding domain (RBD) located in the S1 subunit to the angiotensin converting enzyme 2 (ACE2) on the cell surface [124]. Cryo-EM analysis revealed conformational changes of the pre-fusion spike protein related to the RBD positioning. Thus, the RBD can be present in an “up” or “down” configuration, whereas the interaction with the ACE2 receptor is only mediated by the binding in the “up” positioning [124, 125]. The RBD:ACE2 interface has been shown to be an attractive target for potent virus neutralisation by antibodies [126, 127] or nanobodies [128, 129]. Neutralisation can be mediated by various mechanisms, such as competition for the ACE2 binding or stabilization the all-down state of the RBDs. Thus, the position of the RBD can have implications for the accessibility of the epitopes and subsequently neutralisation efficiency [130].

3.2.5.3 Signal-Regulatory Protein Alpha (SIRPα)

The signal-regulatory protein alpha (SIRPα) is a member of the SIRP family consisting of three individual proteins namely SIRPα, SIRPβ and SIRPγ. SIRPα (also known as SHPS-1 or CD172a) is expressed on the cell surface of monocytes, macrophages, granulocytes, dendritic cells and to varying levels on neurons with high expression in synapse rich areas of the brain [131]. Complexation with CD47, which is expressed on virtually all cells including erythrocytes and platelets, leads to inhibition of the phagocytosis. Therefore, CD47 is often referred to as “don’t-eat-me” signal. The level of CD47 expression varies and can therefore be downregulated with

cell aging, leading to higher levels of phagocytosis. Simultaneously, overexpression is associated with suppressed phagocytosis in various tumour types [132].

SIRPα consists of three Ig-like extracellular domains, a transmembrane region and a short cytoplasmic region [133]. The interaction with CD47 is mediated through the V-set domain one, which shows a sequence dependent polymorphism known to have no effect on the interaction [134]. Furthermore, the extracellular domain (ECD) of SIRPα is highly N-glycosylated, which, while not essential for function, may reduce the affinity to CD47 upon hyperglycosylation [135].

4 Aims and Objectives

Epitope mapping of proteins encompassing multiple posttranslational modification (PTMs) such as disulphide bonds and heterogeneous N-glycosylation patterns remains challenging for HDX-MS analyses. However, a high number of diagnostic and therapeutic Nb and Ab targets are extracellular displaying both, highly N-glycosylated and disulphide-bonded antigens. The aim of this thesis was to address these challenges with the development of mass spectrometric methods to characterise conformational epitopes of extracellular proteins and protein domains.

Main objectives:

- Establishing a HDX-MS method and setup a prerequisite for epitope mapping encompassing the following requirements:
    - An HPLC-setup, capable to maintain cold temperatures during the analysis.
    - A efficient proteolysis under HDX-quenching conditions yielding high sequence coverage and redundancy to set up a bottom-up HDX-MS workflow.
    - Controlling the back exchange, intra-, and interday variance of the manually performed HDX-MS analysis.
- The established method was applied to map epitopes of nanobodies and antibodies of various antigens.
- To decide evidence based which are the lead interaction partners among multiple binding candidates, the method was adapted to be capable for increased throughput in order to screen for epitopes.
- The established method was adapted to map challenging proteins that encompass multiple PTMs. Therefore, a novel enzyme (PNGase) was characterised and it encompassed the following properties:
    - A broad N-glycan hydrolysis spectrum.
    - An acidic working range suitable for deglycosylation under HDX-MS quenching conditions.
    - A high activity to facilitate short deglycosylation times.
    - Resistance against commonly applied concentrations of denaturing and reducing agents.
    - High activities for native protein deglycosylation.

The results presented here define a versatile platform for evidence-based epitope screening via HDX-MS. Furthermore, the expanded protocol utilized by the presented deglycosylation enzyme will help the HDX-MS community to extract HDX data from highly N-glycosylated and disulphide-bonded antigens.

5 Results

5.1 Establishing Hydrogen-Deuterium Exchange Mass Spectrometry

5.1.1 HDX-LC-MS Experimental Setup

A key to the performance of HDX studies is the maintenance of low temperatures and acidic pH in order to minimize the back exchange during the analysis of deuterium labelled samples. Within the present work, an HDX-LC-MS system was designed that can be mounted and removed in a flexible way to also allow LC-MS/MS standard analyses. Based on a publication of Villar *et al.* [136], a tailor-made Semi-Automated Interface for HD exchange (SAIDE) [136] from MéCour was designed for this purpose (Figure 9). This interface, hereinafter referred to as SAIDE, is capable to maintain a constant temperature of 0 °C during chromatographic separation, which is mediated by coolant flow (-4 °C) through the side walls (Figure 10). It was mounted on a small mobile table that allows easy connection and removal to the HPLC pumps and the mass spectrometer (Figure 9).

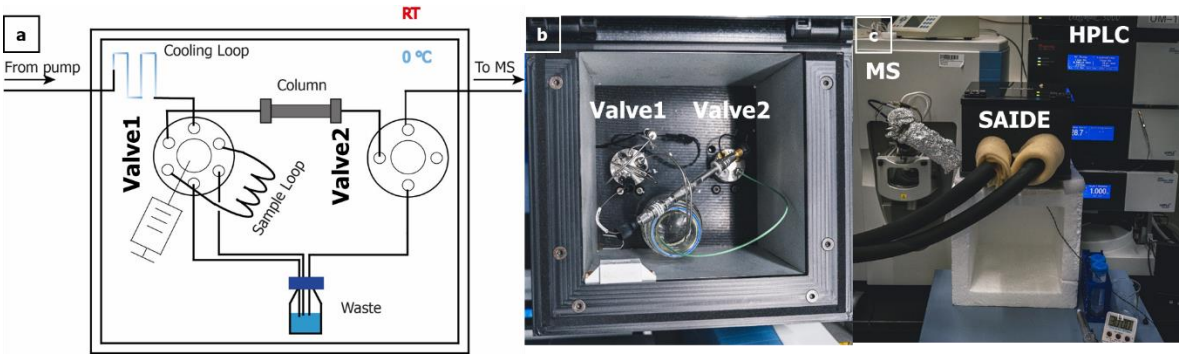

Figure 9: Scheme (a) and pictures showing the top view with open lid, (b) and the front view, (c) of the tailor made cooling-device (SAIDE) maintaining reproducible, constant low temperature for the separation of deuterium-labelled peptides. *The SAIDE houses a stainless steel cooling loop (15 cm) chilling the mobile phase prior chromatography, two two-way valves for sample desalting (6-port, valve1) and injection (4-port, valve2), a sample loop (20 µL), a chromatographic column and a waste (a, b). The samples are injected manually in a vertical manner from the outside of the device into the sample loop using valve 1 with a front-end needle port. The SAIDE interfaced the high-pressure HPLC "loading pump" with the mass spectrometer (c).*

The device houses a solvent cooling loop, two manual two-way valves, a stainless steel sample loop (20 µL) and the chromatographic column with a length of 50 mm (Figure 9). The HPLC eluents are kept, mixed and delivered by a high high-pressure pumps at room temperature (RT). Subsequently, a 15 cm long cooling capillary loop is used to chill the eluent prior to its contact with the injected sample. Due to the thermal conductivity and pressure stability, all capillaries in front of the column are made of stainless steel. The manual two-way 4-port valve

is used to direct the first minutes of the chromatographic gradient (≥2 min, depending on the salt concentration of the quench and labelling buffers) to the waste (Figure 9, valve 2). The two-way 6-port valve enables sample injection by switching the sample loop in and out of the HPLC flow. The injection is performed manually through the front-end needle port of the injection valve (6-port valve, valve 1). Furthermore, this valve is equipped with an electric contact closure that simultaneously triggers the start of the programmed LC gradient and data acquisition by the mass spectrometer allowing precise chromatography.

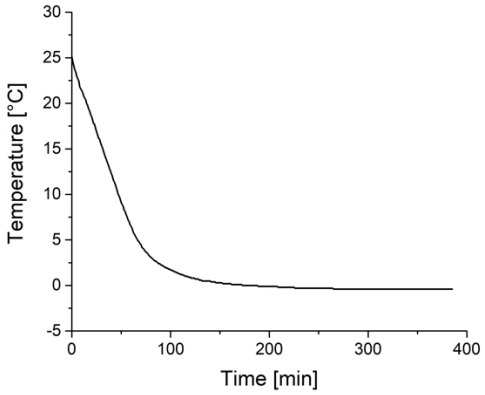

Figure 10: SAIDE temperature profile inside the cooling chamber measured at the column. *The SAIDE maintain a constant temperature of 0 °C during chromatographic separation, which is mediated by coolant flow of polypropylene glycol at -4 °C. After an equilibration time of ~150 minutes, the interior reaches 0 °C.*

To minimise temperature changes of the samples during the injection process, the glass syringes used for sample injection are conditioned within the SAIDE to approximately 0 °C until use. As a consequence of the low temperature within the SAIDE, the viscosity of the mobile phase and subsequently the pump back pressure increases. Therefore, the maximum flow rate for the used column and SAIDE was 50 µL/min resulting in an overall back-pressure of 350 - 400 bar (92% aqueous concentration). Mobile phase compositions with water content greater than 92% are to be avoided as this leads to clogging of the capillaries due to the formation of ice crystals at 0 °C. High salt concentrations of the injected samples, the high pressure (> 350 bar) on the system and the low pH of 2.5 of the eluents lead to rapid wear of the stainless steel valves and connectors. Therefore, the initially installed 6-port valve from ViciValco was replaced by a Rheodyne valve. The latter can easily be rinsed in both valve positions using a glass syringe via the needle port after each analytical run. Post separation, the valve and sample loop are flushed with 8% MeCN with 0.1% formic acid removing remaining buffer salts followed by 80% MeCN with 0.1% formic acid in order to remove potential peptide carry over. Thus, the applied flushing contributes to the extended life time of the Rheodyne valve lasting

>1500 injection (>2 years), compared to the valve from ViciValco that had to be replaced after approximately 500 injections (1.5 years).

5.1.2 Peptic Proteolysis

The first step in the applied HDX bottom-up protein analysis approach is the enzymatic proteolysis (Figure 6). Among the enzymes with an optimal pH working range of 2-3, pepsin was chosen. Highly efficient pepsin proteolysis is possible within short time at low temperature and acidic pH, however the enzyme is non-specific. Therefore, the peptides generated cannot be predicted and automatically identified as it is the case using e.g. trypsin in standard proteomic bottom-up analysis. The obtained peptide length is variable and depends on structure accessibility of cleavage sites and therefore on efficient opening of intramolecular bonds and on the availability of preferred cleavage residues. On the other hand, the assignment of the deuterium exchange to individual amino acids highly depends on the length and overlap of neighbouring peptides. Higher amino acid residue overlap yields redundant HDX information. Thus, the optimization of the peptic digest aimed to the generation of overlapping and short peptides that span as much of the protein sequence as possible.

To achieve this goal, generic but also protein-specific proteolysis parameters were investigated. Generic proteolysis parameters are optimal pH, temperature, duration and enzyme-to-substrate ratio (E:S). They were investigated using Annexin-A1, which at the same time also contained the first epitope to be elucidated. However, protein-specific proteolysis parameters are also related to the individual protein structure defined by intramolecular bonds and interactions and need to be adapted for each individual protein. Proteolysis was performed at pH 2.5 as it results in the lowest back exchange.

5.1.2.1 Proteolysis Temperature and Time

The influence of the proteolysis time and temperature on the number of identified peptides and their length was assessed by performing the proteolysis of ANXA1 for 5 and 10 min at 0 °C and 2 min at 20 °C using a typically E:S of 1:1 (M:M) (Figure 11) [67]. After five minutes of proteolysis, 152 peptides could be identified with an average length of 20.3 amino acids (aa). By doubling the digestion time, the number of peptides increased by 13% and the peptide length shortened to an average length of 18.7 aa (Figure 11b). The number of peptides could not be increased further upon short digestion at 20 °C (Figure 11a). However, proteolysis at higher temperature (20 °C) was beneficial to the distribution of the peptide length leading to a reduction of the average length of 15.4 aa (Figure 11b).

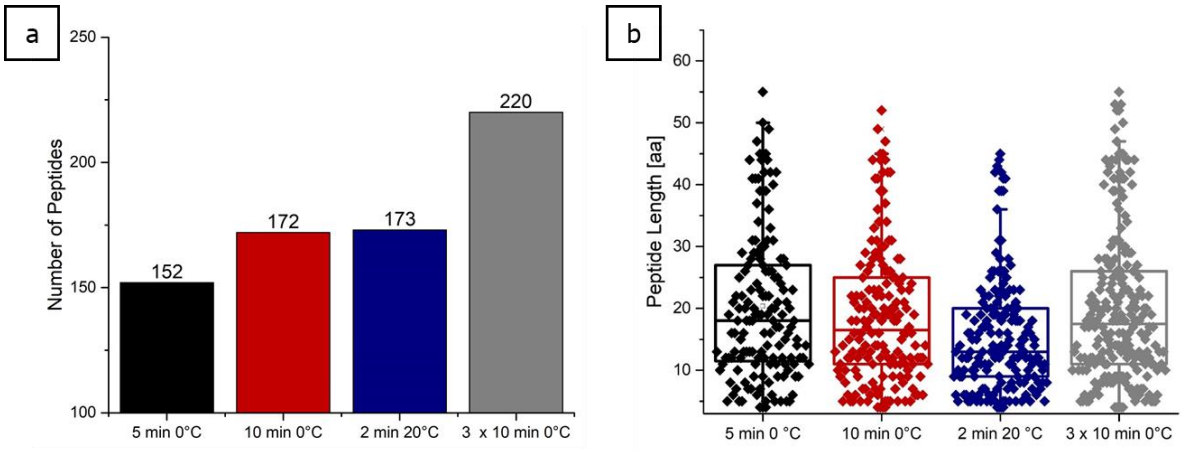

Figure 11: Examination of optimal generic proteolysis conditions. *(a) The number of peptides identified by mass accuracy in MS1 and by MSMS fragmentation pattern after different proteolysis periods and temperatures. Single experiments for 5 min/0 °C, 10 min/0 °C and 2 min/20 °C and a combination of three independent proteolysis experiments 10 min/0 °C. (b) The distribution of the peptide length for different digestion conditions using a box plot. (E:S = 1:1 M:M)*

With respect to the number of peptides and average peptide length, proteolysis conditions of 10 min at 0 °C were chosen for subsequent HDX analysis. These prevent an increase of the back exchange caused by the increased temperatures. The observed back exchange of the different proteolysis conditions can be found in 5.1.4.

The number of identified peptides was further increased by 28% (+48 peptides) using a combination of three independent sample preparations and MSMS analysis prepared using the same protocol (10 min; 0 °C). While most of the peptides (152) were commonly identified in each experiments additionally 68 peptides were identified (Figure 12a). This can be explained by the limited, incomplete proteolysis in combination with the promiscuous cleavage spectrum of pepsin and the semi random sampling in a TopN data dependent MSMS analysis. Consequently, a combined peptide identification list from at least three technical replicates was included in the generic workflow.

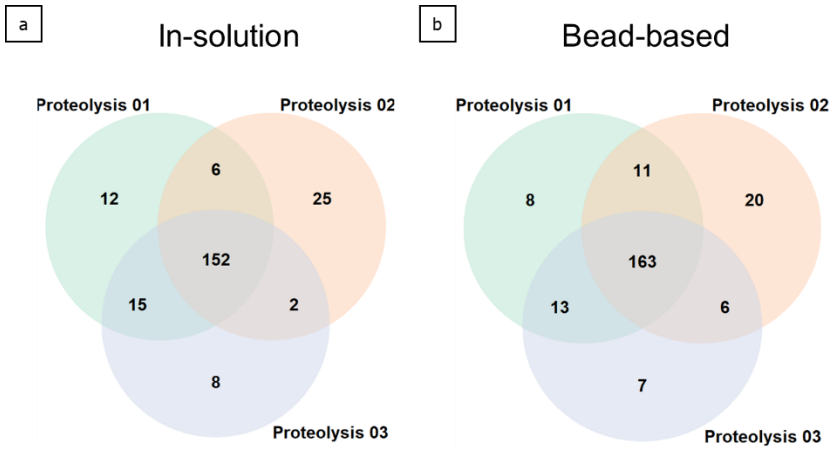

Figure 12: Venn diagram of identified peptides by tandem mass spectrometry of three independent peptic proteolysis experiments of the in-solution (a) or the bead-based (b) protocol.

5.1.2.2 Comparison of Two Proteolysis Protocols (E:S – ratio)

To further improve the enzymatic digestion, proteolysis was evaluated using a higher E:S ratio. Therefore, pepsin immobilised on beads (hereinafter referred to as bead-based proteolysis) was compared to the above described pepsin in-solution (hereinafter referred to as in-solution proteolysis). Using the immobilized-pepsin protocol, a high E:S ratio can be achieved resulting in an excess of pepsin while pepsin can be removed after the proteolysis. The peptide lists of both approaches were generated in independent triplicates. Again, the combination of three replicates leads to an increase of the number of identified peptides by 17%. The bead-based proteolysis showed a slightly higher reproducibility leading to 163 peptides identified in all replicates, 30 peptide identified in 2 of 3 experiments and 35 peptides identified in only one experiment (Figure 12b). Both strategies resulted in identification of a comparable number of 220 and 228 identified peptides for the in-solution and the bead-based digest, respectively (Figure 12, Figure 13). However, with use of immobilised pepsin the proteolysis time could be reduced from 10 to 1 minutes. Furthermore, the bead-based digestion protocol resulted in a sharp decrease of the peptide length distribution leading to an average peptide length of 15 aa compared to the 21 aa of the in-solution digest (Figure 13b). Consequently, more peptides elute earlier in the chromatographic gradient, reducing the risk of higher back exchange (Figure 13c).

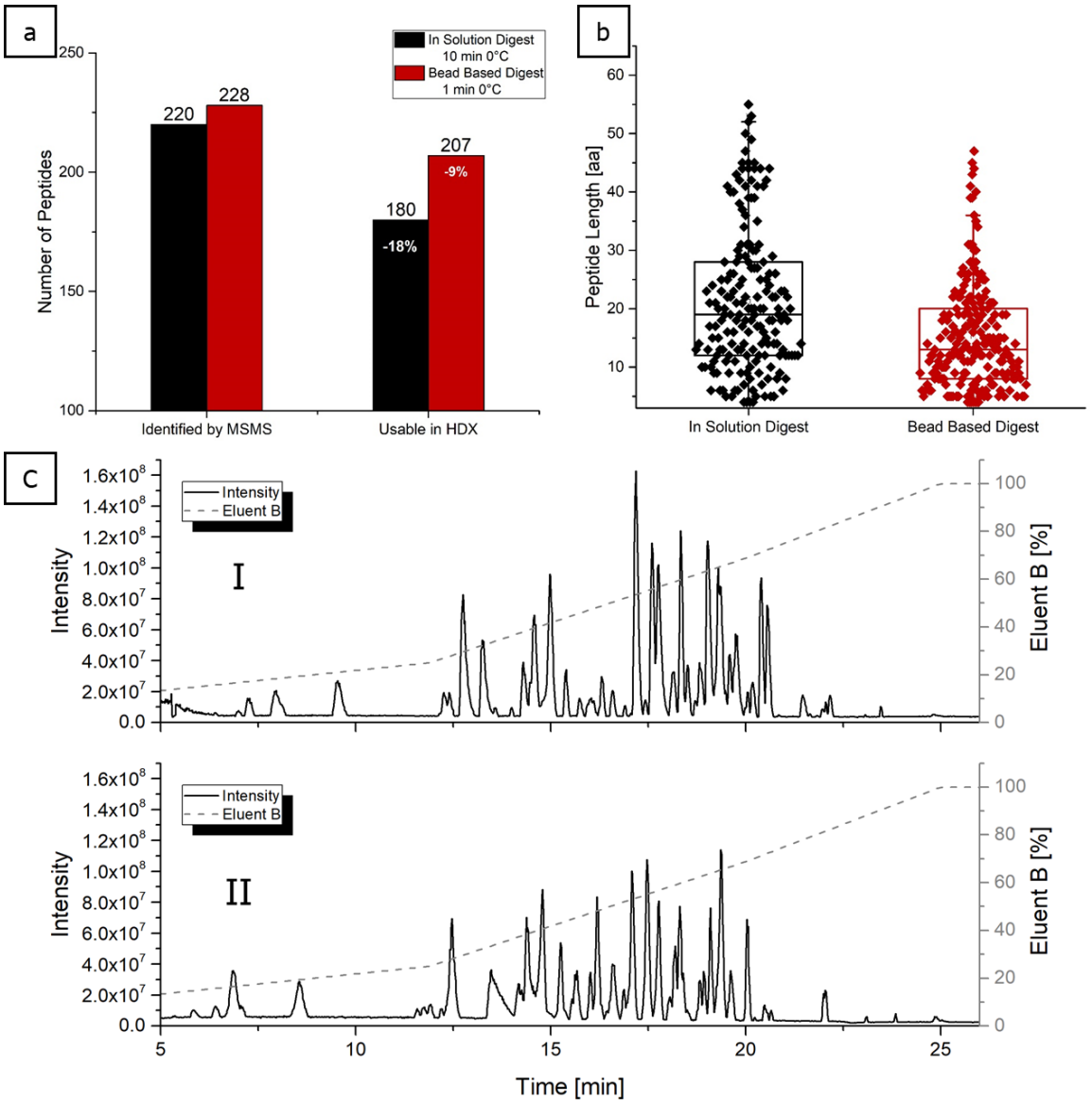

Figure 13: Comparison of the bead-based with an in-solution proteolysis on ANXA1. *ANXA1 was digested at 0 °C using pepsin immobilized on beads and pepsin in-solution for 1 and 10 min, respectively. (a) The pooled number of identified peptides from three independent digestions and analysis experiments. MSMS-identified and peptides with good isotopic assignment that can be used to extract HDX information. (b) The peptide length distribution for the in-solution (180 peptides) and the bead-based (207 peptides) proteolysis as box plots. (c) Base peak subtracted chromatogram (300-2000 m/z) of the in-solution (I) and bead-based (II) digestion protocol.*

5.1.2.3 Evaluation of Two Proteolysis Protocols in HDX-MS Analysis

Besides the number of identified peptides the performance of both proteolysis strategies in an HDX-MS analysis has to be evaluated. Since the calculation of the centroid mass shift upon deuteration requires a good assignment of the isotopic peptide patterns, HDX analysis depends on the data quality of the identified peptides. Low signal to noise ratios (S/N) and co-eluting peptides can lead to poor isotopic assignment resulting in uncertainty in the calculated centroid mass shift and thus the deuterium uptake. Therefore, these peptides are excluded

manually and automatically by the analysis software (HDExaminer) during the analysis process. To evaluate the number of excluded peptides, both proteolysis strategies were compared in an HDX analysis of ANXA1. Thus, HDX of ANXA1 that was labelled for 5 and 500 min was analysed in independent triplicates. Only a subset of the initially identified peptides could be used to extract valuable HDX data. Thus, 9% of the peptides of the based digest and 18% of the in-solution digest could not be used to extract HDX data (Figure 13a). Most peptides elute within a time window of 12 to 20 minutes in both experiments However, the bead-based proteolysis resulted in smaller ANXA1 peptides, eluting in peaks with high intensity across the whole chromatographic gradient. This led to less co-elution and a higher signal to noise ratio (Figure 13c).

Next, peptide HDX reproducibility of both proteolysis strategies was compared. For direct comparison, only peptic peptides with identical sequences were used. This peptide list comprised 106 peptides. The plotted standard deviations (SD) of the average peptide HDX of independent technical replicates (n=3) revealed a higher HDX reproducibility of the bead-based digest (range: <0.001 – 0.429 Da) compared to the in-solution proteolysis strategy (range: 0.001 – 0.804 Da (Figure 14).

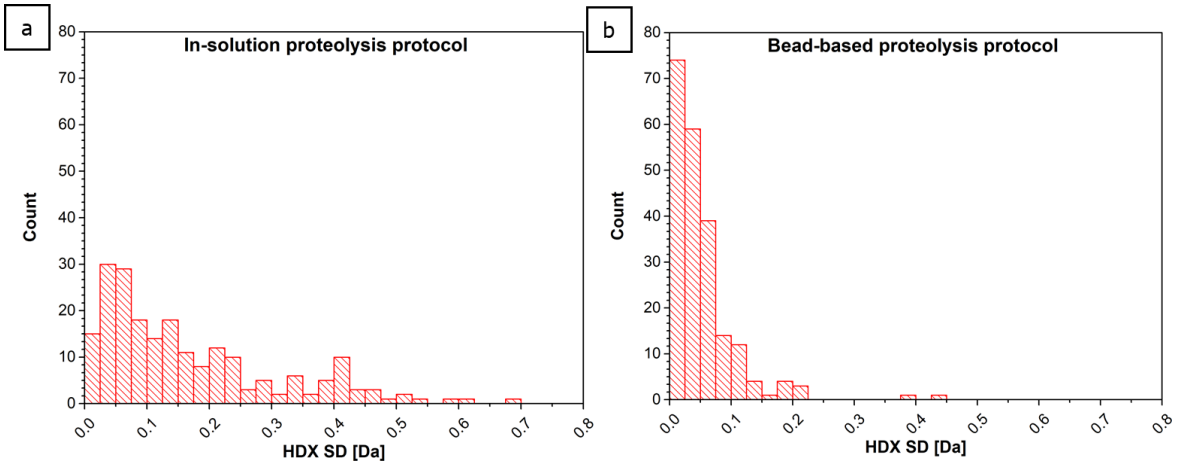

Figure 14: HDX reproducibility using the in-solution (a) and the bead-based (b) proteolysis protocol. *The histograms comprise HDX standard deviation of 106 peptic peptides after two labelling time points. Only peptides identical in their sequence were used for the analysis of both proteolysis protocols.*

This might be due to the shorter preparation time using immobilized pepsin, which is completed after one minute limiting possible variations of the back exchange in the resulting peptides. Furthermore, peptides undergo HDX even under HDX-quenching conditions, which occurs independent on their native structure in the protein (non-native on exchange). Both kinetics can vary for peptide subpopulations und thus might result in higher HDX standard deviations for the prolonged proteolysis. A summary of the parameters used to compare the two proteolytic strategies can be found in Table 1.

Table 1: Comparison of the proteolysis results and HDX conditions using pepsin in-solution and immobilised on beads.

Characteristic parameters	In-solution digest	Bead-based digest
Identified ANXA1 peptides	220	228
Proteolysis conditions	10 min; 0 °C; E:S 1:1 (M:M)	1 min; 0 °C; enzyme excess
Deuteration time points	5 & 500 min	5 & 500 min
Distribution of HDX SD	<0.001-0.804 Da	<0.001-0.429 Da
Peptides usable for HDX	180 (81.8%)	207 (90.8%)
Average peptide length [aa]	21.3	15.2
Sequence coverage	100%	100%

As a consequence, the bead-based proteolysis approach was chosen as standard method for HDX analyses and applied for subsequent epitope mapping studies on RBD (see 5.3.2) and SIRPα (see 5.3.3).

5.1.3 Determination of Peptide Carry Over

As a next step, potential peptide carryover between HDX HPLC separations was examined. Within HDX experiments, carryover can lead to false bimodal (EX1) HDX kinetics resulting in misinterpretation of the HDX data [137]. To eliminate the carryover, a rinse (wash) run was inserted between each sample run. Since carryover depends not only on the sample amount loaded on column and the sensitivity of detection but also on the physicochemical properties of the analyte and the completeness of protein hydrolysis, it is both method and analyte specific. Therefore, potential carryover was examined for each analysed protein. The efficiency of the washing gradient was assessed by injection of a blank sample consisting of eluent A. No peptides were identified by MS1 and MSMS. EICs were examined to be less than 10% of the previous run in each of the case studies described in 5.3.1, 5.3.2 and 5.3.3.

5.1.4 Determination of the Deuterium-Hydrogen Back Exchange

After quenching of the HDX reaction, proteins and subsequently peptides are exposed to elevated concentration of hydrogen-containing oxonium ions that cause an acid catalysed deuterium-hydrogen back exchange (Figure 5). This back exchange needs to be kept to a minimum for performing high-resolution HDX-MS experiments. The enzymatic digestion step of the HDX workflow was assessed for its impact on back exchange.

5.1.4.1 Generation of a Peptide Standard for Determination of the Back Exchange

To assess the back exchange a fully deuterated, artificially generated peptide mixture was used. It allows a determination of the back exchange, regardless of complete protein deuteration, denaturation and protein proteolysis. A mixture consisting of 14 synthetic peptides with different length and amino acid composition was chosen (Table 2), taking into account that the back exchange varies between different amino acid residues and increases with chromatographic retention time. In order to achieve a complete deuteration, the peptide mixture was lyophilized and deuterated by reconstitution in 99.9% deuterated water and incubation overnight at 20 °C.

Table 2: List of the synthetic peptides for back exchange determination [110]. *carbamidomethylated cysteine.

#No	Sequence	Length	Retention time [min]
1	LTIEELK	7	16.3
2	FNNYQVR	7	7.9
3	MSDSVILR	8	14.5
4	SEC*HVDFFR	9	17.3
5	TVAAFGGEK	9	5.1
6	IVVLC*GQEAVK	11	14.8
7	LQDEIDAALPNK	12	15.8
8	GTTLITNLSSVLK	13	20.4
9	AAATEDATPAALEK	14	11.4
10	ISIIPQDPILFPGSLR	16	21
11	EQLDSLVC*LESAILEVLR	18	23.4
12	LSDRPQLPYLEAFILETFR	19	22.7
13	AMDSFPGPPTHWLFGHALEIQK	22	20.6
14	VYGPVFTLYFGSKPTVVVHGYEAVK	25	20.7

5.1.4.2 Calculation of the Back Exchange

Each difference between the experimentally found and the theoretic maximum deuterium content of the peptide can be directly attributed to the back exchange of the LC-MS analysis. The back exchange was calculated using the following equation:

$$Back\ exchange\ [\%] = \left(1 - \frac{m_{100\%} - m_{0\%}}{N * D_{frac}}\right) * 100 \qquad \text{Equation 13 [74]}$$

where $m_{0\%}$ is the non-deuterated peptide centroid mass, N is the theoretical number of exchangeable backbone amides, D_{frac} is the fraction of D/H present in the labelling buffer (e.g. 0.8, 0.9 or 1) and $m_{100\%}$ is the experimentally achieved, fully labelled centroid mass. N represents the amino acid residue count of each peptide except proline and the first two N-terminal residues. Fully deuterated peptide samples were quenched by acidification to pH 2.5, aliquoted and then snap frozen in liquid nitrogen until analysis.

5.1.4.3 Determination of the Back Exchange during LC-MS Analysis and for a Simulated Protein Proteolysis

Immediate injection of the fully deuterated peptides defines the chromatography-dependent back exchange. The average deuterium back exchange at pH 2.5 was 21% (Figure 15a, 0 min). Next, a proteolysis step was simulated for different time periods at 0 °C and the average examined back exchange from technical triplicates was assessed (Figure 15a). An average back exchange of the peptides mixtures after immediate injection (0 min) was 21% (1 – 42%) and a maximum of 33% (17 - 50%) after 20 min digest was examined (Figure 15a). An approximate increase of 0.6% back exchange per minute of incubation at 0 °C and pH 2.5 was observed. Additionally, a simulated proteolysis under non-HDX conditions at 20 °C was performed for 2 or 10 min and analysed in single measurements (Figure 15a). Sample incubation for 2 min at 20 °C showed a similar back exchange as incubation for 20 min at 0 °C. Notably, the back exchange appears to be reaching an equilibrium maximum value after 10 minutes at 20 °C as the range of the back exchange distribution is at a minimum here (40-54 %) (Figure 15a).

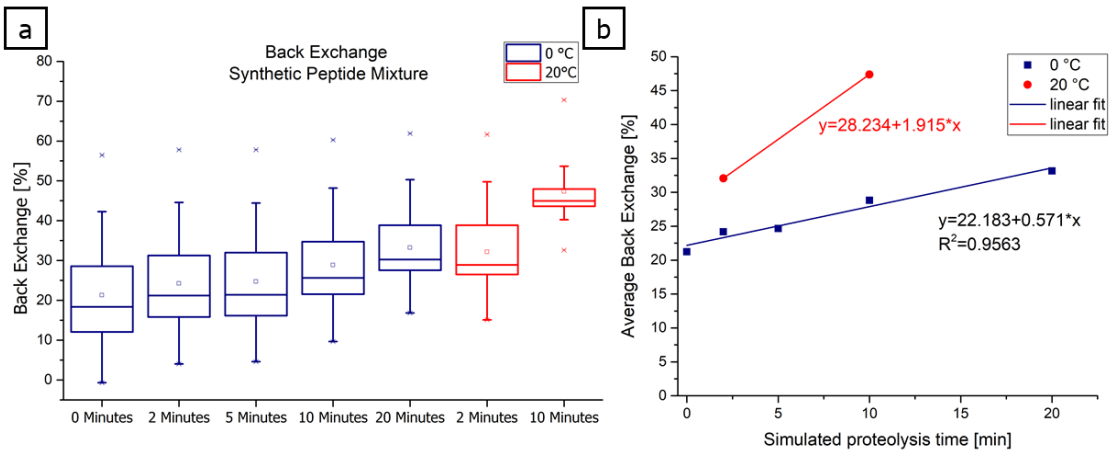

Figure 15: Back exchange assessment using a fully deuterated synthetic peptide mixture. *The box plots consisted of the average back exchange data determined from 14 peptides in technical triplicates. Values exceeding 1.5 times the interquartile range are outliers shown as asterisks. The average back exchange of the peptides is depicted as squares within the boxes. (a) Back exchange within a mixture of 14 peptides differing in length and amino acid composition after full labelling (99.9% D_2O; overnight; 20 °C) and 1:1 quenching (v/v) to pH 2.5 with aqueous*

buffer. Digestion was simulated for different time periods at 0 °C and 20 °C. The digestion conditions at 20 °C were performed in single measurements. (b) Average back exchange plotted for 0 °C and 20 °C in dependence of the incubation time.

Plotting of the average back exchange versus the incubation time, revealed approximately four-fold higher reaction speed (slope) (Figure 15b).

5.1.4.4 Comparison of Back Exchange for In-Solution and Bead-Based Protein Digestion

Furthermore, the back exchange for the two previously described proteolysis approaches, the bead-based (1 min) and in-solution digest (10 min) (see 5.1.2) was compared using fully deuterated ANXA1. Deuteration of ANXA1 was induced for 24 h under denaturing conditions using 6 M urea-d4 at 20 °C. Deuterium labelling was performed in 90% D_2O, which also represents the proportion of measurable, slow-exchanging backbone amide protons and therefore the theoretic maximum peptide deuteration (Equation 12, D_{frac}= 0.9). ANXA1-derived peptides were analysed by LC-MS using the above described method.

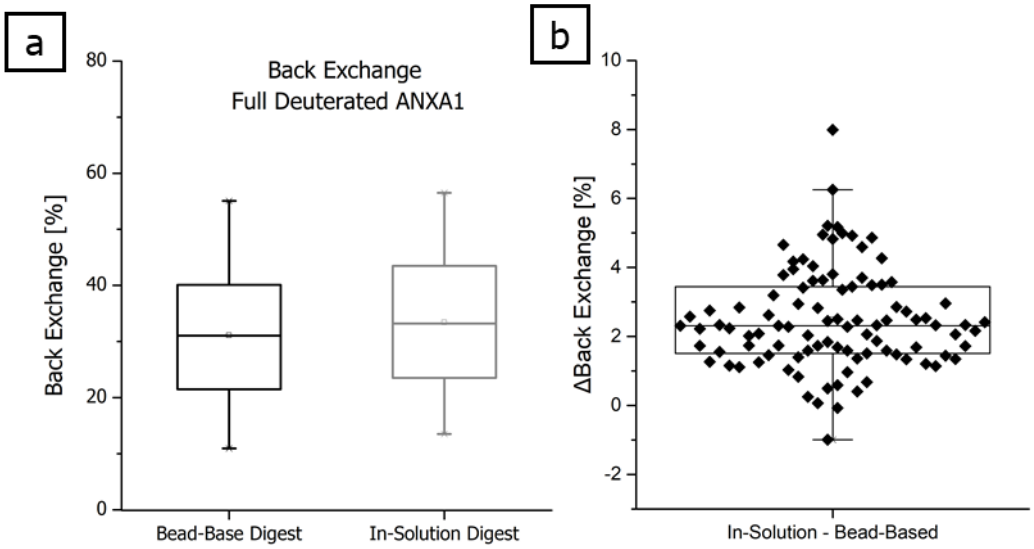

Figure 16: Comparison of the back exchange of two proteolysis approaches using the fully deuterated ANXA1. *(a) Back exchange was examined for 98 peptides of fully deuterated ANXA1 comparing a bead-based (1 min) and an in-solution peptic proteolysis (10 min). Only peptides with identical sequence were included. The box plots consist of the average back exchange determined from triplicate experiments. Values exceeding 1.5 times the interquartile range were defined as outliers and are shown as asterisks. The average back exchange was depicted as squares within the boxes. (b) Differential back exchange of the in-solution and bead-based proteolysis protocol. Observed back exchange values of the peptides of the in-solution digest was subtracted by those of the bead-based digest.*

Again, for direct comparison only peptides identical in sequence were included in this analysis. Plots shown in Figure 16a include the average hydrogen-deuterium exchange data of 98

peptide pairs of ANXA1 measured in independent triplicates. The in-solution digest led to 33% average back exchange ranging from 14% to 56%. The bead-based digest protocol led 31% average back exchange ranging from 11-55%. Peptide-specific differences between both protocols, are shown in Figure 16b. Most peptides show a ~2% higher back exchange using the in-solution proteolysis with some peptides that are more affected by the prolonged proteolysis, ranging from ~3-6% higher back exchange (Figure 16b). While the bead-based proteolysis strategy showed a small reduction in the average back exchange of ANXA1 peptides, it had a large effect for some peptides.

5.1.5 Intra- and Interday Variability of HDX Experiments

The SAIDE interface ensures high flexibility in the use of the mass spectrometer for different LC-MS approaches. However, manual sample handling, the disconnection from the HPLC-MS and the release of the temperature control pose a potential risks to high intra- and interday variability of HDX analyses, which was investigated next.

For these experiments HDX of SIRPα was analysed after deuteration for 5 min and 30 min and the proteolysis was preformed using immobilized pepsin. A HDX-MS analysis campaign is normally performed in more than one day especially if multiple binding partners have to be tested. To minimize potential variability, all samples can be labelled on one day and stored at minus 80 °C upon proteolysis and measurement. Thus, the intraday variability here corresponds to the variability of HDX between different samples of one analysis campaign. It was assessed using independent technical replicates (n=3) that were labelled on the same day and measured consecutively within the same week. In order to assess differences in the manual labelling and due to the disconnection of the SAIDE, the analysis campaign was repeated nine weeks later. The variability between these two experimental campaigns here corresponds to the interday variability.

5.1.5.1 Intraday Variability

Within the first experimental campaign 90 SIRPα peptides were identified and included in the HDX data analysis. Two peptides were only detected within the first campaign and removed from the whole analysis. The remaining 88 peptides eluted within a retention time window of ±1 min showing a reproducible chromatography, manual injection and valve switch. The intraday variability was assessed using HDX standard deviations (SD) of independent technical replicates (n=3) of both experimental campaigns (Figure 17). Overall, the comparison led to 176 standard deviations for each campaign ranging from 0.006 to 0.408 Da (campaign 01) and 0.003 to 0.249 Da (campaign 02). Each campaign showed a small intraday variability with most of the SDs below 0.1 Da.

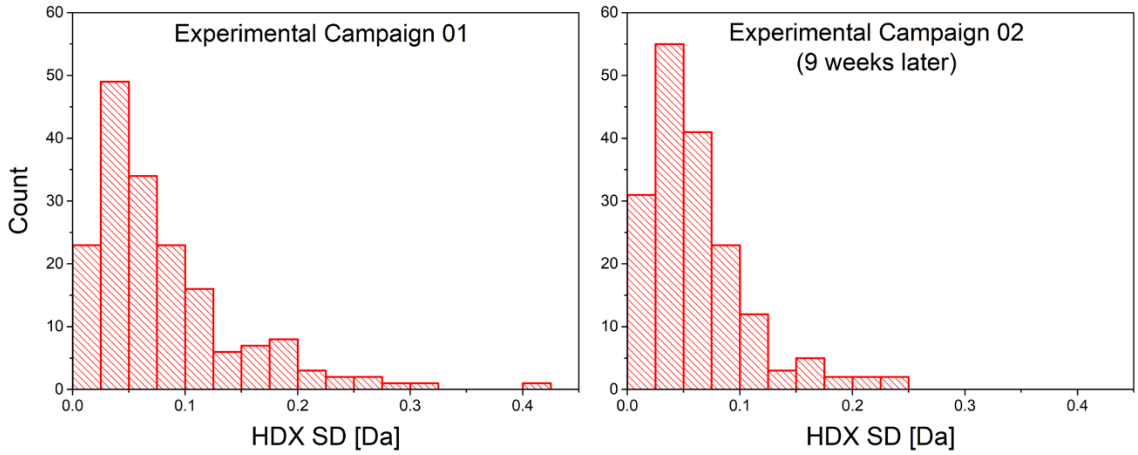

Figure 17: Distribution of the HDX standard deviation of two experiments performed nine weeks apart. *Standard deviation of the deuterium uptake of 88 SIPRα peptic peptides (176 SDs) of each experimental campaign are plotted. (n = 3; SIPRα deuteration = 5 and 30 min)*

5.1.5.2 Interday Variability

Next, the HDX interday variability was assessed. To detect meaningful differences in the differential HX-MS data, a global minimum detectable difference ($\Delta\overline{HX}$ threshold) was calculated using the equations as described [138]. This threshold is calculated on the basis of the HDX standard deviations of the technical replicates of two states (here, campaign 01 and 02) and displays the global minimal detectable HDX mass difference of two states on basis of a chosen confidence level. The calculations of the $\Delta\overline{HX}$ threshold are also implemented in the HDExaminer software according to the following equations.

First, a pooled standard deviation (s_p) for all N experimental HDX standard deviation (s_j) standard and the corresponding sample size (n_j) is calculated:

$$s_p = \sqrt{\frac{\sum_{j=1}^{N} s_j^2\,(n_j - 1))}{\sum_{j=1}^{N}(n_j - 1)}} \qquad \text{Equation 14 [138]}$$

With s_p a standard error of the mean (SEM) was calculated with the sample size (n), equal to the number of replicates:

$$SEM_{\Delta\overline{HX}} = \sqrt{\frac{{s^2}_p}{n_a} + \frac{{s^2}_p}{n_b}} \qquad \text{Equation 15 [138]}$$

On basis of the SEM and the Student's t-distribution, the degrees of freedom (df) and a significance level (α) the confidence interval (CI) was calculated. This CI displays the global $\Delta\overline{HX}$ threshold.

$$df = n_a + n_b - 2 \qquad \text{Equation 16 [138]}$$

$$\pm CI_{\Delta\overline{HX}} = t_{\frac{\alpha}{2},df} * SEM_{\Delta\overline{HX}} \qquad \text{Equation 17 [138]}$$

Any difference greater than this CI ($\Delta\overline{HX}$ threshold) indicates a significant HDX difference between the two states.

The comparison of both experiments resulted in a minimal detectable difference ($\Delta\overline{HX}$ threshold) of 0.21 Da ($p \leq 0.05$). Additionally, the statistical significance of each peptide HDX difference ($\Delta\overline{HX}$, m_b-m_a) was examined pairwise using the Student's t-test ($p \leq 0.05$). With the $\Delta\overline{HX}$ threshold and the p-values, a hybrid approach was used for significance testing. Based on these criteria none of the peptides showed a significant difference between both experimental campaigns and most of the HDX values differed only in ≤0.1 Da (Figure 18a). However, in the second analysis campaign, a slight correlation of higher deuteration was observed for the absolute (Figure 18a) and the relative HDX differences (Figure 18b). Notably, all peptides summed HDX difference are below 5%, chosen as significance criteria for the following case studies using two time points (Figure 18b). A drift of HDX can be easily detected within an experimental campaign. However, to increase the reproducibility for the following case studies, a separate negative control (intrinsic HDX of the protein alone) was prepared for each analysis campaign. In summary, these experiments showed a high reproducibility and low interday variance of the manual HDX-MS workflow. As per consensus guidelines [74], HDX uptake plots of all peptides (Figure A8) and a HDX data table (Table A1) can be found in the appendix.

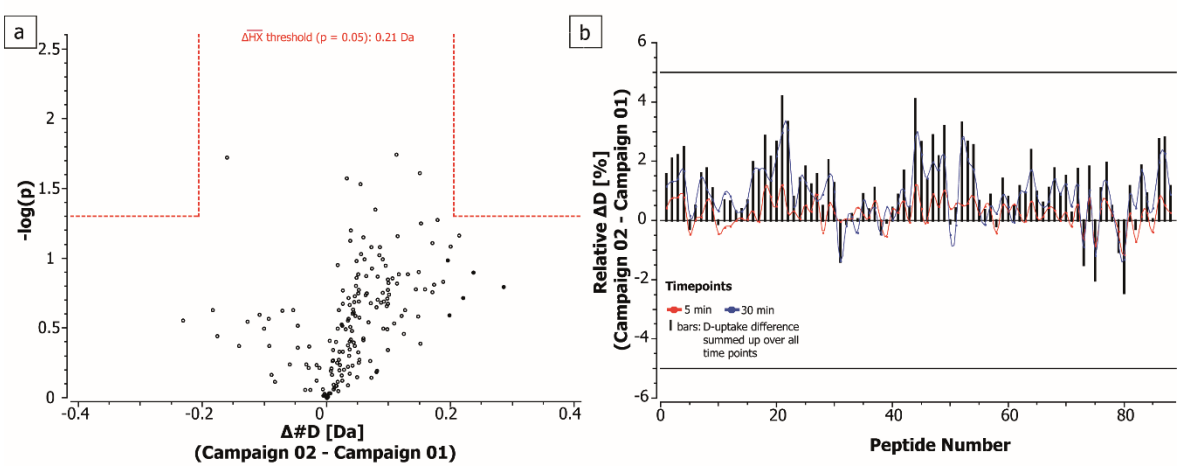

Figure 18: Interday variability using manual sample preparation and the SAIDE. *The interday variability of HDX measurements was assessed using a SIRPα proteolysis, which was analysed in triplicate in two separate analysis campaigns, nine weeks apart from each other with interimed disconnection of the SAIDE cooling chamber. (deuteration= 5 and 30 minutes). (a) The HDX difference for 88 peptides was plotted against p-value as determined by the Student's t-test. Dashed lines: significance level (p=0.05) and the minimal detectable difference ($\Delta\overline{HX}$ threshold). (b) Relative deuteration difference of both experimental campaigns. Peptides are numbered from N- to C-terminus and additionally sorted from shorter to longer peptides. The deuterium uptake is normalised to the exchangeable aa (backbone amide count without proline and the first two N-terminal aa).*

5.2 Enzymatic Deglycosylation with a Novel Acidic PNGase Rc

5.2.1 Expression and Purification

A manuscript including results and figures of the following chapter is published in Analytical Chemistry [139]. Figures of this chapter are reprinted (adapted) with permission from [139]. Copyright 2022 American Chemical Society.

Recently, 13 acidobacterial PNGase A homologues were published, which are referred to as PNGase H^+ variants because of their acidic pH optimum [102]. First, the feasibility of the recombinant expression was investigated for one of these acidic PNGases originating from *Dyella japonica* (PNGase Dj). However, the high level of insoluble enzyme obtained from heterologous expression in *E. coli* prevented the production of a large enough amount of enzyme to justify further characterization and use in HDX (Figure A1). Later, the expression attempt was successfully repeated with another new enzyme variant, which originates from the soil bacterium *Rudaea cellulosilytica* [140] (PNGase Rc). The sequence of this enzyme was kindly provided by Prof. Dr. Josef Voglmeir (GGBRC, Nanjing Agricultural University, China).

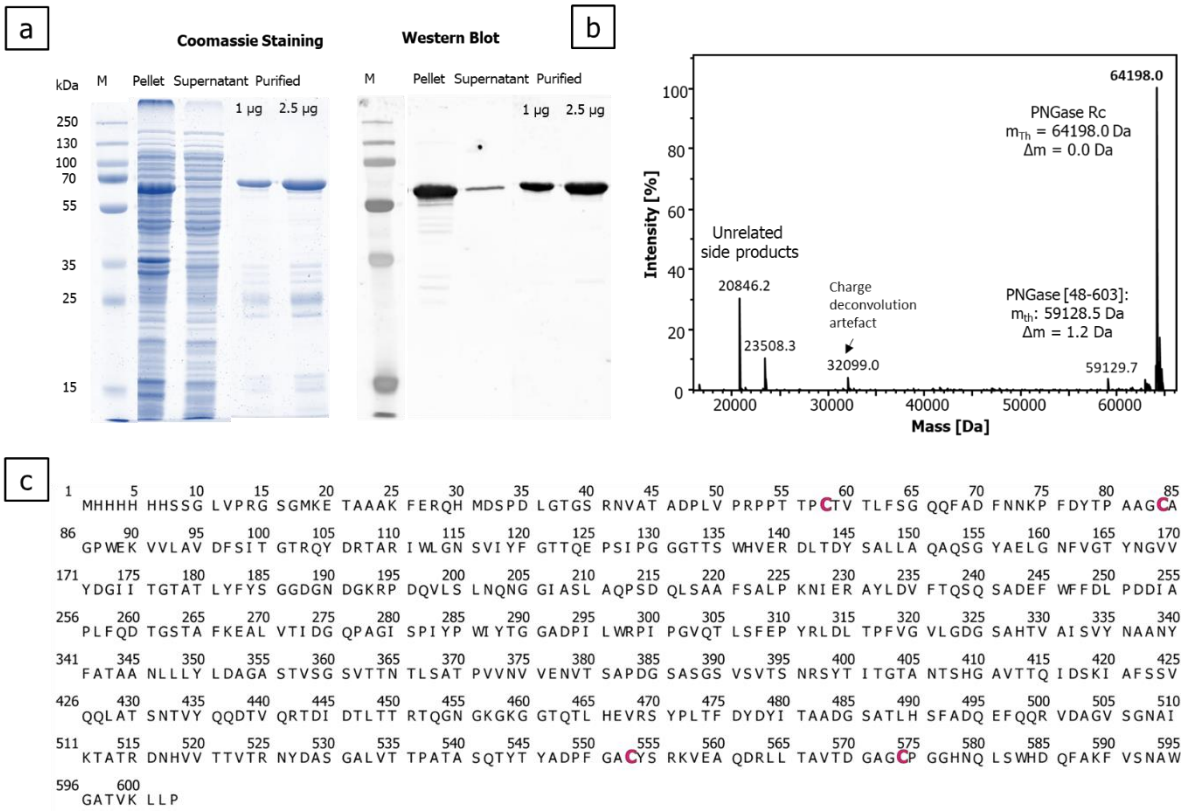

Figure 19: Purification and identity confirmation of the acidic PNGase from Rudaea cellulosilytica (Rc) according to [139]. *(a) SDS-PAGE (left) and western blot analysis (right) of different purification stages of PNGase Rc kindly provided by P. D. Kaiser. For western blot analysis, an anti-His tag antibody was used as primary antibody. Purification using IMAC and SEC led to ~75% purity. (b) Identity and integrity confirmation via intact mass analysis (Mass spectrometer: Bruker MaXis HD Q-TOF). (c) Amino acid sequence of PNGase Rc construct with highlighted cysteine residues.*

Based on the knowledge gained from the experiments on PNGase Dj, the expression and purification of PNGase Rc could be optimised and performed by Dr. Philipp D. Kaiser (Recombinant Antibody Technology Group, NMI, Germany). For the heterologous expression, the ORF encoding for the PNGase Rc was transferred in a bacterial expression vector (pET30a(+)) and a His_6-tag was added. The recombinant enzyme was expressed in *Escherichia coli* strain BL21 (DE3), isolated and purified using immobilized metal ion affinity chromatography (IMAC) followed by size exclusion chromatography (SEC) (Figure 19a). It turned out that a critical parameter for the expression of the PNGase Rc in *E.coli* is the induction of the expression vector at low bacterial density (OD_{600} = 0.8) in combination with subsequent cultivation at room temperature (Figure A1). Despite that >90% of the PNGase Rc, as determined by western blot analysis, were found within the insoluble bacterial pellet fraction, overnight expression in one litre bacterial culture yielded ~1.3 mg of enzyme with a purity of ~75% (Figure 19a). The identity of the PNGase Rc in each fraction of the purification process was confirmed by western blot analysis using an anti-His tag antibody (Figure 19a). Furthermore, the integrity of the PNGase Rc construct was confirmed by HPLC-MS (Figure 19b,

c). The theoretical mass of 64,198.0 Da (closed disulphide links) was confirmed using the deconvolution of the mass-to-charge signal series. A minor side peak at 59,129.7 Da was observed corresponding to a truncated enzyme variant lacking the first 47 N-terminal amino acids ($m_{theoretical}$ = 59,128.5 Da). Since it conferred to a common autohydrolysis amino acid motif "DP" it might be artificially introduced by electrospray ionization or originated from the sample itself. The peaks at 20,948.2 and 23,508.3 Da, also detected by SDS-PAGE at similar molecular weights, could not be assigned to the amino acid sequence of the PNGase. Thus, they might be derived from contaminant proteins (Figure 19a,b). Characteristic parameters of the expression, analysis and enzyme are summarized in Table 3.

Table 3: Summary of PNGase Rc expression parameters and physico-chemical characteristics.

PNGase Parameter	Value
Expression host	*E.coli* BL21 (DE3)
Optical bacterial density	OD_{600}=0.8
Induction of the expression	0.1 mM IPTG
Expression conditions	Room temperature, overnight
Exression yield	~1.3 mg from 1 L cell culture after affinity purification and SEC
Purity by SDS-PAGE	~75%
Amino acid residues	603
Molecular weight (all cysteines oxidised)	64189.0 Da
pI*	5.05

*calculated by ProtParam (ExPASy; [141])

5.2.2 Characterisation of PNGase Rc

5.2.2.1 Enzyme Activity

To assess the activity of the enzyme, a mass spectrometry-based assay was developed monitoring the time-dependent N-glycan hydrolysis from the humanized IgG1 anti-HER2 antibody trastuzumab. The Fc region of IgG1 antibodies harbours two N-glycosylation sites at N301 with certain microheterogeneity and no macroheterogeneity. The three major glycoforms of trastuzumab comprise complex biantennary N-glycans differing in their degree of galactosylation [142]. The assay was performed using a molar enzyme-to-substrate ratio (E:S) of 1:44 at pH 2.5 and 37 °C. No denaturation was applied prior the deglycosylation knowing to impede N-deglycsoylation by the PNGases. Deglycosylation led to different

antibody states, with the non-deglycosylated, half deglycosylated and the fully deglycosylated molecules that were relatively quantified (Figure 20).

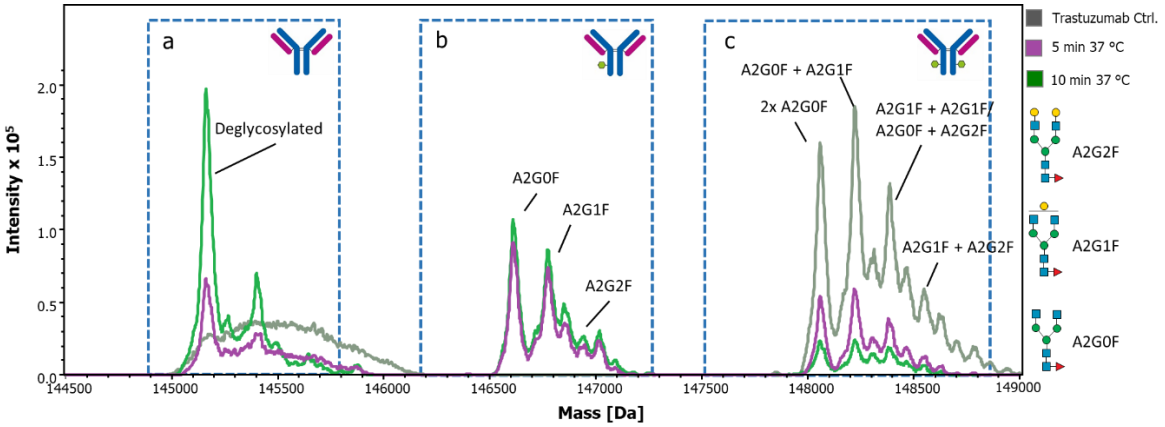

Figure 20: N-Glycosylation states of intact trastuzumab antibody upon deglycosylation using PNGase Rc before (grey) and after incubation for 5 (purple) and 10 minutes (green) as published in [139]. *Deglycosylation led to the three glycosylation states: the completely deglycosylated antibody (a), the half deglycosylated antibody (b) and the fully glycosylated antibody (c). The most abundant N-glycoforms are labelled. N-glycan abbreviations are correlated to glycan symbols according to the Symbol Nomenclature for Glycans (SNFG) [143] at the right hand side of the figure. Deglycosylation was performed at 37 °C and pH 2.5 with PNGase Rc with an E:S of 1:44 (M:M).*

The proportion of the completely deglycosylated IgG1 molecule was used for determination of the enzyme kinetics. Using the above described conditions, 41% and 100% fully deglycosylated intact antibody were obtained after 10 and 40 min incubation, respectively (Figure 21). A velocity ($v = \Delta s/\Delta t$) of the N-glycan release of 5.2%/min was obtained for the PNGase Rc. Next, the determined activity was compared to the widely used, commercially available PNGase F using the same assay but changing the pH to 7.5. Compared to the PNGase Rc, PNGase F showed a ~10 times lower reaction velocity (0.4%/min) (Figure 21). Additionally, the analysis of the enzyme storage stability was assessed after one freeze-thaw cycle and after storage for 42 days at 4 °C. No significant loss in activity was found for none of these conditions (Figure 21).

In summary these findings showed that the novel PNGase exhibits high activity and is also able to hydrolyse complex biantennary type N-glycans bearing a α-1,6-fucosylation on the Asn-linked GlcNAc.

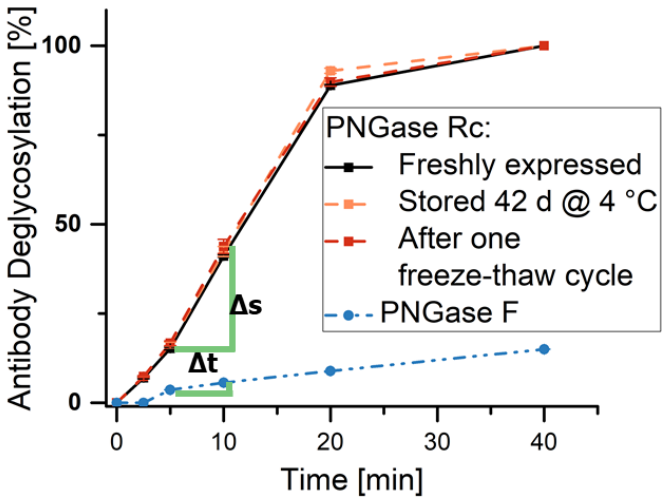

Figure 21: Comparison of deglycosylation kinetics of intact trastuzumab by PNGase Rc and F and the assessment of the storage stability as published in [139] . *Deglycosylation was performed for 2.5, 5, 10, 20 and 40 min at 37 °C and an E:S of 1:44 (M:M) at pH 2.5 or pH 7.5 for PNGase Rc and F, respectively. Activity of PNGase Rc was determined after expression, one freeze-thaw cycle and storage for 42 days at 4 °C. Analysis: RP-C4-LCMS; relative abundance of fully deglycosylated trastuzumab was calculated from peak intensity of the charge-deconvoluted mass after summation of all m/z spectra across the trastuzumab chromatographic peak.*

5.2.2.2 Enzyme Temperature and pH Optimum

Using the assay described above, the temperature and pH optima of the enzyme were determined. Each parameter was changed independently starting from the initial conditions of pH 2.5 and 37 °C and applying a fixed incubation time of 10 min. The temperature optimum for intact deglycosylation was found to be 37 °C while higher temperatures than 50 °C led to an inactivation of the PNGase. Deglycosylation efficiency on ice was insufficient for intact deglycosylation within the applied time range and molar E:S ratio (1:44) (Figure 22). However, the PNGase was able to hydrolyse 6% of one of both N-glycans (half deglycosylated state), indicating a remaining activity for intact protein deglycosylation even at 4 °C (data not shown).

The PNGase Rc has an optimum activity at pH 3.5 with twice the activity compared to the deglycosylation at pH 2.5. The pH working range of the PNGase Rc is 2.5 to 4.5, which suggests that post-HDX deglycosylation under HDX quench conditions is feasible. The low enzyme activity at pH 5.0 can additionally be explained by enzyme precipitation due to its isoelectric point of 5.1. This assumption is supported by the finding that the LC-MS peak for the enzyme disappears in samples measured at pH 5.0 (not shown).

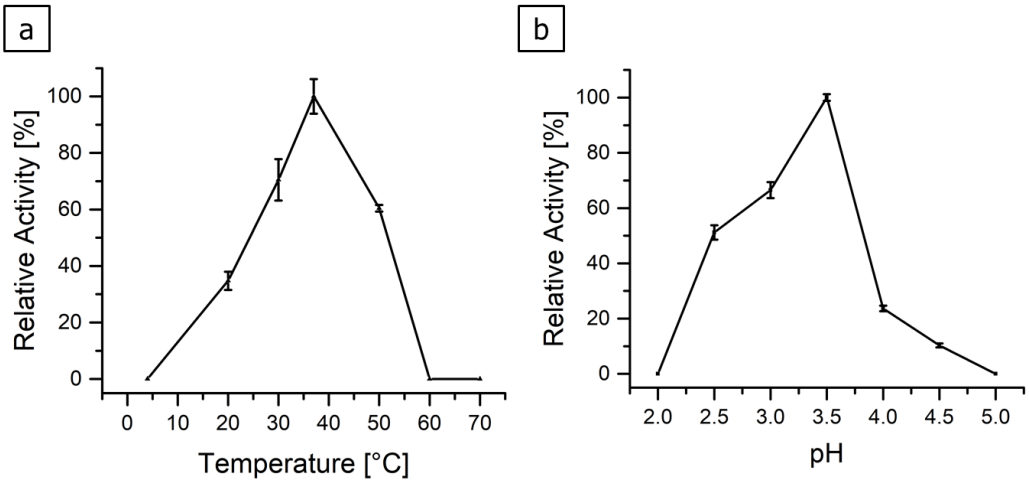

Figure 22: Temperature (a) and pH optimum (b) of PNGase Rc after 10 min deglycosylation of intact trastuzumab as published in [139]. *Parameter for determination of the temperature optimum (a): t = 10 min; pH = 2.5. Parameter for the determination of the pH optimum (b): t = 10 min T = 37 °C. E:S = 1:44 (M:M). Used buffer for pH 2.0: 200 mM glycine-HCl buffer and for pH 2.5 to 5.0: 100 mM citrate-NaOH.*

5.2.2.3 Enzyme Specificity

The substrate specificity of the PNGase Rc was further evaluated by assessing the N-glycan release from three multiply or very specifically N-glycosylated proteins. For this, deglycosylation of the plant glycoprotein, horseradish peroxidase (HRP), fetuin and ribonuclease B (RNase B) was monitored by SDS-PAGE (Figure 23a-c). As a reference, PNGase F-treated samples with identical experimental conditions but physiological pH were prepared. Heat denaturation, which is known to facilitate deglycosylation of sterically inaccessible sites, was omitted in order to assess the activity of deglycosylation of native glycoproteins [98].

HRP (~44 kDa) contains nine potential glycosylation sites and is occupied mainly (>80%) by oligomannose, xylosylated, core-1,3-fucosylated N-glycans (MMXF) [144]. Incubation for 0.5 h with PNGase Rc resulted in a clear band shift towards the deglycosylated HRP (~34 kDa). It was completely deglycosylated after incubation for 3 h. Here, PNGase F served as a negative control for deglycosylation of HRP, known to be unable to release α-1,3-core-fucosylated N-glycans [145].

The second protein, RNase B contains a single N-glycosylation site that is occupied by high-mannose type glycans (Man5-9GlcNAc2) [146]. Incubation of RNase B (~17 kDa) with any enzyme for 30 min resulted in the appearance of a new protein band at the molecular weight of the deglycosylated protein (~14 kDa). However, these band became clearly visible only after overnight incubation using PNGase Rc but with higher intensity compared to the PNGase F (Figure 23b). Thus, these results led to the conclusion that the novel PNGase Rc hydrolyses high-mannose N-glycans more efficiently than PNGase F.

Finally, fetuin from fetal calf serum (48.4 kDa) was used as substrate encompassing three N- and four O-linked glycans with a high degree of sialylation [147]. When interpreting the data, it must be taken into account that the hydrolysis of glycans by both PNGases is limited to N-linked glycans only. PNGase Rc showed the onset of deglycosylation within 30 min, resulting in the disappearance of the protein band with the highest molecular weight, corresponding the glycosylated fetuin (Figure 23c). A comparable N-glycan hydrolysis using PNGase F was observed at an incubation of 6 hours. These results reveal a higher activity of the PNGase Rc in deglycosylating natively folded proteins compared to the widely applied PNGase F.

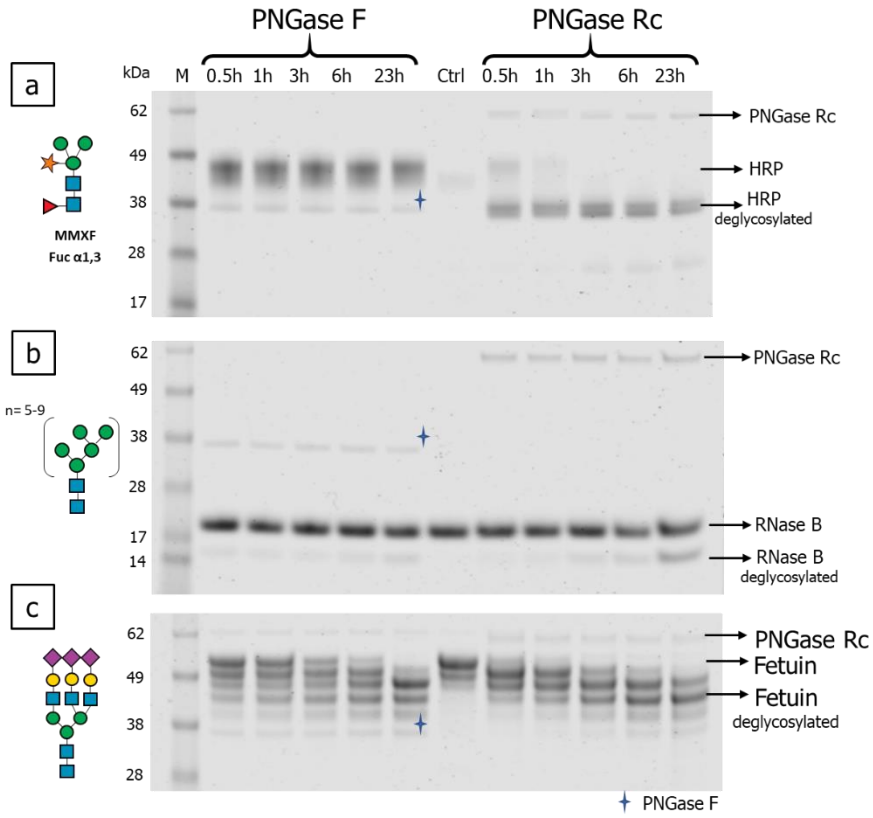

Figure 23: Monitoring intact protein N-glycan hydrolysis by PNGase Rc and F of (a) HRP, (b) RNase B and (c) fetuin adapted from [139]. *Proteins were incubated for various times with PNGase Rc or F at 37 °C and pH 3.5 or 7.5, respectively. Deglycosylation was performed at a molar E:S of 1:48 and deglycosylation efficiencies were monitored by SDS-PAGE followed by Coomassie staining at indicated time points. Main N-glycan species of the proteins are depicted according to the Symbol Nomenclature for Glycans (SNFG) [143] at the left hand side of the figure. Non-Glycosylated HRP negative control (Ctrl) was incubated for 24 h at 37 °C and pH 3.5 without PNGase.*

5.2.2.4 Integration of PNGase Rc into the HDX-MS Workflow

The high activity of PNGase Rc at pH 2.5 provides an opportunity to integrate the enzyme into the HDX workflow for protein-protein interaction analysis, which was evaluated next. Performing N-deglycosylation after pepsin digestion ensures antigen-antibody binding in their native conformation while providing comprehensive sequence coverage. Furthermore, N-glycan hydrolysis was shown to be more effective on peptides than on natively folded proteins [148]. The integration of the deglycosylation step into the HDX-MS workflow was tested using a tryptic digest of trastuzumab. Thus, deglycosylation of the antibody peptide ^{296}EEQYNSTYR^{304} including the N-glycosylation site of the Fc region was monitored. The glycosylation pattern was annotated on basis of the exact masses. The efficiency of deglycosylation was relatively quantified using the extracted ion chromatograms (EIC, included masses see Table 19). The deglycosylated peptide area was monitored relative to the sum of glycosylated and deglycosylated peptide peak areas (Figure 24).

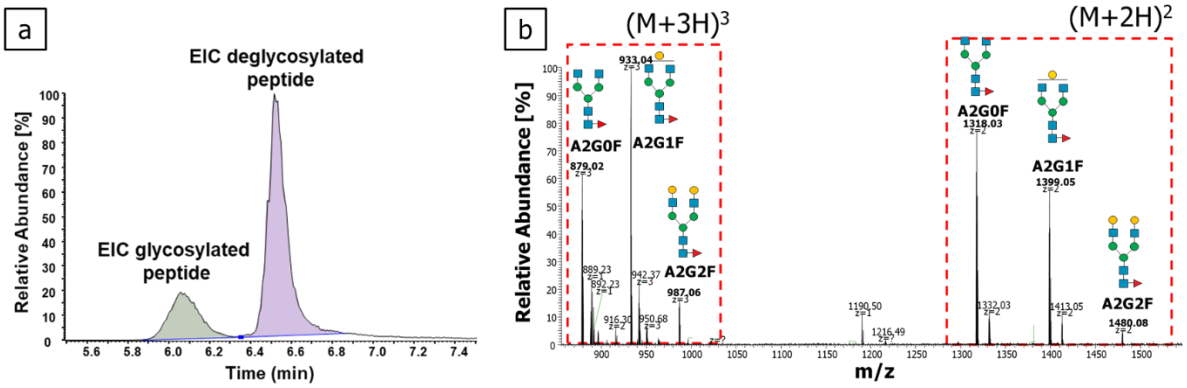

Figure 24: Peptide deglycosylation efficiency of PNGase Rc implemented in the HDX-MS workflow according to [139]. *(a) EIC of the deglycosylated and glycosylated tryptic peptide EEQYNSTYR for the peptide-based deglycosylation assay with a molar E:S ratio of 1:10.5; pH = 2.5, t = 2 min, T = 0 °C. (b) m/z spectrum summed up over the chromatographic retention time range from minute 5.8 to 6.5 of a sample without deglycosylation. N-glycosylated peptide species of the tryptic peptide were annotated. Glycans: SNFG [143].*

Deglycosylation was performed for 2 minutes under HDX quenching conditions at pH 2.5 in a water-ice bath (~0 °C). To evaluate the E:S ratio resulting in a complete deglycosylation, increasing enzyme concentrations were used (Figure 25a). Notably, residual trypsin from the proteolysis is inactive at this pH which protects PNGase Rc from being proteolysed. A complete deglycosylation was obtained at the applied hydrolysis conditions using a E:S of 1:2.6. In order to reduce disulphide bonds, and therefore increase the proteolysis efficiency and subsequently the resulting sequence coverage, reducing and denaturing agents are required for HDX-MS analysis. Thus, the proteolysis is typically performed in presence 1-3 M GdmCl or 1-4 M urea and ~250 mM TCEP, depending of the number of disulphide bonds [67, 107]. The tolerance of

the enzyme against each of these substances was evaluated using the above described assay with increasing amounts of TCEP, urea and GdmCl. The enzyme showed almost no activity loss in presence of 200 mM TCEP and 2 M urea (Figure 25a-b). It showed lower tolerance against GdmCl compared to urea, showing a drop in activity at a concentration of 1 M GdmCl already (Figure 25c). However, these experiments clearly indicate a possible integration into the established semi-automatic HDX-MS workflow for post-proteolysis deglycosylation under harsh denaturing and reducing HDX-quenching conditions.

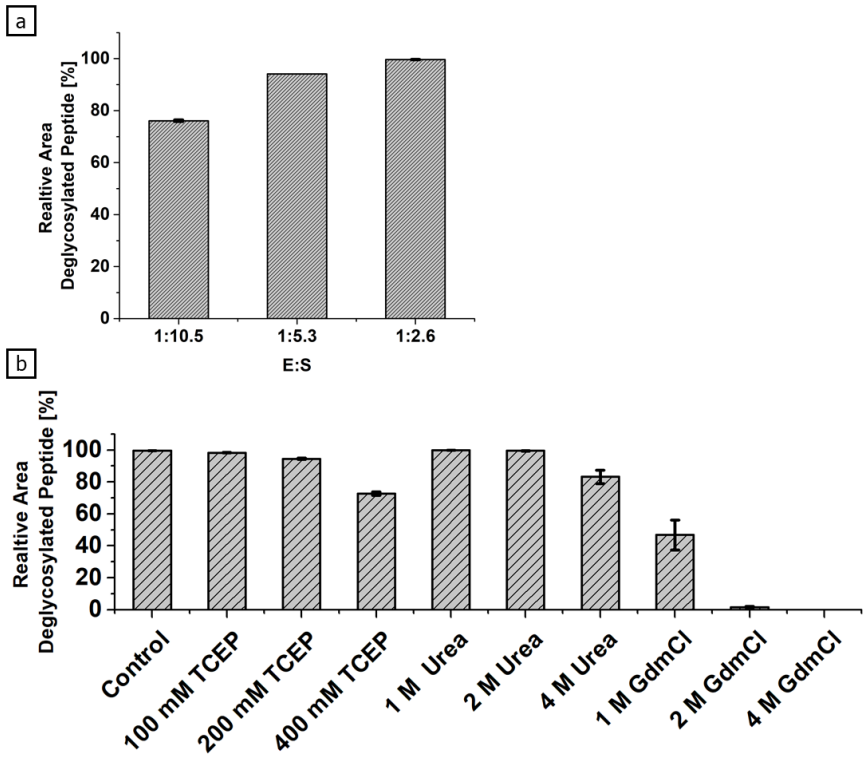

Figure 25: Influence of various E:S ratios (a), concentrations of TCEP (b), urea (c) and GdmCl (d) on the peptide deglycosylation using PNGase Rc under HDX quenching conditions according to [139] . *The peptide deglycosylation assay using the tryptic peptide EEQYNSTYR was applied (pH = 2.5, t = 2 min, T = 0 °C). Deglycosylated peptide area was monitored relative to the sum of glycosylated and deglycosylated peptide peak areas (see Figure 24a). (a) Deglycosylation activity using different E:S ratios. Tolerance of the PNGase Rc using an E:S of 1:2.6 towards increasing concentrations of TCEP, urea and GdmCl.*

5.3 Epitope Characterisation Case Studies

5.3.1 Annexin-A1: A Calcium-Binding Antigen

This work has been published in 2021 [110]. Within this study, the epitope mapping of an anti-ANXA1 antibody considered for clinical applications was examined. Typically, an HDX-MS experiment starts by determining proteolytic conditions that result in high sequence coverage and peptide count in order to extract HDX data of the whole molecule. ANXA1 was used to establish generic protocols and validate the setup and workflow for conducting HDX experiments. These experiments are presented in other sections of this work (see 5.1.2; 5.1.4). For ANXA1 both, the bead-based and in-solution proteolysis workflow were carried out (see 5.1.2). HDX data from the in-solution digest will be discussed in detail within this section. Additionally, HDX-MS data of the bead-based approach can be found in the appendix.
The proteolysis for 10 min at 0 °C led to 180 peptides with an average redundancy of 11 amino acids resulting in 100% coverage of the sequence.

5.3.1.1 Determination of the Binding Affinity

To calculate the amount of antigen bound during the complex formation and thus ensuring a saturated antigen:antibody interface, the equilibrium dissociation constant was determined by surface plasmon resonance (SPR) prior to the HDX-MS experiments. For ANXA1, known to undergo structural changes upon calcium binding [111], it is of particular interest to monitor the equilibrium constant of both the apo and the holo conformational states. Thus, the binding affinity was determined in presence (holo-state) or absence (apo-state) of 1 mM Ca^{2+}. Whereas an equilibrium dissociation constant (K_D) of 2.66 nM was determined for the calcium-bound holo-state of ANXA1 (Figure 26 a), no binding of the anti-ANXA1-antibody to the apo-state of ANXA1 was observed (Figure 26 b). This proves that the antibody only binds to the calcium-complexed ANXA1 [110].

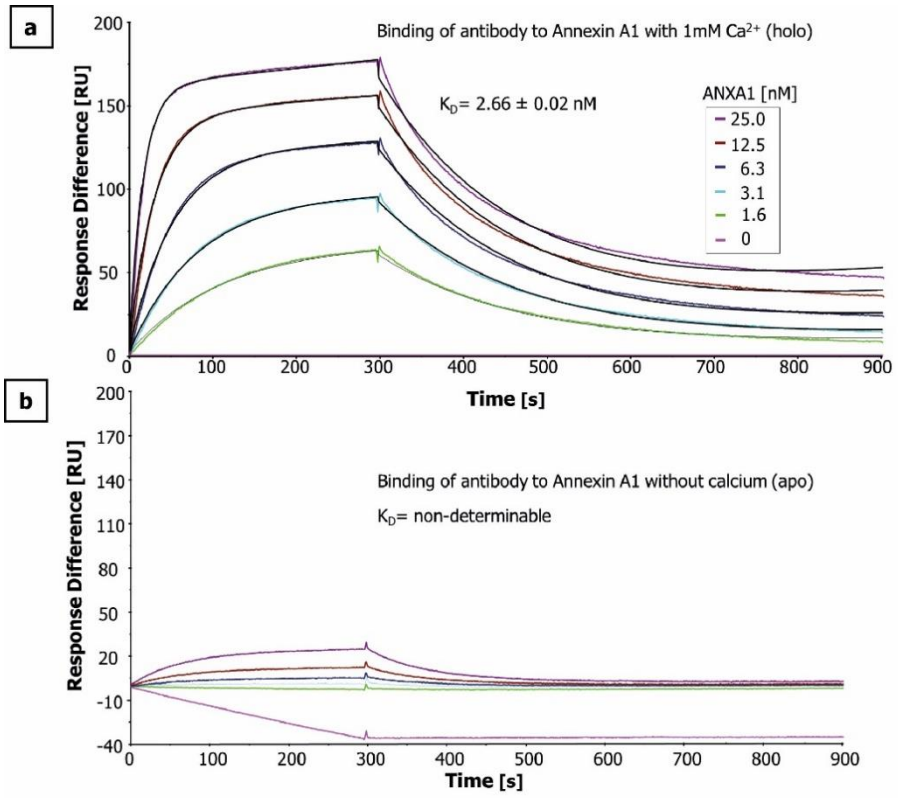

Figure 26: Binding affinity determination of the anti-ANXA1 antibody by SPR analysis as published in [110]. *Anti-human IgG was covalently coupled to a CM5-chip, which was used to capture the anti-ANXA1 antibody. The binding kinetic of five concentrations of ANXA1 (ranging from 1.6 to 25 nM) in presence (a) and absence (b) of calcium was examined. All measurements were performed in technical, independent triplicates and the obtained data were evaluated by the 1:1 Langmuir binding model. One representative sensorgram of each state is shown [110].*

5.3.1.2 HDX Kinetics of ANXA1

Because of the finding that the anti-ANXA1 antibody binds exclusively to the holo-state of ANXA1, HDX experiments were conducted in the presence of 1 mM Ca^{2+}. The intrinsic deuteration kinetic of ANXA1 was determined using continuous HDX labelling for different time periods. According to the consensus guidelines [74], labelling reactions were performed over a wide time window of four orders of magnitude (0.5; 5; 50; 500 min) with one additional long deuteration time point (24 h). A sequence coverage map of ANXA1 for peptides used to extract HDX information is shown in Figure A2. Figure 27 shows the relative deuterium uptake for ANXA1 peptides, which are numbered from the N- to the C-terminus and are additionally sorted from short to long peptides. Notably, a rapid deuterium uptake was observed for the first 10 peptides reaching a saturation within the first 0.5 minutes (60-80%). This suggests a high solvent accessibility of the N-terminus in the ANXA1 holo-state. The observed deuterium uptake for peptides covering the accessible N-terminus as well as the first α-helix of repeat I (peptide no. ~10-20, Figure 27) slowed down. The ANXA1 core (repeat I-IV) is highly structured as it mainly consists of α-helices. The α-helices are connected by loops known

known to undergo fast hydrogen-deuterium exchange. Thus, an alternating high and low deuterium uptake was observed for the peptides covering the core repeats of ANXA1. Within the core (repeat I - IV), an average deuterium uptake of 21% of the easily accessible amide hydrogens was determined after 0.5 min labelling. Thereafter, a slow (+5%) deuterium uptake kinetic was observed with some peptides showing an ongoing uptake after 24 h deuteration. Of all repeats comprising the core, repeat III (peptide number ~105-155) showed an overall higher initial deuterium uptake of 26% on average after 0.5 min labelling. A complete deuteration on ANXA1 was attempted in the presence of 6 M urea-d4 for 24 h at 20°C. While peptides covering the structured protein repeats I, II and IV showed a high increase in deuteration, the more accessible peptides covering the N-terminus as well as repeat III showed only a slight increase in deuterium uptake even after additional denaturation (Figure 27, Figure A3). This suggests that repeat III undergoes a molecular "breathing" with fast opening of the core structure (k_{open}) compared to the other repeats comprising the core [110].

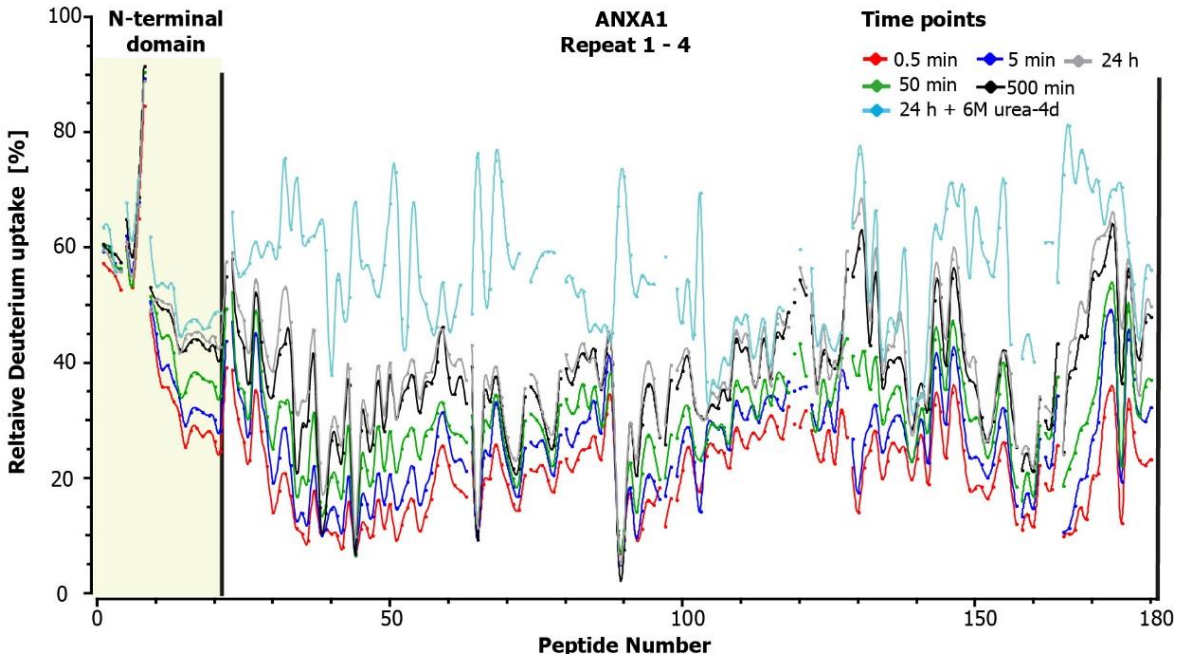

Figure 27: Deuterium uptake kinetics of ANXA1 derived peptides depicted by a summary uptake plot. *Adapted from [110]. Peptides are numbered from N- to C-terminus and additionally sorted from shorter to longer peptides. The deuterium uptake is normalised to the exchangeable aa (backbone amide count without proline and the first two N-terminal aa). HDX was performed in 90% D_2O, shown is the average of independent technical triplicates.*

5.3.1.3 HDX-MS Epitope Mapping

The comparison of HDX data of ANXA1 alone and in complex with an anti-ANXA1 antibody revealed significant HDX reduction within peptides covering the N-terminus and repeat III (Figure 28a). Based on the $\Delta\overline{HX}$ threshold of 0.64 Da and the average peptide length of 21 aa, a global significance line of 16% was calculated. If the summed deuteration difference of a peptide in the bound and unbound state was found to be >16%, this peptide was considered protected from HDX. The highest HDX protection upon antibody binding was found within repeat III at peptide numbers from 105 – 149 comprising amino acid residues 182 to 278. Using the software HDExaminer with the data obtained from overlapping peptides, an amino acid resolved heatmap was generated (Figure 28 c). It revealed three regions showing meaningful HDX differences upon antibody binding. The highest HDX difference was found in two regions that are assigned more precisely to residues 199-210 (region 1) and 223-236 (region 2). Peptide examples 182-226 and 223-234 covering these regions show high deuteration difference of >2 Da (25%) and >5 Da (12%) after 24 h labelling (Figure 28b II, III). According to the consensus guidelines [74], epitope mapping HDX uptake plots of all peptides (Figure A9 and Figure A10) and the HDX data table (Table A2) can be found in the appendix for both workflows [110].

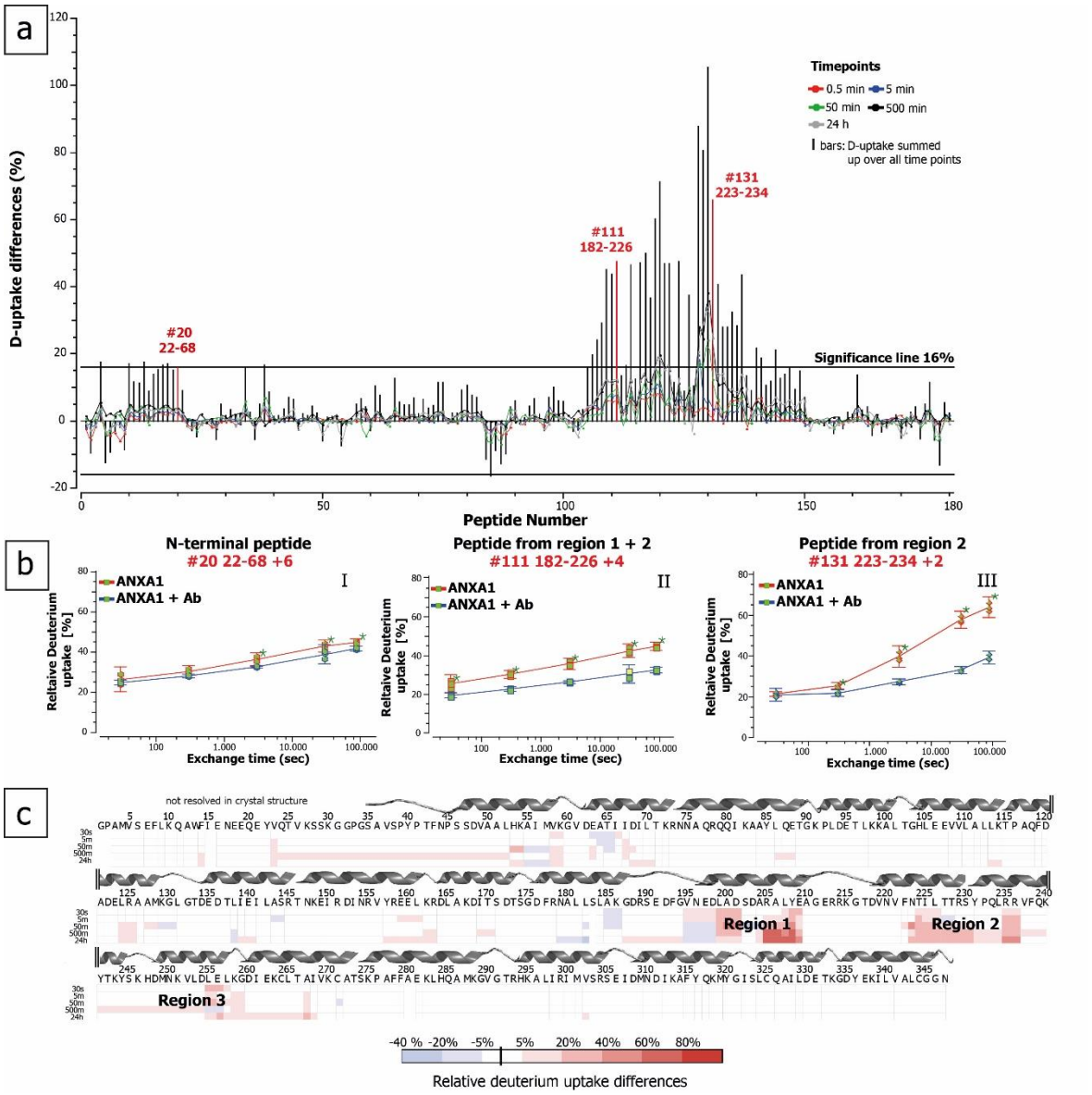

Figure 28: Results of the epitope mapping using the in-solution pepsin digest revealed deuteration differences within three regions of repeat III as published in [110]. *(a) Differential deuterium uptake of ANXA1 derived peptides with and without ANXA1:Ab complex formation. Peptide numbering see Figure 27. (b) Deuterium uptake plots of example peptides from the N-terminal region (I) and two epitope regions (II and III) alone and complexed by the antibody. The asterisk indicated statistical significant differences revealed by Student's t-test (α=0.05). (c) Heat map of anti-ANXA1 antibody epitope regions using the data from overlapping peptides. Secondary structural elements are depicted as symbols based on the X-ray structure ANXA1 (PDB ID: 1AIN [149]).*

A third region showed smaller but statistically significant HDX differences. Peptides covering this region were found to be inconsistent in the HDX protection upon binding (Figure A9; uptake plots). Furthermore, only some deuteration time points showed statistical significant differences (Student's t-test, p≤0.05). After 24 h labelling, 6.6% HDX difference was observed (Figure 29). However, HDX data of the bead-based digest with lower back exchange and higher reproducibility ($\Delta\overline{HX}$ threshold = 0.25 Da) revealed significant HDX difference upon antibody

binding of 3.5 and 5.2% after 5 and 500 min deuteration, respectively. Consistent HDX protection for peptides covering this region were observed using the bead-based digest (Figure 29, Figure A10). This suggests that some amino acids of this region contribute to the binding site as well.

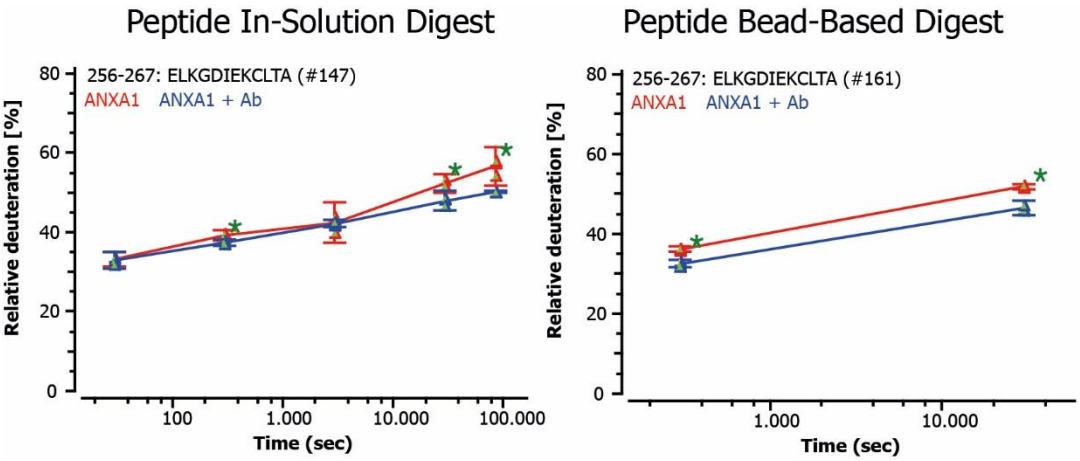

Figure 29: Comparison of uptake plots of a peptide covering the epitope region 3 between the bead-based and the in-solution digest. *The relative deuterium uptake normalised to the exchangeable aa (number of backbone amides without proline and the first two N-terminal aa). Statistical significance was determined using the Student's t-test (α = 0.05). Statistical significant differences were indicated by green asterisks.*

Additionally, a fourth region in repeat I, close to the N-terminus and distinct to repeat III shows modest (<4% per time point) but significant reduction in HDX upon antibody binding (Figure 28, Figure A4). This reduction might be due to allosteric changes in the dynamics or conformation of ANXA1 upon antibody binding opposed to a direct interaction that might altered the backbone amide HDX [110].

The binding regions one and two are in close proximity to each other within the three-dimensional structure (~30 Å) and constitute one spatial surface of ANXA1. These regions are located on two α-helices in repeat III of ANXA1 (Figure 30, helix A and B). The third region is located in three spatially close α-helices of repeat III (helix C, D and E). All three regions are within a distance of 30 Å and therefore can directly interact with an antibody binding site. Furthermore, repeat III undergoes a rearrangements upon calcium binding leading to major structural changes (Figure 29b, PDB ID: 1MCX [150] and 1HM6 [111]). This further supports the refinement of the epitope region to repeat III, taking into account that the anti-ANXA1 antibody binds exclusively to the holo-state of ANXA1 [110].

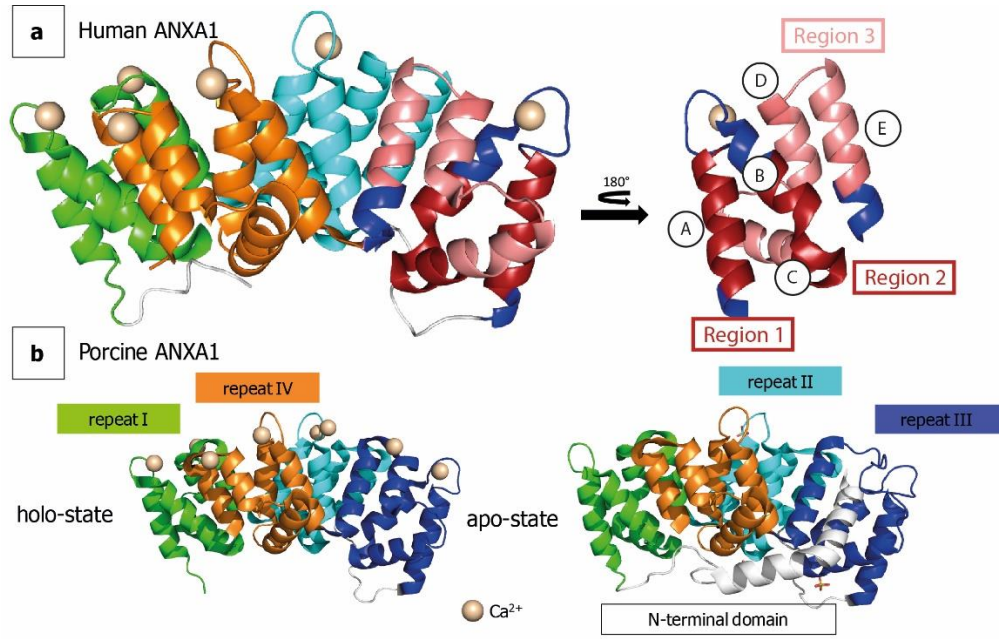

Figure 30: HDX-MS results mapped on the X-ray structure of human ANXA1 as published in [110]. *(a) Ribbon diagram of human ANXA1 complexed with calcium and with the binding regions 1-3 in repeat III of ANXA1 (PDB code: 1AIN [149]). According to Weng et al. [149], the five α-helices were named from A-E. Region with HDX protection of >40% upon antibody complexation are shown in dark red (regions 1 and 2) and the third region with 20 - 40% protection were depicted in light red. (b) Ribbon diagram of porcine holo-ANXA1 (left panel, PDB ID: 1MCX [150]) and apo-ANXA1 (right panel, PDB ID: 1HM6 [111]) showed the conformational switch within repeat III [110].*

With ANXA1, the proof-of-concept for performing epitope mapping experiments with the established experimental workflow and manual setup could be confirmed. However, the application to a larger number of proteins including molecules with multiple post-translational modifications such as disulphide bonds or glycosylations remained to be evaluated.

5.3.2 SARS-CoV-2 - Receptor-Binding Domain (RBD): Method Throughput with Seven Nanobodies

5.3.2.1 Method Adaptations for Increased Throughput

The aim of this study was the epitope screening of seven nanobodies targeting the receptor-binding domain (RBD) of SARS-CoV-2 in a short period of time. The screening aimed to select nanobodies (Nbs) whose epitope regions overlap with the ACE2:RBD interface. This allows evidence based identification of nanobodies that should have the potential to prevent the virus from penetrating human cells by blocking the major host receptor. The herein described wild-type RBD, derived from the first isolated virus strain, Wuhan-Hu-1 strain and is a glycoprotein containing two N-glycan consensus sequences and four disulphide bonds (Figure 32). The RBD protein with C-terminal His_6-tag was recombinantly produced and purified in-house in Expi293 cells, capable of N- and O-glycosylating proteins. Identity and integrity were proven using mass spectrometry (Figure 31). N-deglycosylation of the RBD using PNGase F was successfully achieved and the theoretical molecular mass of 26034.1 Da of the RBD could be confirmed. The analysis furthermore revealed extensive of O-glycosylation (>95%) of the RBD. A tryptic peptide map analysis assigned the O-glycosylation to serine 8 (Ser325 in Spike SARS-CoV-2) [151].

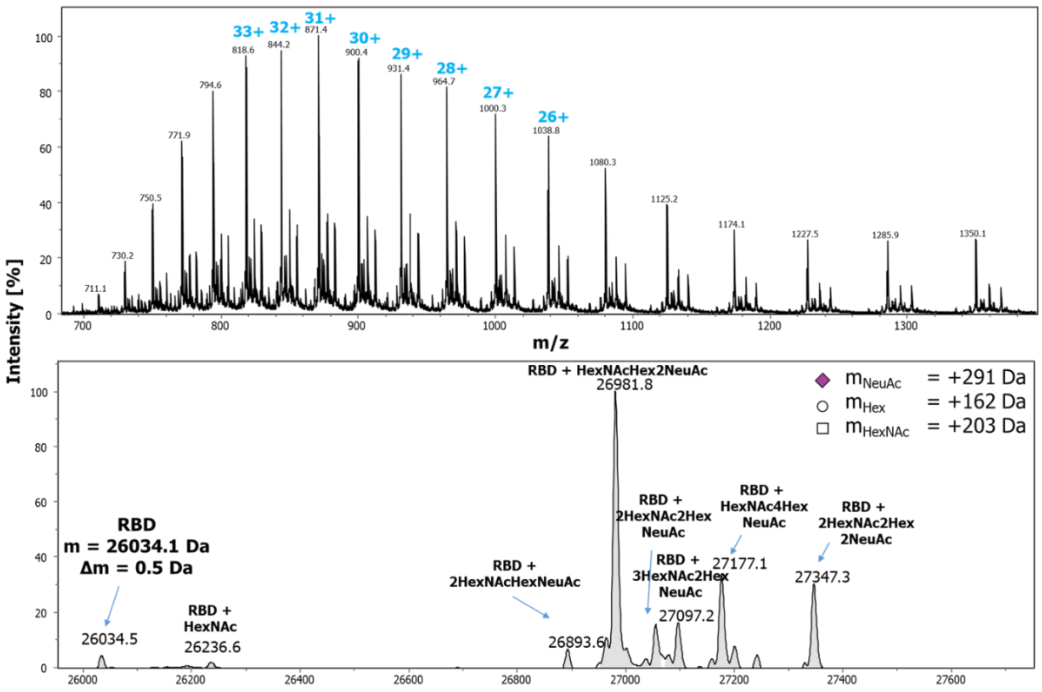

Figure 31: ESI mass spectrum of wild-type RBD (Wuhan-HU-1) showing the m/z charge envelope (upper panel) and the charge deconvoluted mass spectrum (lower panel). *RBD was reduced and denatured followed by an N-deglycosylation using PNGase F. Peaks showing the protein with O-glycosylations are labelled.*

Generation of a peptide list

Using the HDX-MS workflow with pepsin immobilized on beads developed for ANXA1, the feasibility of the HDX-based epitope mapping for the RBD was investigated. The applied feasibility criterion was a high sequence coverage considering peptides with non-overlapping isotopic pattern after LC separation. The former might be hampered by incomplete digestion or lack of identification due to e.g. closed disulphide bonds or glycosylations.

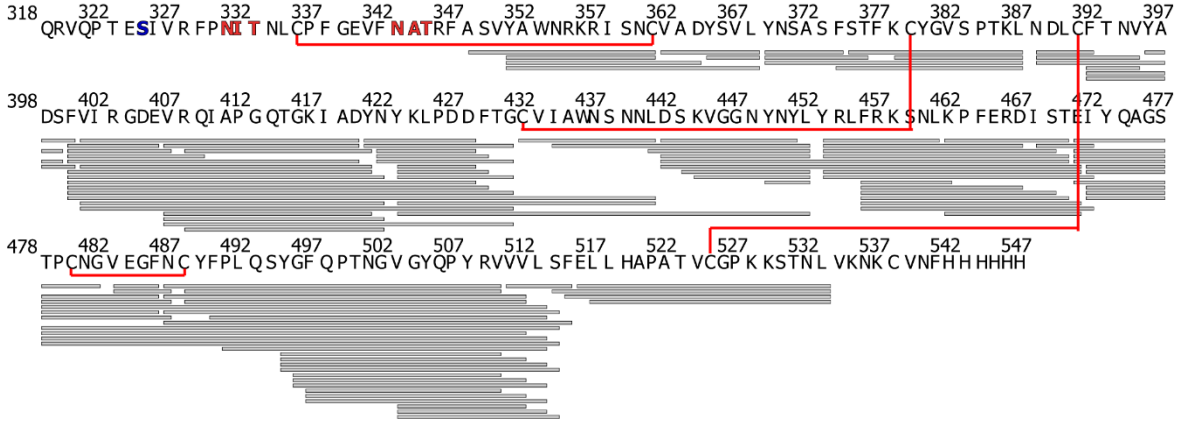

Figure 32: Sequence coverage map of RBD after pepsin proteolysis and exclusion of peptides with overlapping isotopic pattern in LC-MS analysis. *112 peptides covering 81% of the RBD of SARS-CoV-2 were identified. Each bar represents one peptide, red lines indicates the disulphide bonds. N-glycosylation consensus sequences shown in bold red. O-glycosylation as determined by tryptic peptide map shown in bold blue.*

In order to increase the number of identified peptides different, quenching and digestion conditions were used. These included a proteolysis with and without additional reduction for 60 sec at 20 °C and different concentrations of TCEP (100-200 mM) or the RBD (38-73 µM) as well as different amounts of pepsin beads (20 or 30 µL) (Table 20). The proteolysis conditions do not alter the peptide retention time or pepsin cleavage sites [107]. Identified peptides can be pooled and the generated peptide list can be used for analysis in a later experiments, under HDX compatible proteolysis conditions. The combined pool comprised 112 peptic peptides covering 81% of the RBD's sequence (Figure 32). Although fewer peptides were found covering cysteine residues compared to the other regions, disulphide bond hydrolysis was sufficient to cover these regions well. However, no coverage of the RBD's N-terminal end was achieved, which can be explained by the presence of the N- and O-glycosylation. Since these residues are distant from the RBD:ACE2 interface in the three-dimensional structure missing HDX data in this region is uncritical for the applied epitope mapping experiments.

Determination of the intrinsic HDX kinetics

The bottleneck of the established workflow and setup regarding high throughput was the time requirement for the HPLC-MS analysis in combination with the manual sample handling. Therefore, HDX epitope screening was performed with a limited number of labelling time points which might impair HDX sensitivity. To compensate for this, the labelling time points were chosen on basis of the intrinsic deuteration kinetics of the RBD. Slow intrinsic deuterium uptake consequently results in minor detectable HDX differences upon Nb binding. The RBD intrinsic HDX kinetic was examined for 0.5, 5, 10, 50 min and 24 h deuteration time (Figure 33).

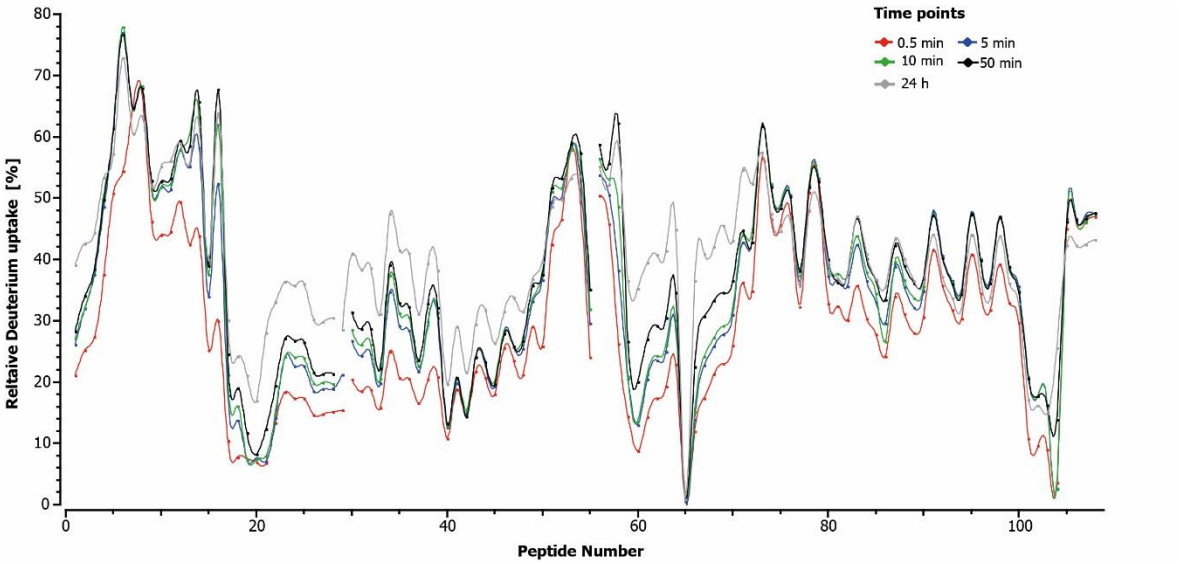

Figure 33: Deuterium uptake kinetics of RBD peptides. *The RBD HDX was examined after 0.5, 5, 10, 50 min and 24 h labelling in 90% deuterated PBS at 25 °C. For peptide numbering see Figure 27. The relative deuterium uptake was normalised to the exchangeable aa (backbone amide count without, proline and the first two N-terminal aa). Analysis was performed in duplicate and the average HDX is shown.*

The average global intrinsic deuterium uptake of the RBD after 50 min was 37.5%. Two regions covering amino acid residues 392-441 (peptide number 17-50) and 453-472 (peptide number 61-71) showed structural resistance to deuteration. Both region showed an average deuterium uptake of 24.7 and 27.3% after 50 min labelling, respectively. With respect to those regions, and in order to potentially increase the sensitivity by detection of fast and slow effect on the HDX upon Nb binding, deuteration times of 5 and 50 min were chosen for HDX epitope mapping. Conditions for the subsequent HDX epitope mapping experiments are summarized in Table 4. HDX uptake plots of all peptides (Figure A11) and the HDX data table (Table A3) can be found in the appendix. It should be noted that peptides are numbered consecutively within an HDX experiment. This means that the peptide numbering of one and the same peptide can

vary between different experiments. The assignment of the peptide numbers can be found in appendix (Figure A11-A18).

Table 4: Summary of HDX conditions for epitope mapping of various Nb binding partners on the RBD

Experimental parameter	Used conditions
HDX reaction details	1x PBS pH 7.4, 90% D_2O, 25 °C
Deuteration time points	5 & 50 min
Proteolysis conditions	2 min on-ice, 30 µL pepsin beads
Reduction and denaturation conditions	100 mM TCEP; 4 M GdmCl
Back exchange determined by synthetic peptide mixture (see 5.1.4)	24% (4-45%).

5.3.2.2 Epitope Mapping

Binding kinetics

Seven Nbs with high affinity to the RBD were included to the HDX-MS epitope analysis as published in Wagner *et al.* [46]. The individual binding affinities (Table 5) of the Nbs obtained from biolayer interferometry (BLI) using biotinylated RBD and were kindly provided by Teresa Wagner (Recombinant Antibody Technology Group, NMI, Germany).

Table 5: Binding affinity of the individual Nbs chosen for HDX-MS epitope mapping (adapted from [46]). *Affinities were determined with BLI analysis by Teresa Wagner (Recombinant Antibody Technology Group, NMI, Germany).*

	K_D (nM)	k_{on} (10^5 M^{-1} s^{-1})	k_{off} (10^{-2} s^{-1})	R^2
NM1221	22.70	1.30 ± 0.034	0.296 ± 0.010	0.956
NM1222	17.96	1.64 ± 0.013	0.294 ± 0.003	0.995
NM1223	3.82	0.70 ± 0.004	0.027 ± 0.001	0.999
NM1224	8.34	3.20 ± 0.042	0.267 ± 0.005	0.987
NM1226	3.66	3.14 ± 0.025	0.115 ± 0.002	0.992
NM1228	1.37	4.66 ±0.039	0.064 ± 0.001	0.996
NM1230	8.23	2.01 ± 0.015	0.166 ± 0.002	0.996

Epitope elucidation

On basis of the determined binding affinities (K_D), a molar ratio of Nbs to RBD was calculated [72] ensuring a >95% complex formation during HDX labelling. As per consensus guidelines [74], a summary of HDX parameters and results for the different Nbs is shown in Table 6. On basis of the standard deviations determined by the replicate analysis of each Nb (n = 3), a $\Delta\overline{HX}$ significance threshold of 0.17-0.26 Da ($p \leq 0.05$) was obtained, indicating a high reproducibility of the HDX epitope mapping data (see 5.1.5).

As a general rule, a peptide was considered as protected from HDX upon Nb binding, if both states showed ≥5% HDX difference. In contrast, the peptides HDX was considered as unaffected by the Nb binding, if the difference between bound and unbound state was <3%. Protected regions were spatially mapped on the RBD crystal structure (PDB ID: 6M17 [152]) and compared to the previously described RBD:ACE2 interaction sites [152, 153] (Figure 34, Figure A6).

While both members of Nb-Set1 (NM1226, NM1228) interact with the RBD at the lower back side (back view), both showed a slightly different binding interface (Figure 34B, C). Upon NM1226 binding mainly one region covering 370–387 (Figure 34B, Figure A5) was examined as protected. The same region also was covered by NM1228, which displayed additional protection in amino acid residues 489-514, covering a large stretch of the RBD:ACE2 interface.

NM1230, NM1221 and NM1222 (Nb-Set2) showed highly similar HDX protection upon binding located in two regions, which can be explained by their highly similar CDR regions [46] (Figure 34 D-F, Figure A5). Region one consists of amino acids 432-452 covering two amino acids involved in ACE2 binding (G446, Y449). The second region covered amino acids 487-496, which overlaps with the RBD:ACE2 interface.

Nanobody NM1224 (Nb-Set4) showed an interaction site distinct from the other Nbs [46]. A high HDX protection (<-15% - <-25%) present at both time points was determined upon binding, located at the lower right side with region 454-472 (Figure 32G, Figure A15). The second region showed weaker protection reaching the significant threshold of 5% only at prolonged exposure to deuterium (50 min). Both regions comprise amino acid residues corresponding to the RBD:ACE2 interface.

NM1223 (Nb-Set3) showed HDX reduction in residues at the lower front of the RBD indicating a non-competitive binding with that of the RBD:ACE2. The spatial distance of this protected region to the RBD:ACE2 interface suggested that a clash of the Nb with the ACE2 is unlikely to occur. [46]

Table 6: Summary of HDX-MS parameters of epitope mapping of different Nbs on the RBD of SARS-CoV-2 as per consensus guidelines [74]. *Additionally, significant differences between the bound and unbound in HDX uptake plots were tested by the Student's t-test (p≤0.05).*

Summary of HDX parameter							
States	RBD & RBD bound by **NM1221**	RBD & RBD bound by **NM1222**	RBD & RBD bound by **NM1223**	RBD & RBD bound by **NM1224**	RBD & RBD bound by **NM1226**	RBD & RBD bound by **NM1228**	RBD & RBD bound by **NM1230**
Av. peptide length (AA)	15.7 (s_d=7.0)	15.6 (s_d=7.1)	15.8 (s_d=7.5)	15.6 (s_d=7.3)	15.5 (s_d= 7.0)	16.1 (s_d= 7.6)	16.1 (s_d= 7.5)
Av. redundancy (AA)	5.6	5.7	5.8	5.7	5.9	6.4	5.7
Number of identified peptides	82	84	84	84	87	91	82
Sequence coverage	74%	80%	81%	81%	79%	79%	79%
$\Delta\overline{HX}$ threshold (p≤0.05)	0.18 Da	0.17 Da	0.22 Da	0.26 Da	0.21 Da	0.20 Da	0.19 Da
$\Delta\overline{HX}$ threshold (p≤0.01)	0.29 Da	0.28 Da	0.37 Da	0.43 Da	0.36 Da	0.33 Da	0.32 Da
Complexed RBD during labelling	96.6%	97.4%	99.6%	97.9%	99.1%	99.6%	98.6%

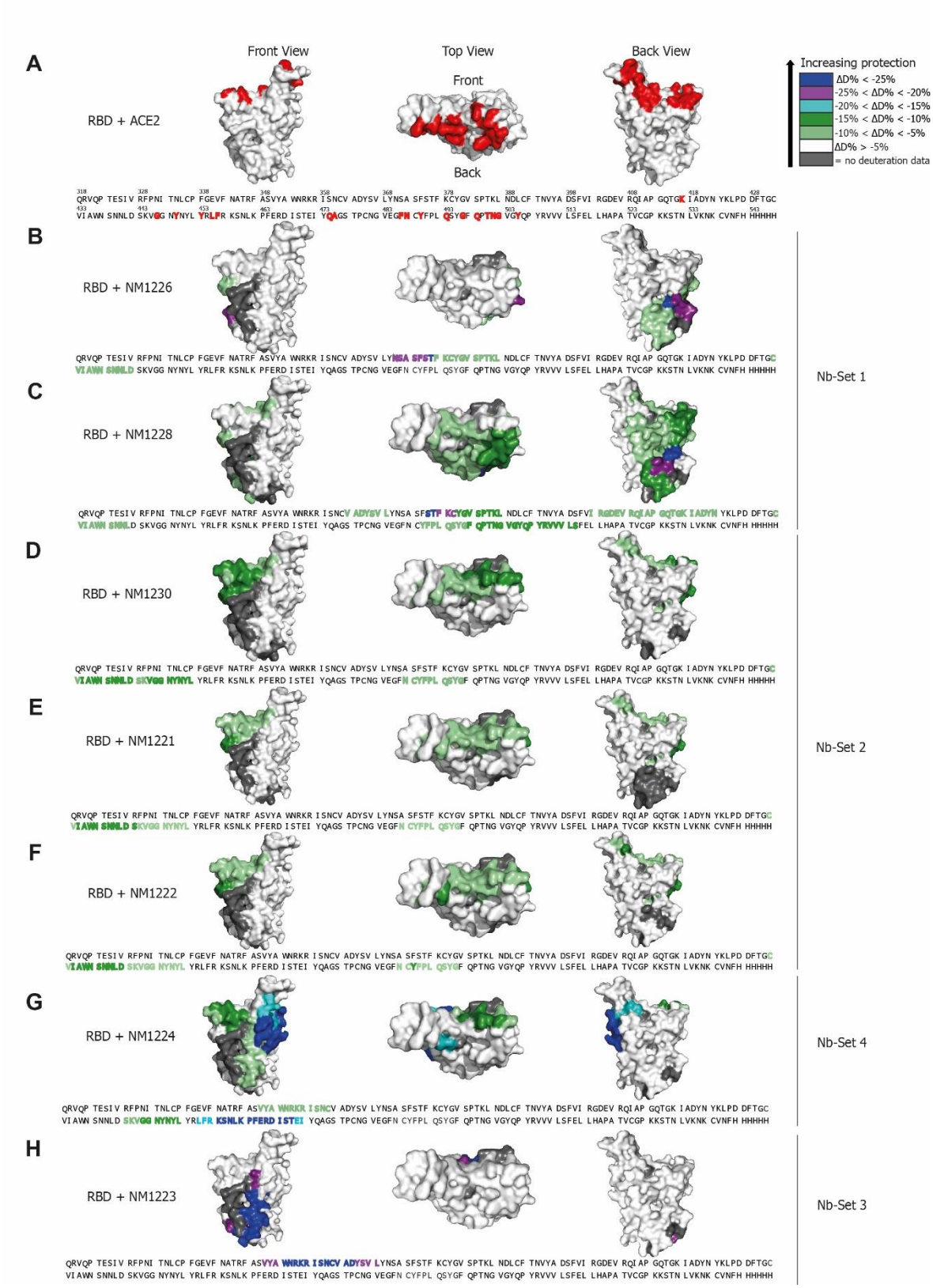

Figure 34: HDX-MS epitope mapping data mapped onto the surface structure model of RBD (PDB ID: 6M17 [152]) compared to the RBD:ACE2 interface as published in [46]. *The strength of protection upon Nb binding is highlighted in different colours. (A) Amino acid residues of the RBD involved in the RBD:ACE2 interaction site [152, 153] are shown in red. (B-H) Regions protected from deuterium uptake upon binding of different Nbs.*

Due to the restrictions of the time points, the throughput was increased leading to a data acquisition time of 79 h. This showed the feasibility of throughput analysis with the manual sample handling and the SAIDE setup for epitope screening. Furthermore, comparison of the peptides HDX kinetics of the RBD bound by individual Nbs improves the certainty of an epitope mapping campaign. In particular, unique effects on the HDX exchange upon individual Nb:RBD incubation can be confidentially attributed to the certain Nb. Moreover, if one Nb effects the HDX of region on the targeted molecule, false negative identification due to low sensitivity (low intrinsic HDX or high back exchange) can be excluded. According to the consensus guidelines [74], epitope mapping HDX uptake plots of all peptides and epitope mapping experiments (Figure A12-18) as well as a HDX data table (Table A3) can be found in the appendix.

5.3.2.3 Comparison of HDX-MS Results with X-Ray Crystallography

Two Nbs that are potent in their neutralization of the SARS-CoV-2 infection of a human cell line were selected for further analysis. Thus, NM1226 and NM1230 showing HDX reduction on different RBD residues and among the highest obtained affinities were selected for high-resolution epitope mapping by X-ray crystallography by the Stehle laboratory (Interfaculty Institute of Biochemistry, Eberhard Karls University, Tuebingen, Germany). Amino acids involved in the binding were observed by X-ray crystallography using a distance cutoff of <4 Å. A comparison of the crystal structure data (PDB ID: 7NKT, 7B27 [46]) with HDX-MS data shows that both methods result in similar binding interfaces of the Nbs to the RBD (Figure 35A). Therefore, an HDX-MS method validation by X-ray crystallography was possible.

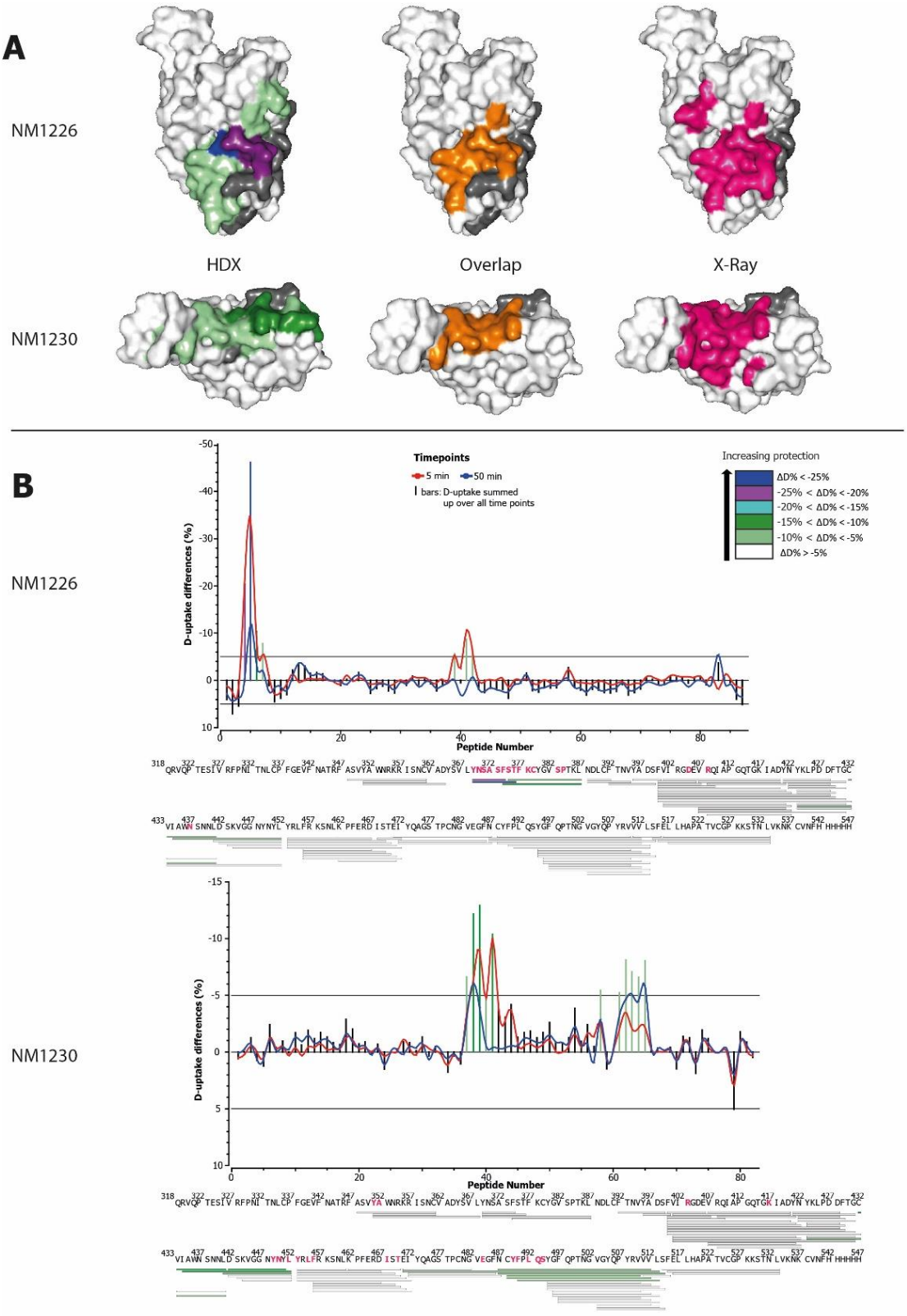

Figure 35: Comparison of HDX-MS and X-ray epitope data of Nb NM1226 (PDB ID: 7NKT [46]) and NM1230 (PDB ID: 7B27 [46]). *(A) Epitope residues mapped on the surface model of the RBD for X-ray epitope analysis (pink), HDX-MS analysis (colour-dependent on the HDX protection (%)) and overlapping residues (orange) (PDB code: 6M17 [152]). (B) Adapted from [46]. Peptides are colour coded by the degree of HDX protection (%). Peptide numbering see Figure 27. Amino acids found to be involved in binding by X-ray are highlighted in pink.*

For more precise comparison of both methods, the obtained HDX-MS data were treated as a classifier problem and analysed using a confusion matrix (Table 7). Assuming that the X-ray data are the true epitope values each residue that is determined by HDX-MS can be individual classified. If both approaches show that the residue belongs to the binding interface is classified as true positive (TP). In contrast, if a residue shows a no significant difference in HDX and is not part of the epitope determined by the X-ray analysis it is classified as true negative (TN). The other scenarios were a peptide is considered as part of the interface by only one of the approaches leads to classification as false positive (FP) or false negative (FN) identifications (Table 7).

Table 7: Confusion matrix comparing the results epitope mapping data of HDX-MS and X-ray crystallography assuming the X-ray data to show true epitope residues.

		HDX-MS	
		+	-
Crystallography	+	**True Positive (TP)**	*False Negative (FN)*
	-	*False Positive (FP)*	**True Negative (TN)**

The confusion matrix allows a calculation of the sensitivity ($\frac{TP}{TP+FN}$) and specificity ($\frac{TN}{TN+FP}$) of the HDX-MS epitope mapping.

The determined sensitivity and specificity for the HDX-MS epitope analysis of NM1226 was 0.75 and 0.93, respectively. To eliminate FP identifications throughout the multiple epitope analysis a rather high $\Delta\overline{HX}$ threshold corresponding to the 99% confidence level was used. This subsequently ensures a high specificity to distinguish between similar epitopes of different Nbs at the expense of the sensitivity. In general, if the interface consists of several amino acids that are close together in the primary sequence the detection of HDX protection is facilitated. Therefore, consistency with X-ray crystallography data is higher for binding regions of this type. However, the interface of NM1230:RBD as determined by X-ray, comprised several residues, scattered over the sequence of the RBD in the primary as well as the 3D structure. These are challenging to detect using HDX-MS, especially if they belong to long peptides were uptake differences of <1% per time point were observed. Thus no reduction in HDX was observed for this aa resulting in a lower sensitivity (0.44) but comparable specificity (0.88) compared to the determined epitope of NM1226 (Figure 35B). Since the two N-terminal aa of each peptide were known to lose their label rapidly, missing aa coverage further explains FN identification by HDX-MS.

A special case of FN identification was examined for the interaction of both Nbs with residues of the above described region showing low intrinsic HDX (Figure 33). Based on the significance

threshold for the throughput analysis, no meaningful differences were detected for peptides covering aa D405 and R408, which however were detected as part of the binding interface by X-ray crystallography (Figure 35B). Peptic peptides covering this region are structured into a β-sheet and α-helix and consequently showed very low intrinsic deuterium uptake (covering aa 400-409, see Figure 33). Thus, a minor insignificant HDX protection for Nb NM1226 and no HDX protection for NM1230 was found by HDX-MS at the applied time regime (Figure 36). This FN identification might be a result of the screening approach using less time points and might be covered by HDX-MS monitoring a prolonged kinetic.

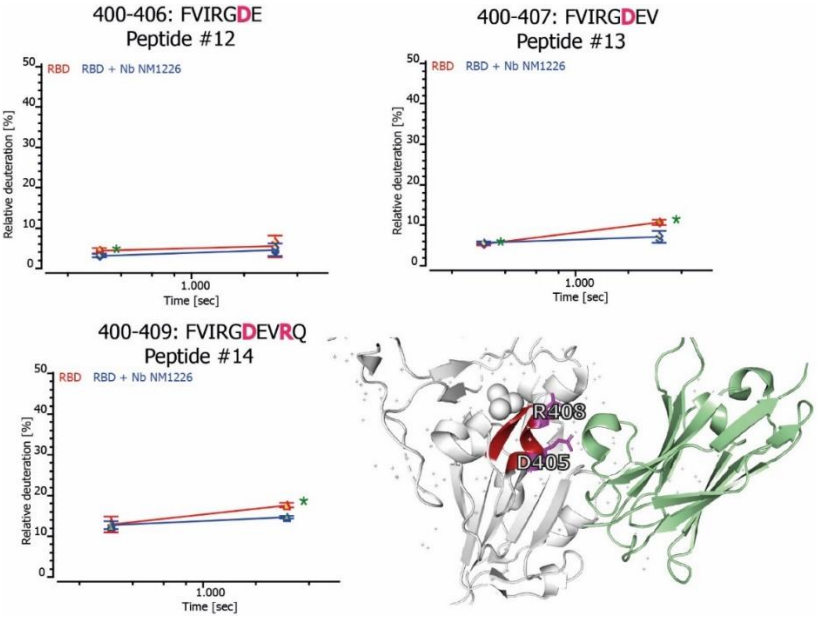

Figure 36: HDX example of peptides covering two amino acids belonging to the epitope of NM1226 below the global threshold of 5%. *The peptides covering the amino acids (D405 and R408, bold pink letters) were defined as part of the epitope by X-ray analysis but not by HDX. These peptides are hidden within the core (PDB ID 7NKT [46]) and show low intrinsic deuterium uptake. The shortest peptide showed an uptake of only ~5%.*

In summary, the HDX-MS data were in good agreement with the high-resolution epitope mapping results using X-ray crystallography. Using the screening approach with a strict $\Delta\overline{HX}$ threshold, contact regions comprising contiguous contact residues can be detected by HDX-MS. For detailed analysis with higher sensitivity, more time points and broader time regime (seconds to hours) need to be applied to detect faster and slower HDX changes upon binding.

5.3.3 Signal-Regulatory Protein Alpha (SIRPα): Epitope Mapping of Highly Glycosylated Target Proteins

Parts of the following chapter are published in [139]. Some figures of chapter are reprinted (adapted) with permission from [139]. Copyright 2022 American Chemical Society. In this case study, the epitope mapping of different Nbs raised against the multiply N-glycosylated signal regulatory protein alpha (SIRPα) was performed via HDX-MS. As described, the approach consists of an in-silico assessment of the target protein with regard to posttranslational modifications such as N-glycosylation and disulphide bonds. Thereafter, a quality control of the intact sample and an assessment of the sequence coverage after proteolysis under HDX conditions was performed. This preliminary work, enabled a batch analysis of different interaction partners with the target protein SIRPα in the adapted HDX-MS workflow.

5.3.3.1 In-Silico Assessment and Quality Control of SIRPα

The in-silico assessment of the full length extracellular part of SIRPα (~37 kDa) revealed three disulphide bonds and five potential N-glycosylation motifs. The commercially available protein was next analysed intact for assessment of the identity and integrity by MS. To obtain resolvable mass spectrometry data the protein must be deglycosylated. Due to the high number of potential N-glycosylation sites, a comparison of a conventional PNGase F and the new PNGase Rc was performed. Whereas, PNGase F incubation overnight led to an incomplete N-glycan release, full deglycosylation of SIRPα was achieved using PNGase Rc with the same E:S ratio (Figure 37).

The theoretical molecular mass of 38538.4 Da was confirmed. Notably, deglycosylation leads to a deamidation of the asparagine that is subsequently converted into an aspartic acid resulting in an increase in mass by +0.98 Da per N-glycosylation site. The experimental mass deviated by ~4 Da from the theoretical mass suggesting that 4 of the 5 potential N-glycosylation sites are occupied.

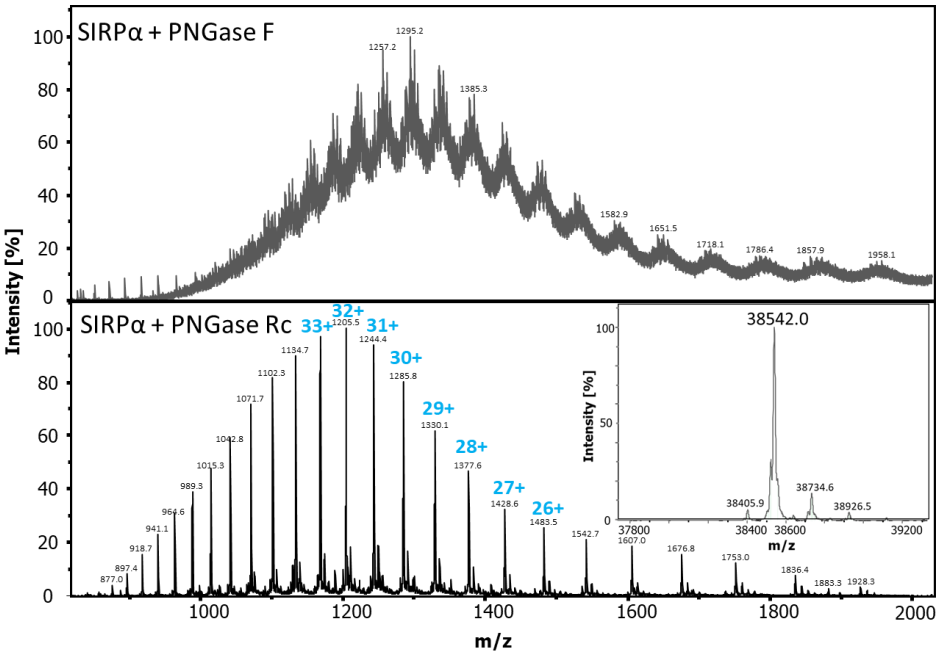

Figure 37: ESI mass spectrum of SIRPα with charge envelope after overnight deglycosylation using PNGase F (upper panel) and PNGase Rc (lower panel) as published in [139]. *Deglycosylation: t = overnight; T = 37 °C; Enzyme to substrate ratio: 1:45 (M:M); at pH 2.5 and pH 7.4 for PNGase Rc and F, respectively. Samples were desalted by a short RP-C4-LCMS gradient and MS spectra were summed across the chromatographic peak of SIRPα. The inlayer in the lower panel displays the charge-deconvoluted masses of SIRPα.*

In a next step, the N-glycosylation profile was determined to evaluate the micro-, and macroheterogeneity. Therefore, a tryptic proteolysis of SIRPα was used followed by HPLC-MS/MS detection. This analysis revealed a high microheterogeneity of most of the N-glycan sites (Figure 38). With respect to the macroheterogeneity, an almost fully occupied N240 and N262 were found, while more than 10% of N215, more than 30% of N80, and 90% of N289 were identified to be non-occupied with N-glycans.

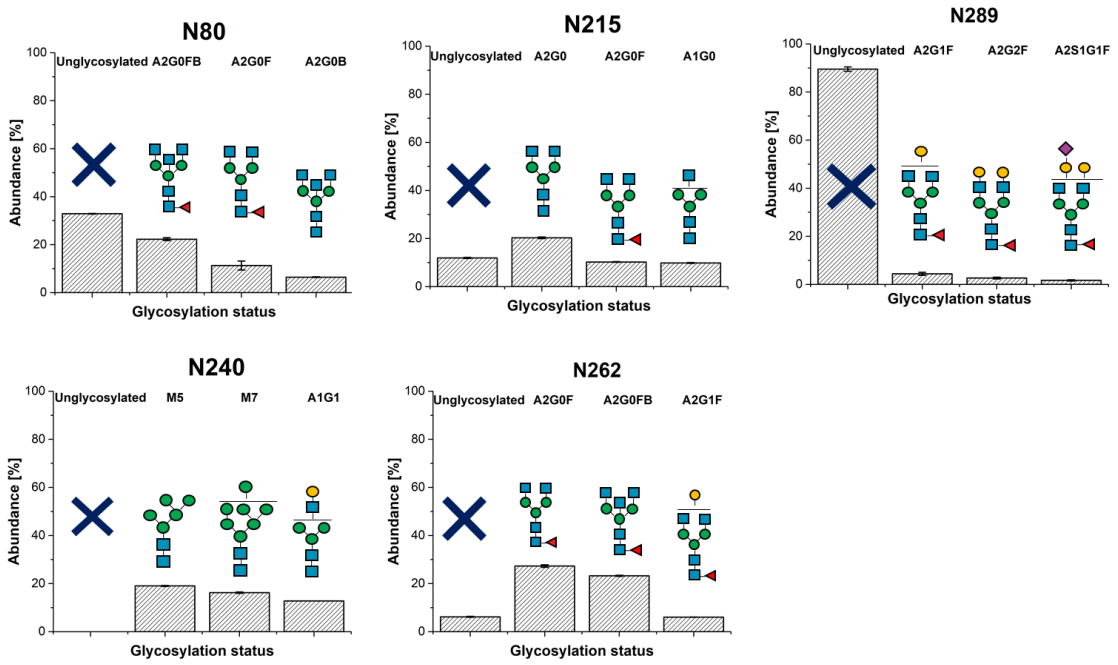

Figure 38: Examination of the micro-, and macroheterogeneity of the five possible N-glycosylation of SIRPα as published in [139]. *SIRPα was proteolysed overnight at 37°C using trypsin. HCD fragmentation was applied and peptides were identified by BioPharma Finder v4.1.53.14. Identified N-glycan species are relatively quantified. The three most abundant found N-glycans are shown.*

5.3.3.2 Peptide Map and Sequence Coverage with and without Deglycosylation by PNGase Rc under HDX Conditions

Generation of a peptide list

For improved peptide identification proteolysis was performed using different proteolysis conditions with respect to the TCEP concentration and the digestion time (Table 21) and identified peptides were combined in a peptide list.

The digestion of SIRPα performed under denaturing and reducing conditions using 100 mM TCEP and 2 M GdmCl led to the identification of 107 peptides covering 81% of its sequence. The sequence coverage of SIRPα's cysteines shows a successful disulphide hydrolysis under these conditions. However, low sequence coverage near the N-glycan motifs of N215 and N262 and no coverage near amino acid N240 was obtained (Figure 39). In contrast, a good coverage near the potential N-glycosylated asparagine N80 and N289 was found by peptide mapping. These data were in good agreement with the findings of the N-glycosylation analysis of the micro-, and macroheterogeneity of SIRPα.

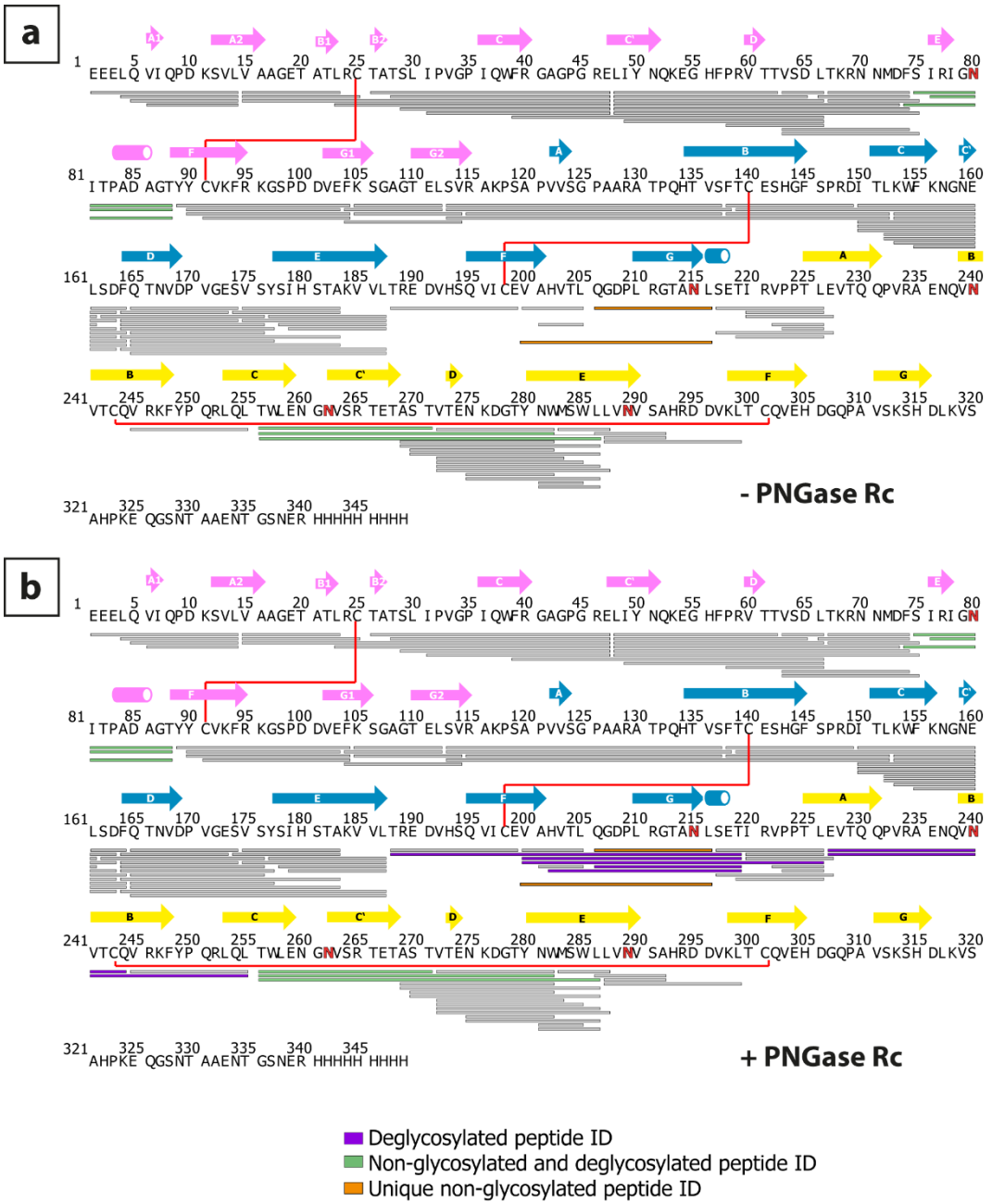

Figure 39: Sequence coverage of identified SIRPα peptides with (a) and without deglycosylation (b) using PNGase Rc according to [139]. *HPLC-MSMS identified peptides (grey) after 2 min proteolysis at 0 °C using immobilised pepsin. Unique peptides (purple) were identified using post-proteolysis deglycosylation for 2 min at 0 °C with PNGase Rc. Some peptides were identified as non-glycosylated species only (orange), while other peptides were be identified in non-glycosylated and deglycosylation version (pale green). Disulphide bonds are depicted with red lines and the N-glycosylated asparagine residues are highlighted in red. Amino acids involved in a secondary structure elements are depicted with arrows (β-sheet) and tubes (α-helix) according to [133]. These are highlighted according to their associated domains in pink (domain 1), deep teal (domain 2) or yellow (domain 3).*

To increase the sequence coverage, deglycosylation with PNGase Rc was applied post-proteolysis under HDX quench conditions (pH 2.5; 0 °C). With the additional deglycosylation step of 2 min, seven additional peptides spanning the N-glycosylation sites could be identified leading to a sequence coverage of 86%. Deglycosylation added sequence coverage and peptide redundancy to the region close to N240 and improved the coverage of residues adjacent to N215. Both residues were observed almost fully glycosylated. Two peptides, 206-216 and 200-216 covering N215 were found only as the non-glycosylated species. Since the corresponding deglycosylated peptides were not found, it suggests that N-glycosylation hindered pepsin from cleavage at favourable cleavage sites. Peptides spanning the N-glycan motif at N289 were only identified in the unoccupied manner, which can be explained by the mostly unoccupied glycosylation site. Notably, all non-glycosylated peptides could be identified independently of the additional deglycosylation by PNGase Rc.

Pepsin bead removal prevents the PNGase Rc from being proteolysed. Nevertheless, a potential interference of PNGase Rc peptides with target-specific peptides was assessed by applying a data base search against the PNGase Rc protein sequence and a manual check of RT and MS interference with SIRPα peptides. Only four PNGase Rc peptides were identified of which one interfered in sequence with SIRPα due to sequence homology. This peptide was removed from the peptide list and further analyses.

Chromatographic separation of the non-glycosylated and deglycosylated peptides

As described above, deamidation due to the deglycosylation leads to a mass increase by 0.98 Da and enables a chromatographic separation of the non-glycosylated and deglycosylated species of a peptide (Figure 40). Although, no change in sequence coverage was obtained for N80, the deglycosylation resulted in approximately three times higher signal intensity of the deglycosylated versus the non-glycosylated peptide (Figure 40). Consequently, more reliable HDX information were obtained for this region as well. However, in order to distinguish between the mass increases by HDX and deamidation a chromatographic separation is essential. In summary these experiments showed the feasibility of the introduction of a deglycosylation step into the established HDX-MS workflow and the benefits of it. Therefore, further experiments were conducted with the additional deglycosylation step using the PNGase Rc.

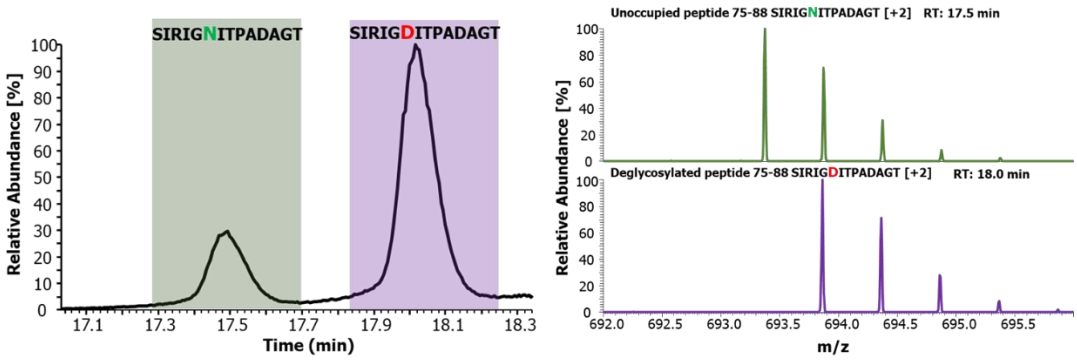

Figure 40: Extracted ion chromatogram of a SIRPα peptide (aa S75-T88) (left) and the summed m/z spectra of each peak (right) as published in [139]. *The deamidation of the amino acid asparagine caused by deglycosylation resulted in a mass increase of +0.98 Da and a chromatographic separation of the two peptide species*

5.3.3.3 Post-HDX Deglycosylation for Epitope Mapping

Epitope mapping was conducted according to the experiments on the RBD and a short (5 min) and prolonged (30 min) deuteration time point was chosen in order to detect fast and slow effects on the HDX kinetic of SIRPα caused by the Nbs (see also Figure A7). Proteolysis parameters as listed in Table 8 were used for each HDX-MS experiment. 114 peptides were used to extract HDX information yielding 86% sequence coverage.

Table 8: Summary of HDX conditions for epitope mapping of SIRPα

Experimental parameter	Conditions used
Deuteration buffer and temperature	1x PBS pH 7.4, 90% D_2O, 25 °C,
Deuteration time points	5 & 30 min
Proteolysis conditions	2 min on-ice, 30 µL pepsin beads
Deglycosylation conditions	2 min deglycosylation, 5 µL (4 µM) PNGase Rc
Reduction and denaturation conditions	100 mM TCEP; 4 M GdmCl
Back exchange determined by synthetic peptide mixture (see 5.1.4; 5 min)	25% (5-45%).

Back exchange examination of the HDX-MS post-HDX workflow

In order to estimate the additional back exchange, the intrinsic HDX of SIRPα was probed with and without additional deglycosylation. Thus, SIRPα HDX was determined in independent technical triplicate labelled for 5 and 30 min in D_2O with and without additional deglycosylation step (Figure 41a). The HDX was observed using 90 peptides. A minor decrease of the average peptide HDX of ~0.7 and ~1.2% after 5 and 30 min labelling was found, respectively. The slight increase in the back exchange is worth the ability to obtain additional

sequence coverage and redundancy and the detection of potential epitopes in proximity to N-glycan moieties.

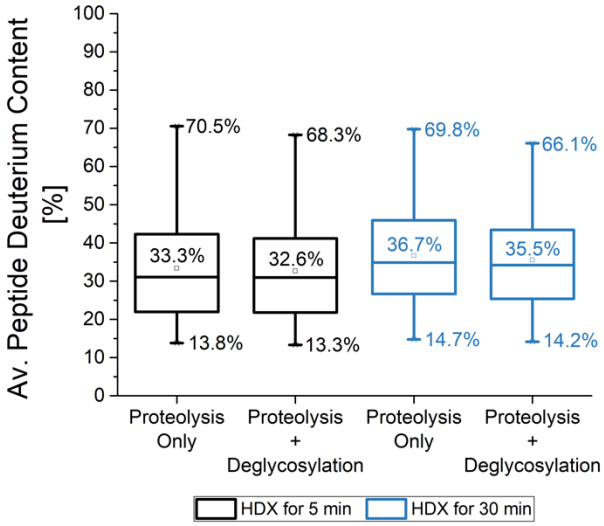

Figure 41: Deuterium uptake of SIRPα with and without additional deglycosylation for 2 min at 0 °C as published in [139]. *Average HDX of 90 peptic peptides obtained from SIRPα proteolysis determined in independent triplicates. The average, minimal and maximal observed HDX values are depicted.*

Binding kinetics

Within this case study the epitope of four Nbs were examined (Table 9). The Nb binding affinities were used to calculate the concentrations needed to ensure a high amount (≥95%) of bound receptor during HDX.

Table 9: Binding affinity of the individual Nbs chosen for HDX-MS epitope mapping. *Affinities were determined with BLI analysis by Teresa Wagner (Recombinant Antibody Technology Group, NMI, Germany).*

	K_D (nM)	k_{on} (10^5 M^{-1} s^{-1})	k_{off} (10^{-2} s^{-1})	R^2
Nb 01	19.96	6.16 ± 0.067	1.229 ± 0.004	0.972
Nb 02	0.46	20.43 ± 0.083	0.094 ± 0.000	0.992
Nb 03	25.88	4.92 ± 0.091	1.274 ± 0.008	0.913
Nb 04	0.12	15.19 ± 0.073	0.018 ± 0.000	0.995

Epitope mapping

HDX protection was analysed using similar HDX thresholds as used for the SARS-CoV-2 case study. In brief, a peptide was considered as protected, if it showed a ≥5% HDX difference between bound and unbound state. On the other hand, the peptide HDX was considered as unaffected by the Nb binding, if the difference between bound and unbound state was <3%. The determined HDX inhibition in SIRPα due to the different Nbs was mapped on the crystal structure a SIRPα (PDB ID: 2wng [133] Figure 42). This crystal structure showed a different subtype of SIRPα than subtype v1, used for HDX analysis. The sequence only differs in the sequence of domain 1 and showed 97% sequence identity determined by BLASTp. However, the observed HDX results were mapped with respect to the amino acid position.

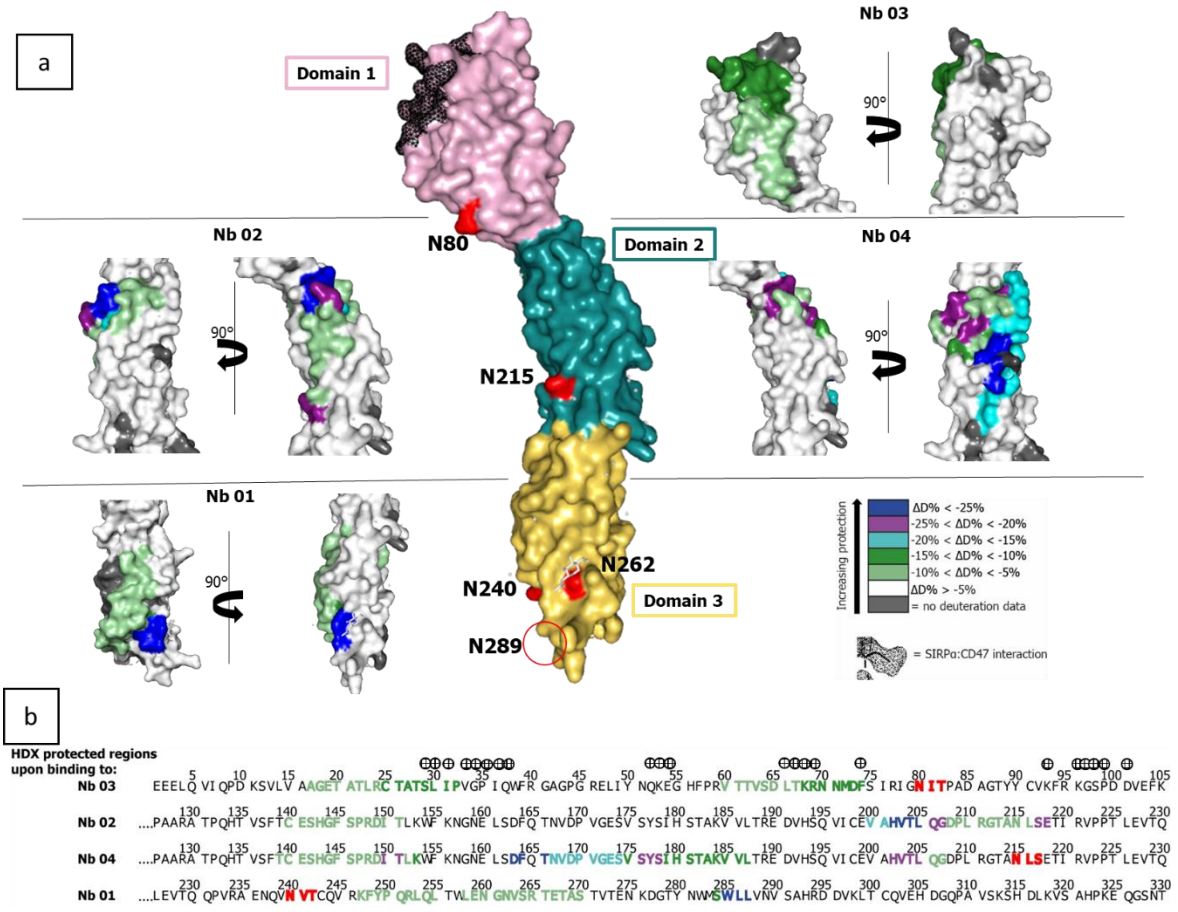

Figure 42: HDX-protected regions of SIRPα upon binding to different Nbs mapped on the surface structure model of the ECD (PDB ID: 2wng [133]). *(a) The middle panel shows SIRPα with coloured domains. The panels to the right and left showed the HDX protection of the different nanobodies mapped on the corresponding domains. The selected structure differs in the sequence of domain 1 with the subtype v1 used for HDX-MS. Asparagine residues with potential glycosylation are shown in red. N289 is not resolved in the X-ray structure and highlighted by a red circle. (b) HDX protected regions mapped in the primary sequence of SIRPα subtype v1. Direct and indirect contact residues of the SIRPα:CD4 [134] are denoted as dots over the sequence stretch of Nb 03.*

Binding of Nb 01 resulted in HDX reduction located in domain 3 within two regions (K247-S270, S284-L287) close to the glycosylated N240 and N262 residues (Figure 42). The elucidation of this binding site benefited from the deglycosylation that led to higher redundancy and additional sequence coverage to extract valuable HDX information. Thus, residues L226-R246 could be excluded from the binding interface showing no significant HDX-protection (Figure 41, Figure 42).

Incubation with Nb 02 and 04 cause HDX protection in domain 2 in residues C140-K153 and V200-G207. Furthermore, Nb 04 showed, high and unique HDX reduction in peptides covering residues D163-L187, suggesting an interaction with SIRPα opposed to the interaction with Nb 02. Both were in proximity to the glycosylation site N215 and also benefitted from deglycosylation.

SIRPα incubation with Nb 03 resulted in HDX protection within domain 1. However, HDX reduction with 5 and 30 min labelling time regime led to inconsistent results and for some peptides insignificant protection (<5%) using the applied HDX threshold. Notably, this nanobody shows the lowest affinity among the four analysed nanobodies (Table 9). Therefore, the HDX analysis was conducted with adjusted time points of 0.5 and 5 min (Figure 42).

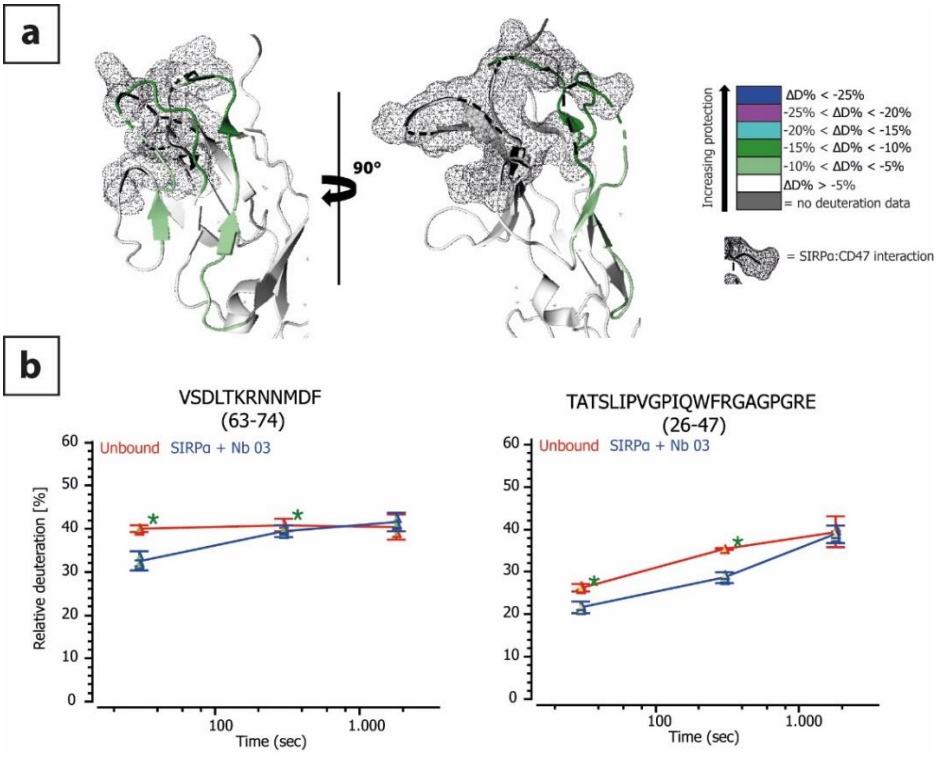

Figure 43: Epitope mapping results of Nb 03 mapped on the X-ray structure (PDB ID: 2wng [133]) (a) and the HDX kinetic example peptides belonging to the Nb 03 (b). *SIRPα:CD47 contact residues shown by a mesh structural model are based on [134]. Analysis was performed in technical replicates (n = 3) and the average HDX is plotted. Error bars show the 95% confidence interval. Asterisks show a significant differences based on the Student's t-test (p≤0.05).*

Consequently, two regions covering aa A17-P32 and V60-F74 showed a significance reduction in deuterium exchange upon binding. Regions with HDX protection by Nb 03 showed partial overlap of with residues of the CD47:SIRPα interface as described by Hatherley et al. [134] which might result in a potential competition for the binding to SIRPα (Figure 43). However, large parts of the CD47:SIRPα interface remained uncovered and the observed HDX reduction suggests an interaction opposed those of CD47 and SIRPα. As per consensus guidelines [74], epitope mapping HDX uptake plots of all peptides and epitope mapping experiments (Figure A20-23) and the HDX data table (Table A4) can be found in the appendix. A summary of HDX parameter for the epitope mapping is shown in Table 10. In summary, the HDX-MS epitope screening workflow could be successfully expanded by a deglycosylation step using the novel PNGase Rc post-HDX. This increased the sequence coverage, the peptide redundancy.

Table 10: Summary of HDX-MS parameters of epitope mapping of anti-SIRPα-Nbs as per consensus guidelines [74].

HDX parameters				
States	SIRPα & SIRPα bound by **Nb 01**	SIRPα & SIRPα bound by **Nb 02**	SIRPα & SIRPα bound by **Nb 03**	SIRPα & SIRPα bound by **Nb 04**
HDX reaction detail	1x PBS pH 7.4, 25 °C, 90% D_2O	1x PBS pH 7.4, 25 °C, 90% D_2O	1x PBS pH 7.4, 25 °C, 90% D_2O	1x PBS pH 7.4, 25 °C, 90% D_2O
Deuteration time points	5 & 30 min	5 & 30 min	0.5 & 5 min	5 & 30 min
Average peptide length (AA)	14.3 (s_d= 7.0)	14.2 (s_d = 6.6)	14.9 (s_d = 7.1)	14.3 (s_d = 6.7)
Average redundancy (AA)	4.2	4.4	4.4	4.3
Number of used peptides	102	108	104	105
Sequence coverage	83%	86%	86%	86%
$\Delta\overline{HX}$ threshold for each time point (p≤0.05)	0.22 Da	0.27 Da	0.22 Da	0.23 Da
$\Delta\overline{HX}$ threshold for each time point (p≤0.01)	0.37 Da	0.44 Da	0.36 Da	0.38 Da
Complexed SIRPα during labelling	94.7%	99.9%	95.9%	97.1%

Simultaneously binding of Nb 02 and Nb 04

Next, further characterization aimed to evaluate a potential competition on the SIRPα binding of Nbs 02 and 04. As determined by HDX-MS epitope mapping, both Nbs interact with domain 2 and showed HDX protection in common residues. However, the examined HDX-kinetic revealed differences in their binding behaviours for this region (V200-G207, Figure 44). While peptides covering this region showed high, persisting HDX protection for both time points upon binding to Nb 02, the HDX protection caused by Nb 04 was lost after labelling for 30 min (Figure 44a). Comparable K_Ds of both Nbs 0.46 (Nb 02) and 0.12 nM (Nb 04) suggested that differences in the HDX protection kinetics were not originated in their binding affinity. Furthermore, Nb 04 showed unique HDX protection on the opposite site of domain 2. This region, showed the highest HDX protection upon binding of this Nb, which also persisted with prolonged labelling (30 min) (Figure A23),

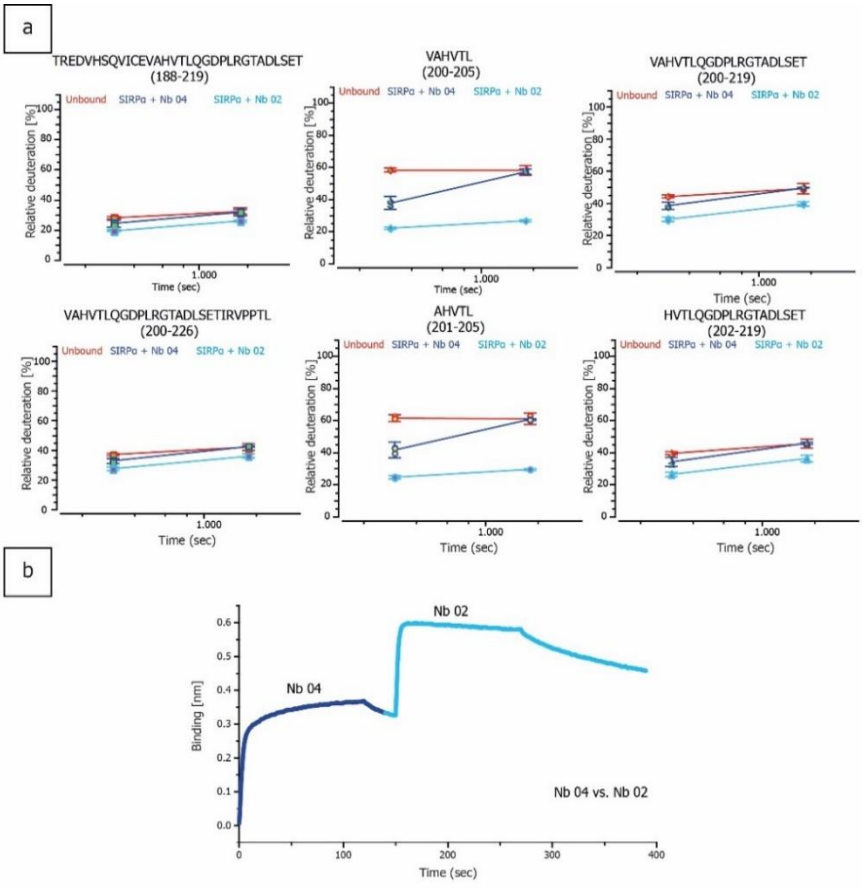

Figure 44: HDX kinetics of SIRPα:Nb 02 and SIRPα:Nb 04 for overlapping epitope regions despite simultaneous binding capability *(a) Relative deuterium uptake in overlapping epitope regions for Nb 02 and Nb 04. Error bars show 95% confidence level. (b) Biolayer interferometry (BLI) with consecutive binding of Nb 04 and Nb 02. SIRPα was biotinylated and immobilised on streptavidin sensors. 500 nM of Nb 04 was loaded first and the ongoing kinetic after 500 nM Nb 02 binding revealed that both Nbs could bind simultaneously.*

This suggested that these amino acids are not directly involved or involved with higher dynamic or lower affinity in the binding of Nb 04 compared to Nb 02. Thus, both Nbs might be able to bind simultaneously. This assumption could be confirmed by an epitope binning experiment, performed and kindly provided by Teresa Wagner (Recombinant Antibody Technology Group, NMI, Germany) (Figure 44b).

6 Discussion

6.1 Hydrogen-Deuterium Exchange Mass Spectrometry

HDX analyses require short analysis times with low temperature and pH throughout the experiment from quenching of the labelling reaction to the analysis by mass spectrometry [67]. Thus, the establishment of HDX-MS analysis protocols and a setup represents the first and most important. Within the first part of this thesis, a tailor-made semi-automated interface for HDX (SAIDE) and HPLC-MS method were established and validated. In combination with an optimised proteolysis protocol using immobilised pepsin on beads, HDX could be monitored on a high number of peptides with low back exchange, inter-, and intraday variance leading to a high reproducibility.

Since HDX-MS analyses got increasing attention over the last years, fully automated systems dedicated to HDX were developed from companies such as Waters Corp., ThermoFisher Scientific and LEAP technologies [92, 127, 154]. After empirical examination of the quench and digest conditions within a first, "feasibility" stage [107] these systems provide a fully automated sample preparation from labelling to injection followed by an online digestion with pepsin-packed columns and detection by HPLC-MS. Hence, automated analysis can lead to very low variance, increased reproducibility and higher throughput of HDX data acquisition [155-157]. However, if the number of samples in a laboratory does not justify the purchase of an independent HDX system in terms of space, investment and maintenance costs, it is very beneficial to use a flexible HDX module. It allows mounting and removal from an HPLC-MS instrumentation used for conventional chromatography as well. With handling expertise and using a standardized work flow, manual sample preparation (labelling, quenching and proteolysis) and analysis (e.g. injection, valve switching) can also lead to a high reproducibility [67, 136]. Moreover, manual off-line sample preparation offers advantages such as pooled sample preparation of an analysis campaign avoiding potential protein degradation [158] and the possibility of post-proteolysis sample preparation steps such as deglycosylation. To evaluate the HDX reproducibility with manual sample handling the protein Annexin-A1 was used. The established in-solution proteolysis approach using pepsin showed adequate HDX reproducibility low standard deviations. Using immobilized pepsin the proteolysis efficiency and subsequently the HDX reproducibility was improved and was comparable to automated HDX analysis of complex samples described by Hageman *et al.* [138]. However, both proteolysis approaches were suitable for epitope mapping of a therapeutic antibody targeting ANXA1 (see 7.3.3.1). Additionally, the proteolysis time could be reduced by 90% to only one minute with simultaneously slightly increasing number of identified peptides, peptide recovery and decreasing peptide length. This improvement in proteolytic efficiency is mainly achieved

through the increased enzyme to protein ratio compared to the in-solution approach [67]. Further improvement is reported to be achievable using the online digestion with a cartridge packed with immobilised pepsin [67]. Improvements in proteolysis efficiency are attributed to the applied pressure and reduced manual sample preparation [159]. However, online digestion requires a separate HPLC pump and off-line pepsin digestion is known to show less sample carry over [107, 160].

A low HDX intraday and interday variance of the herein described manual HDX workflow was confirmed for SIRPα. However, the comparison of two analysis campaigns measured nine weeks apart (interday variability) revealed a slight global shift in HDX. To avoid these shifts in the following epitope mapping experiments the unbound protein labelling was repeated for each analysis campaign.

Another important HDX-MS parameter, which needs to be controlled and monitored, is the loss of the deuterium label (back exchange) during the analysis [74, 161]. Using immobilized pepsin the average back exchange was improved compared to the in-solution digest. Full deuterium labelling of an intact, natively folded protein can be difficult, even when labelling in presence of denaturants [92, 162]. In order to avoid an overestimation of the back exchange, a fully deuterated mixture of standard peptides was used as well. Both approaches yielded a back exchange comparable to the one reported in literature of ~30% [161]. Furthermore, the achieved back exchange fulfilled the criteria of the community-based recommendations of performing HDX-MS experiments, which suggest to keep the back exchange to a minimum with only few peptides exceeding 50% [74]. However, even small reductions in the back exchange can improve the achievable HDX sensitivity. Typically peptide separation for HDX-MS analyses range from 5 to 20 minutes [67, 68, 96, 161, 163]. With the herein used chromatographic gradient a peptide separation was achieved after 20 min. Thus, further improvements on the back exchange might be achieved by shortened chromatographic run time which in contrast encourage peptide co-elution and low S/N values. This optimised HDX-MS workflow was used as generic starting point for the epitope mapping of different antigens.

6.2 Enzymatic Deglycosylation with the Novel Acidic PNGase Rc

Findings of this chapter were already discussed in [139]. PNGases are indispensable for characterization of protein glycosylation or for making proteins accessible to mass spectrometric and structural analysis [164-166]. Commercial PNGases, are sometimes inefficient in deglycosylation of natively folded proteins with multiple, complex or sterically inaccessible N-glycosylation sites. This can lead to low sequence coverage in bottom-up HPLC-MS experiments and failure to obtain an intact mass signal in top-down analysis. The here presented novel acidic PNGase from soil bacteria *Rudeae cellulosilytica* (Rc) was recombinantly expressed in *E.coli* with high yield and sufficient purity. The enzyme showed high activity with a broad N-glycan hydrolysis spectrum from peptides and intact proteins. The acidic pH optimum of PNGase Rc enabled a integration post-proteolysis under HDX quench additionally to the established HDX-MS workflow.

Peptide N-Glycanases differ in their substrate specificity in terms of the N-glycans they can hydrolyse and their susceptibility to protein conformation [101]. The nature of fucosylation of the core GlcNAc especially influence the enzymatic hydrolysis specificity. Of the widely used commercially available PNGase F and PNGase A, only the latter can hydrolyse N-glycan moieties with a α-1,3 core fucosylation [98]. While PNGase F can be recombinantly expressed in *E.coli*, expression of PNGase A is not possible in simple prokaryotes [98, 102]. Two acidic PNGase variants, isolated from *Terriglobus roseus* (Tr) [103] and *Dyella japonica* (Dj) [102] have been described recently. These enzymes exhibit a broad cleavage spectrum and improved working conditions [102, 103]. However, their availability is still limited as they were not produced on large scale, yet. The PNGase Rc presented here could be obtained by expression in *E. coli* and yields ~1.3 mg per 1 L of bacterial culture with sufficient purity. Compared to other acidic PNGases, PNGase Rc shows <50% sequence homology and encompass less disulphide bonds (Table 11)

Table 11: Determined sequence homology between the PNgase Rc and the recently published acidic PNGases Dj, Tr using BLASTp as published in [139].

	Rc	**Dj**	**Tr**
Rc	-	45%	47%
Dj	45%	-	47%
Tr	47%	47%	-

The PNGase Rc showed a broad N-glycan release spectrum included high-mannose and complex biantennary type N-glycans with α-1,3 and 1,6-fucosylation. This enables the hydrolysis of glycans as they occur on proteins of plants, mammals and invertebrates [167, 168]. Due to the higher deglycosylation activity compared to the widely used PNGase F, PNGase Rc might serve as valuable alternative for intact MS analysis of N-glycosylated biopharmaceuticals such as antibodies [164, 165]. Moreover, the data showed that the PNGase Rc is largely insensitive to the protein conformation. In particular, the enzyme showed an improved deglycosylation efficiency on natively folded RNase B, which was previously shown to be resistant to deglycosylation by PNGase F due to sterically hindrance [169]. This ability provides new applications such as deglycosylation of natively folded proteins prior to structural analyses such as X-ray crystallography or investigation of the influence of N-glycans on PPIs via biological assays.

Furthermore, the PNGase Rc displays a stable PNGase variant showing tolerance against reducing and denaturing agents. Under HDX quenching conditions, the enzyme retained ~80% of its activity in presence of 4 M urea and tolerated concentrations of 0.4 M TCEP or 1 M GdmCl. Due to its acidic pH optimum the improved activity, stability and broad cleavage specificity, the PNGase Rc is of special interest for HDX-MS analysis. This was demonstrated by the elucidation of four Nb epitopes targeting the multiple N-glycosylated extracellular receptor SIRPα (see 6.3.2).

6.3 Epitope Characterisation Case Studies

6.3.1 Annexin-A1: A Calcium-Binding Antigen

This study revealed the binding region of a mAb which is intended for clinical application binding exclusively to the calcium bound ANXA1.

The intrinsic deuteration kinetics of ANXA1 revealed a deuterium incorporation of ≥60% for peptides covering the N-terminus. This suggested an accessible and therefore expelled N-terminus from the ANXA1 core. To the best of author's knowledge this was the first report of HDX-MS measurements supporting the X-ray crystallographic results of an expelled N-terminus from the ANXA1 core after Ca^{2+} binding [150]. The N-terminal amino acids could only be resolved in apo state and are therefore missing in the published crystallographic structures of intact ANXA1 (Figure 30) [111, 149]. Furthermore, the intrinsic HDX kinetics of ANXA1 revealed a pattern of high and low deuteration in an alternating manner. This pattern correlates with the three-dimensional, crystallographic structure of ANXA1 consisting of 20 α-helices, whose aas show higher and lower solvent accessibility in an alternating behaviour (Figure 27, Figure 30). Moreover, this explains the relatively high initial deuteration of the core repeats I-IV (21%) within the first 30 s labelling, followed by a sluggish increase over time. With exception of repeat III, the core repeats showed high increase in deuterium uptake under denaturing conditions. The slow deuteration for peptides covering repeat III showed a similar uptake behaviour as the N-terminal peptides suggesting a higher flexibility of this core repeat. Hence, this suggests that repeat III showed higher accessibility to solvent (and antibody).

Upon antibody binding, the main inhibition from HDX was found in repeat III, which was further narrowed down to two regions showing deuteration difference of >40% differences (Figure 28). They consist of α-helices A and B/C, which undergo extensive structural changes upon calcium binding as determined by X-ray crystallography [111, 150]. Phe221; Leu225, Phe237 and Val268 form only in apo state a hydrophobic pocket harbouring the N-terminal domain [150]. These amino acids are exactly within the determined antibody binding region. In holo state, ANXA1 is activated and the N-terminus is released from the core and interactions with the plasma membrane or dimer formation are triggered [112]. A third region within repeat III showed protection of 20-40% that covers two amino acid patches belonging to the α-helices D and E. As shown by X-ray crystallography the α-helix D of repeat III is only present in holo-ANXA1 and becomes unstructured without calcium [150]. These conformational changes might prevent the antibody from binding to ANXA1 in apo state, supporting the findings of SPR analysis that showed no binding of the anti-ANXA1 antibody to that state. Therefore, the antibody specifically target the biological active from of ANXA1 making it an attractive therapeutic candidate. One of the possible applications could be the treatment of T-

cell mediated diseases reducing the concentration of holo-ANXA1. It has previously been shown that the T cell activation is impaired and differentiation of $CD4^+$ T-cells into Th2 cells is increase at low levels of holo-ANXA1 [118]. A reduction in the T-cell activity was already reported for the original, murine antibody [12]. For the antibody presented here, further experiments are required to investigate the influence of the binding on the biological function of ANXA1. [110]

6.3.2 SARS-CoV-2 - Receptor-Binding Domain (RBD): Method Throughput with Seven Nanobodies

In 2021, the SARS-CoV-2 pandemic has been evolving rapidly, hence higher throughput screening of multiple binding candidates to the RBD were demanded. As part of this study, the established HDX workflow of ANXA1 was adapted to screen multiple Nb interfaces. This led to the epitope elucidation of seven Nbs targeting the RBD of SARS-CoV-2, which were further compared to the RBD:ACE2 interface. The identified Nb binding interface of Nbs NM1226 and NM1230 were in good agreement with high resolution X-ray analysis.

Monitoring of HDX kinetics is generally recommended to be performed using labelling time points spanning four orders of magnitude [74]. Although a high sensitivity can be achieved using the recommended number of time points, Zhu *et al.* [170] recently demonstrated the benefits of a screening approach using two time points only. Herein, a similar approach was applied leading to an increased throughput by ~40% (127 to 79 h). As they can be analysed within one analysis campaign, this lowered the risk of protein degradation and inter-day variances between the individual Nb analyses [74, 158]. Selected Nbs for HDX analysis were previously grouped into several Nb-sets with respect to a similar binding behaviour determined by epitope binning experiments [46]. These were confirmed by HDX-MS analysis.

Epitope mapping revealed four Nbs (NM1221, 1222, 1230, 1224 and 1228) that displayed deuterium protection in residues overlapping with the ACE2:RBD interface. Furthermore, as shown in Wagner *et al.* [46], each of them showed neutralization potential for the virus and the RBD confirming the HDX-MS results. The examined HDX protected region of NM1223 did neither show overlapping residues nor neutralizing efficiency [46]. HDX analysis revealed no overlapping residues with the RBD:ACE2 interface of NM1226. Interestingly, the epitope showed a high overlap with the determined cryptic epitope of a SARS-CoV specific antibody CR3022 described by Yuan *et al.* [171]. This epitope is only present in the RBD “up”-configuration on the S-protein. Detailed epitope mapping via X-ray analysis was conducted for the most potent Nb candidates (NM1226 and NM1230) by Prof. Dr. Thilo Stehle and co-workers. The analysis revealed that the RBD:NM1226 binding led to steric collision that

prohibits the ACE2 recruitment resulting in a neutralisation of viral infection with wild-type SARS-CoV-2 [46].

X-ray epitope analysis of the Nbs NM1226 and NM1230 were in high accordance to the HDX data. If higher sensitivity is needed a wider time regime might be applied enabling the detection short lasting and accumulation of HDX protection effects [30, 172]. However, these experiments have shown that the modified, manual HDX-MS approach serves valuable throughput and sensitivity. To briefly summarize the outcomes of Wagner *et al.* [46], on basis of the neutralization, binding kinetic, X-ray and HDX-MS experiments synergistical Nbs NM1226 and 1230 were genetically fused to a biparatopic Nb (bipNb). This bipNb then was used to establish a high throughput multiplex assay (NeutrobodyPlex) for the determination of SARS-CoV-2 neutralizing antibody concentration in blood plasma samples of infected or vaccinated individuals [46].

6.3.3 Signal-Regulatory Protein Alpha (SIRPα): Epitope Mapping of Highly Glycosylated Target Proteins

Within this case study, the binding regions of four nanobodies targeting the highly glycosylated receptor SIRPα were elucidated using a modified epitope screening workflow. PNGase Rc was applied displaying the first routine in-solution implementation of an member of the acidic PNGases for epitope analysis. Sequence coverage and redundancy near N-glycan motifs could be increased using a deglycosylation step of only 2 min post-HDX under HDX quench conditions. This enabled the detection of four Nbs:SIRPα interfaces in their native conformation.

The implementation of a deglycosylation step post-HDX was first published by Jensen *et al.* using the PNGase A [65]. Recently, the same group expanded their protocols implementing the acidic PNGase Tr. They obtained almost complete sequence coverage of the model protein α1-antichymotrypsin encompassing five N-glycosylated sites [162]. However, no denaturation and reduction was applied for their HDX-MS analyses [162]. Denaturing and reducing agents such as urea, GdmCl and TCEP are required in most cases for proteolysis to improve protein sequence coverage, especially for proteins containing multiple disulphide bonds [67, 73, 107, 163]. While PNGase A shows an almost complete loss of activity in presence of these substances [65], the herein used PNGase Rc was added to the workflow without adaptations of the proteolysis conditions. Thus, reduction of all disulphide bonds of SIRPα was achieved. A significant increase in sequence coverage and redundancy of the peptides in proximity to the N-glycosylation sites was obtained.

The epitope mapping experiments revealed the interface region all four Nbs. For the elucidation of the binding interface of Nb 03, the labelling time points had to be adjusted since

observed difference were less significant in the initially selected time points. This behaviour might be a result of a high k_{off} rate in combination with the high intrinsic deuterium uptake (k_{ch}) of the binding region. Consequently, the binding is very dynamic and HDX might occur while the complex is released and before re-complexation (k_{on}) takes place [30, 172]. Notably, this behaviour was also found for other, also high-affinity binding Nbs at prolonged deuteration times within other projects on the RBD (see Figure A12, A13, A16 and A18 for NM1221; 1222; 1226; 1230, respectively). Thus, it might also be a result of the smaller binding interface of 600 - 800 $Å^2$ [24] compared to an antibody 1600 - 2300 $Å^2$ [22] or the extended CDR3 loop of Nbs that are known for their high flexibility [173] resulting in a higher entropy.

As shown for the recently published Nb set targeting CD4 [174], the here presented Nbs might be candidates for molecular imaging of immune cells such as macrophages. Since, Nb 03 showed some overlapping residues with the CD47:SIRPα interface [134], a competitive antagonism upon binding of the Nb and therefore a blocking of the interaction might be possible.

However, further evaluation is needed to clarify this behaviour since only a small overlap that was opposed to the CD47:SIRPα interface is determined by HDX-MS. The specificity of the Nbs towards other members of the SIRP family and other cell types remains another task as SIRPα is found on various other cell types such as dendritic cells, neurons or granulocytes [131].

7 Materials and Methods

7.1 Materials

7.1.1 Buffers

Table 12: Frequently used buffers

Buffer	Composition
PNGase F deglycosylation buffer, 7.5	100 mM TRIS adjusted to pH 7.5 with 1 M HCl
HEPES HDX buffer, pH 7.4 – stock (200X)	2 M HEPES 200 mM $CaCl_2$ Adjusted to pH 7.4 with 5 M NaOH
HEPES HDX buffer, pH 7.4 (1X)	10 mM HEPES pH 7.4 1 mM $CaCl_2$ 150 mM NaCl (from NaCL stock H_2O/D_2O) Diluted 1:200 from HEPES HDX buffer (200X) stock in H_2O/D_2O
HEPES equilibration buffer, pH 7.4	20 mM HEPES 2 mM $CaCl_2$ 150 mM NaCl (from NaCl stock H_2O)
NaCl stock (H_2O/D2O)	5 M NaCl diluted in H_2O or D_2O
PBS HDX buffer, pH 7.4 – stock (20X)	Ready to use PBS tablets, pH 7.4 solved to 20X in H_2O/D_2O
PBS HDX buffer, pH 7.4 (1X)	PBS HDX buffer stock diluted 1:10 (v/v) with H_2O /D_2O
Pepsin stock	100 µM porcine pepsin solved H_2O in acidified with 10 mM HCl (pH 4.4) Snap frozen aliquots were stored at -20 °C
Quenching buffer, pH 2.5	100 mM ammonium formate adjusted to pH 2.5 with 20% FA
PNGase Rc deglycosylation buffer, **pH 2.5** – stock	1M citric acid adjusted to pH 2.5 with 5 M NaOH
PNGase Rc deglycosylation buffer, **pH 2.5**	100 mM citric acid Diluted 1:10 from PNGase Rc deglycosylation buffer stock in H_2O
PNGase Rc deglycosylation buffer 02, **pH 3.5** – stock	1 M citric acid, adjusted to pH 3.5 with 5 M NaOH
PNGase Rc deglycosylation buffer 02, **pH 3.5**	100 mM Citric acid diluted 1:10 from PNGase Rc deglycosylation buffer 02 stock in H_2O

7.1.2 Commercial Proteins

Table 13: Commercial proteins for HDX and N-deglycosylation analyses

Protein	Supplier	Cat. No.
Fetuin from fetal calf serum	New England Biolabs, Ipswich MA, USA	P6042S
Horseradish peroxidase (HRP)	Sigma-Aldrich, Munich, Germany	P8125-5KU
Human SIRPα	ACROBiosystems, Newark, DE, USA	SIA-H5225
Ribonuclease B (RNase B) from bovine pancreas	New England Biolabs, Ipswich MA, USA	P7817S

7.1.3 Bio-, Chemicals and Reagents

Table 14: Biochemicals, Chemicals and Reagents

Substance	Manufacturer	Cat. No.
4-(2-hydroxyethyl)-1-piperazineethanesulfonic free acid (HEPES)	VWR Life Science, Darmstadt, Germany	0511
Acetonitrile, LCMS CHROMISOLV	Honeywell Riedel-de Haën, Seelze, Germany	34967
Acrylamide mix 30% (ROTIPORESE Gel 30)	Carl Roth, Karlsruhe Germany	3029.1
Ammonia solution (32%)	Carl Roth, Karlsruhe Germany	P093.2
Ammonium formate (AF)	Fluka, Munich, Germany	14266
Ammonium persulfate (APS)	Merck KGaA, Darmstadt, Germany	101200
Calcium chloride ($CaCl_2$)	Carl Roth, Karlsruhe, Germany	CN93.1
Citric acid	Fluka, Munich, Germany	27109
Deuterium oxide (99.9%)	Sigma-Aldrich, Munich, Germany	151882
Dithiothreitol (DTT)	Carl Roth, Karlsruhe Germany	6908.3
DNAseI	AppliChem GmbH, Darmstadt, Germany	APA3778
Ethylenediaminetetraacetic acid tetra sodium salt dihydrate (EDTA)	Sigma-Aldrich, Munich, Germany	ED4SS
Formic acid (FA)	Thermo Scientific, Schwerte, Germany	A117
Glycine	Carl Roth, Karlsruhe, Germany	0079.4
GST Trap resin	Life Technologies, Carlsbad, CA, USA	17-0766-01
Guanidine HCl (GdmCl)	Carl Roth, Karlsruhe, Germany	0037.2
Hydrogen chloride (HCl) 32% ROTIPURAN	Carl Roth, Karlsruhe, Germany	PO74.4

Substance	Manufacturer	Cat. No.
Immidazol	Carl Roth, Karlsruhe, Germany	X998
Iodoacetamide (IAA)	Sigma-Aldrich, Munich, Germany	I6125
isopropyl-β-D-thiogalactopyranoside (IPTG)	Carl Roth, Karlsruhe Germany	CN08
Kanamycin	Carl Roth, Karlsruhe Germany	T832
Lysozyme	AppliChem GmbH, Darmstadt, Germany	A4972.0010
Milk powder	Carl Roth, Karlsruhe Germany	T145.3
Natrium hydroxide (NaOH)	Carl Roth, Karlsruhe, Germany	6771.1
NuPAGE Antioxidant	Life Technologies, Carlsbad, CA, USA	NP0005
NuPAGE LDS sample buffer (4 X)	Life Technologies, Carlsbad, CA, USA	NP0008
NuPAGE MES SDS running buffer (20X)	Life Technologies, Carlsbad, CA, USA	NP0002
NuPAGE Sample Reducing Agent (10X)	Life Technologies, Carlsbad, CA, USA	NP0009
Phenylmethylsulfonylfluorid (PMSF)	Thermo Scientific, Schwerte, Germany	36978
Phosphate buffered saline (PBS, Gibco)	Life technologies, Paisley UK	14190094
Phosphate buffered saline (PBS, tablets)	Sigma-Aldrich, Munich, Germany	P4417
Pierce immobilized porcine pepsin	Thermo Scientific, Schwerte, Germany	20343
PNGase F from *F. meningosepticum*	R&D Systems, Wiesbaden, Germany	9109-GH
Porcine Pepsin (3497 U/mg)	Sigma-Aldrich, Munich, Germany	P6887
PreScission protease	GE Healthcare, Freiburg, Germany	27-0843-01
Protease-Inhibitor Mix B	SERVA Electrophoresis, Heidelberg, Germany	39105
Rapid PNGase F	New England Biolabs, Ipswich MA, USA	P0710S
Rapid PNGase F reducing buffer	New England Biolabs, Ipswich MA, USA	B0718S
Sodium chloride (NaCl)	Carl Roth, Karlsruhe, Germany	P029
Sodium dodecyl sulphate (SDS)	Sigma-Aldrich, Munich, Germany	2326.2
Technical buffer solution pH 2.00	Mettler Toledo, Columbus, USA	51350002
Technical buffer solution pH 4.01	Mettler Toledo, Columbus, USA	51350004
Technical buffer solution pH 7.00	Mettler Toledo, Columbus, USA	51350034
Technical buffer solution pH 9.21	Mettler Toledo, Columbus, USA	51350036
Terrific broth medium	Carl Roth, Karlsruhe, Germany	HP61
Tetramethylethylenediamine (TEMED)	Carl Roth, Karlsruhe, Germany	2367
Trifluoroacetic acid UPLC/MS Optigrade (TFA)	VWR Life Science, Darmstadt, Germany	84868.180
TRIS	Carl Roth, Karlsruhe Germany	AE15.1

Substance	Manufacturer	Cat. No.
Tris(2-carboxyethyl)phosphine (TCEP)	Carl Roth, Karlsruhe, Germany	HN95.2
Trypsin gold (MS-grade)	Promega, Madison, WI, USA	V5280
Urea	Carl Roth, Karlsruhe Germany	2317.2
Urea-d4 (98 atom %D)	Sigma-Aldrich, Munich, Germany	176087
Water, LCMS Ultra CHROMASOLV	Honeywell Riedel-de Haën, Germany	39253

7.1.4 Laboratory Equipment

Table 15: Laboratory equipment

Apparatus / Equipment	Manufacturer
20 µL stainless steel sample loop	Rheodyne, IDEX H&S, Rohnert Park, CA, USA
2-way-4-port valve	ViciValco, Schenkon, Switzerland
2-way-6-port valve (7725i, Rheodyne)	IDEX H&S, Rohnert Park, CA, USA
2-way-6-port valve (C1CF ViciValco)	ViciValco, Schenkon, Switzerland
ÄKTA pure 25 purification system	GE Healthcare Life Sciences, Chicago, USA
Biacore 3000 system	GE Healthcare, Freiburg, Germany
BLItz	Sartorius, Göttingen, Germany
Centrifuge 5415D	Eppendorf, Hamburg, Germany
Centrifuge 5430R	Eppendorf, Hamburg, Germany
Dry freezer Epsilon 1-4 LSC plus	Martin Christ Gefriertrocknungsanlagen, Osterode am Harz, Germany
Ice machine Scotman AF40	Frimont S.p.A., Pogliano Milanese, Italy
Injection Syringe (50µL), VALCO Liquid Syringe C-160	Machery-Nagel, Düren, Germany
Mass spectrometer, MaXis HD UHR q-TOF	Bruker, Bremen, Germany
Mass spectrometer, Orbitrap Eclipse Tribrid Instrument	Thermo Fisher Scientific, Dreieich, Germany
Mass spectrometer, QExactive	Thermo Fisher Scientific, Dreieich, Germany
Microcentrifuge MiniStar blueline	VWR Life Science, Darmstadt, Germany
MiniChiller 280 pump	Huber, Offenburg; Germany
Mixer, Vortex-Genie 2	Scientific Industries, Bohemia, USA
NanoDrop 2000C	Thermo Fisher Scientific, Waltham, USA
NuPAGE system	Life Technologies, Carlsbad, CA, USA
Octet RED96e	Sartorius, Göttingen, Germany
Odyssey imager	LI-COR Biosciences, Lincoln, NE, USA
PerfectBlue semi-dry electro blotter	VWR, Radnor PA, USA
pH-meter, 766 Calimatic	Knick, Berlin, Germany
Pipette 0.1–2.5 µL, Eppendorf Research plus	Eppendorf, Hamburg, Germany
Pipette 100–1000 µL, Eppendorf Res. plus	Eppendorf, Hamburg, Germany

Apparatus / Equipment	Manufacturer
Pipette 10–100 µL, Eppendorf Res. plus	Eppendorf, Hamburg, Germany
Pipette 20–200 µL, Eppendorf Res. plus	Eppendorf, Hamburg, Germany
Pipette 2–20 µL, Eppendorf Res. plus	Eppendorf, Hamburg, Germany
Pipette 50–5000 µL, Eppendorf Res. plus	Eppendorf, Hamburg, Germany
Refrigerated microcentrifuge 5417R	Eppendorf, Hamburg, Germany
SAIDE	MéCour Temperature Control, Groveland, MA, USA
Thermomixer C	Eppendorf, Hamburg, Germany
ThermoMixer, Comfort	Eppendorf, Hamburg, Germany
Thermologger, Trel-8	LogTag CiK Solutions, Karlsruhe, Germany
Typhoon TRIO	GE Healthcare, Freiburg, Germany
UltiMate 3000, RSLCnano	Thermo Fisher Scientific, Dreieich, Germany
Ultrasonic homogenisator, Sonopuls HD70	Bandelin, Berlin, Germany

7.1.5 Consumables

Only commercial suppliers of consumables with a source that could be decisive for the result of the experiments are included to the table.

Table 16: Consumables

Consumables	Manufacturer
Acclaim PepMap trapping column	Thermo Fisher Scientific, Waltham, USA
Acquity BEH C4 column	Waters GmbH, Eschborn, Germany
Acquity BEH M-Class C18 column	Waters GmbH, Eschborn, Germany
Acquity BEH VanGuard C18 guard column	Waters GmbH, Eschborn, Germany
Amersham Protran 0.45 µM nitrolcellulose blotting membrane	GE Healthcare, Freiburg, Germany
Amicon Ultra-15 10K centrifugal device	Merck KGaA, Darmstadt, Germany
Biacore CM5 chip	GE Health Care, Freiburg, Germany
Bio-Spin P-6 gel Tris-buffer columns	BioRad Laboratories GmbH, Feldkirchen, Germany
Blue BANDit dye	VWR Life Science, Darmstadt, Germany
Centri-Sep desalting columns	Princeton separations, Adelphia, NJ, USA
D-Tube Dialyzer	Merck Millipore, Massachusetts, US
Filter inlet, ultrafree MC centrifugal filter devices with durapore membrane (0.22 µm)	Merck Millipore, Darmstadt, Germany
Filter inlet, ultrafree MC centrifugal filter devices with durapore membrane (0.65 µm)	Merck Millipore, Darmstadt, Germany

Consumables	Manufacturer
Glutathione Sepharose 4B	GE Healthcare, Freiburg, Germany
GSTrap FF	GE Health Care, Freiburg, Germany
HiLoad 26/600 Superdex 75 pg column	Cytiva, Marlborough, MA US
HisTrap Columns	Cytiva, Marlborough, MA US
HiTrap desalting column	GE Health Care, Freiburg, Germany
MarvelXact capillary	IDEX H&S, Oak Harbor, WA, USA
NAP-5 columns	GE Healthcare, Freiburg, Germany
NuPAGE 4–12%, 12 Well, Bis-Tris gel	Life Technologies, Carlsbad, CA, USA
pH Strips (1.7-3.8)	Machery-Nagel, Düren, Germany
SeeBlue Plus2 pre-stained standard	Life Technologies, Carlsbad, CA, USA
Streptavidin coated biosensor tips (SA)	Sartorius, Göttingen, German
Streptavidin SAX biosensors	Sartorius, Göttingen, Germany
Zeba Spin Desalting Columns 7K MWCO	Fisher Scientific, Waltham, USA

7.1.6 Software

Table 17: Software

Software	Distributor
Adobe Illustrator CS5	Adobe Systems, San José, CA, USA
BIAevaluation v4.1	GE Healthcare, Freiburg, Germany
BLItzPro software	Sartorius, Göttingen, Germany
Bruker BioTools 3.2 SR6	Bruker Daltonic, Bremen, Germany
Bruker Compass DataAnaylsis v5.3	Bruker Daltonik, Bremen, Germany
Data Analysis HT 12.0 software	Sartorius, Göttingen, Germany
HDExaminer v2.5.1	Sierra Analytics, Modesto, CA, USA
Image Studio v4	LI-COR Biosciences, Lincoln, NE, USA
Mascot v2.3.02	Matrix Science LTD, London, UK
MaxEnt software	Bruker Daltonic, Bremen, Germany
Nanodrop 2000/2000c 1.5	Thermo Fisher Scientific, Waltham, USA
Origin 2015G Sr2	OriginLab, Northampton, USA
Proteome Discoverer v2.1.0.81	Thermo Fisher Scientific, Waltham, USA
PyMOL v2.0.7	Schrödinger, Portland, USA
R v4.2.1	R Consortium, Boston, USA
Xcalibur v4.1.31.9	Thermo Fisher Scientific, Waltham, USA

7.2 General Methods

7.2.1 Labelling Buffers

The use of glass electrodes for pH adjustment in D_2O leads to a 0.4 pH units lower pH readings in D_2O compared to H_2O ($pH/pD_{corrected} = pD_{read}+0.4$) [175].
Both herein used HDX labelling buffers were prepared as stock solution and either no (PBS) or pH adjustments in H_2O was performed (HEPES). Furthermore, the pH of the quenching solution and diluted labelling buffers were examined using pH stripes. Hence, the specified pH within the present work can be referred to as $pD_{corrected}$.

7.2.2 HPLC and MS Methods

7.2.2.1 Intact Protein Analysis

These methods are published in [110].
The LC-MS analysis for intact molecules was performed with a UHPLC system (UltiMate 3000, RSLCnano, Dionex GmbH) coupled to a Q-TOF type mass spectrometer (MaXis HD UHR q-TOF). Desalting and separation was achieved using reversed phase chromatography with an ACQUITY BEH C4 column (1 x 50 mm, particle: 1.7 µm, 300 Å). Proteins were separated using the HPLC method shown in Figure 45. Eluent A (EA): Water with 0.1% FA. Eluent B (EB): 100% MeCN with 0.1% (v/v) FA. After each injection, the column was washed two times by injecting 5 µL eluent A (EA) followed by LC elution with the same gradient. Within this thesis the parameter of the mass spectrometer were adapted to the size of the analysed molecules as followed:
Mass <100 kDa: Dry temperature: 200 °C, Capillary voltage 4500 V; nebulizer 1.8 bar; dry gas: 8 L/min; Funnel 1 RF 400 Vpp; Multipole RF 400 Vpp; quadrupole ion energy 4 eV;. Collision cell parameter: 8.0 eV; Collision RF 1800 Vpp; Transfer time 110 µs; Pre pulse storage 10 µs. Spectra rate was 1 Hz the m/z-range was adapted to the molecule.
Mass >100 kDa: Dry temperature: 200 °C, Capillary voltage 4500 V; nebulizer 1.8 bar; dry gas: 8 L/min; Funnel 1 RF 400 Vpp; Multipole RF 800 Vpp; isCID Energy 120 eV; quadrupole ion energy 5 eV; low mass 1000 m/z. Collision cell parameter: 10.0 eV; Collision RF 4000 Vpp; Transfer time 150 µs; Pre pulse storage 20 µs. Spectra rate was 0.5 Hz.
Data analysis of intact molecules was performed using Bruker Compass DataAnaylsis.

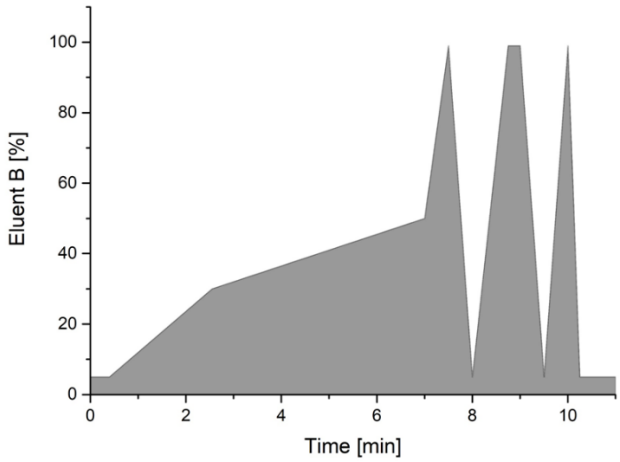

Figure 45: Linear step gradient of eluent B for analysis of intact molecules. *Flow rate: 150 µL/min. Temperature: 75 °C. Eluent A (EA): Water with 0.1% FA. Eluent B (EB): 100% MeCN with 0.1% (v/v) FA. Column: ACQUITY BEH C4; 1 x 50 mm, 1.7 µm, 300 Å particles. HPLC gradient: min 0-0.4, 5% EB; min 0.4-2.6, 5-30% EB, min 2.6-7, 30-50% EB; min 7-7.5, 50-99% EB, min 7.5-8, 99-5% EB, min 8-8.8, 5-99% EB, min 9-9.5, 99-5% EB, min 9.5-10, 5-99% EB, min 10-10.3, 99-5% EB, min 10.3-11, 5% EB.*

7.2.2.2 HDX-LC-MS Peptide Analysis

LC-MS method

The method is published in [46, 110]. HDX samples were analysed using a UHPLC system comprised of RSLC pumps (UltiMate 3000 RSLCnano, Thermo Fisher Scientific), and the SAIDE (see 7.3.1.1) coupled to a Q Exactive mass spectrometer. Separation at 0 °C (measured at the column) was achieved using a ACQUITY BEH C18 column (1 x 50 mm, particle 1.7 µm, 300 Å). Peptides were separated by a HPLC-Method including a two-step linear gradient (20 min) with a flow rate of 50 µL/min shown in Figure 46a. Eluent A (EA): water with 0.1% (v/v) FA. Eluent B (EB): 80% (v/v) MeCN with 0.1% (v/v) FA. Additionally, after each injection a wash method with altering high and low concentrations of eluent EB followed by the column equilibration (10 min) to 10% EB was applied (Figure 46b). MS parameter of the Q Exactive were: Resolution: 70,000; sheath gas flow rate of 25; aux gas flow rate of 5; S-lens RF level: 50, spray voltage: 3.5 kV; capillary temperature: 300 °C; AGC target: 3e+06; maximum injection time: 100 ms. For peptide identification using MSMS HCD fragmentation was applied with following parameters: Resolution: 17.500; AGC target 3e+06 maximum injection time: 250 ms; loop count: 3; TopN: 3; isolation window: 2.0 m/z; fragmentation energy: nce: 25; intensity threshold 1.2e+04; charge state exclusion for: unassigned; ≥8; dynamic exclusion: 10 s.

Valve cleaning

Prior to column equilibration (wash gradient, Figure 46) the 6-port valve was rinsed in both positions (Load, Inject) with 1 mL 8% (v/v) MeCN + 0.1% (v/v) FA followed by 1 mL EB and again with 1 mL 8%(v/v) MeCN + 0.1% (v/v) FA using borosilicate glass syringe. The isolated SAIDE:MS connection was flushed ~5 min with 10% EB (0 °C) prior to each injection.

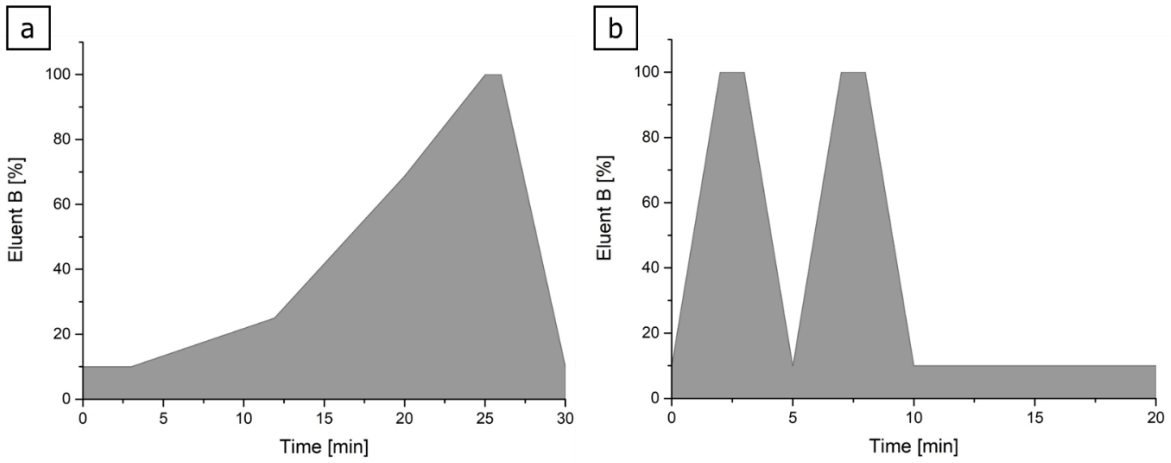

Figure 46: HDX gradient (a) with additional wash and equilibration method (b). *Flow rate: 50 µL/min. Temperature: 0 °C. Eluent A (EA): Water with 0.1% (v/v) FA. Eluent B (EB): 80% (v/v) MeCN with 0.1% (v/v) FA; column: ACQUITY BEH C18, 1 x 50 mm, particle 1.7 µ(m, 300 Å. (a) 30 min stepwise linear gradient for separation of the peptides. HPLC gradient: min 0-3, 10% EB; min 3-11.9, 10-25% EB, min 11.9-20, 25-68.8% EB; min 20-25, 68.8-100% EB, min 26-30, 100-10% EB. (b) The method was run after each separation gradient. This method included the washing of the system followed by 10 min equilibration at 10% eluent B. HPLC gradient: min 0-2, 10-100% EB; min 3-5, 100-10% EB, min 5-7, 10-100% EB; min 8-10, 100-10% EB, min 10-20, 10% EB*

7.2.3 Pepsin Preparation

Immobilized pepsin beads (agarose resin) were prepared freshly prior to each digestion. 50% slurry pepsin beads (50% glycerol in 0.1 M sodium acetate; pH 4.5, and 0.05% sodium azide) were transferred into a tube and washed by dilution in 16 times (v/v) the volume of ice-cold quenching buffer (pH 2.5). Diluted beads were centrifuged at 1000 x g for 3 min at 0 °C and supernatant was discarded. This step was repeated and the settled beads were resolved in an equal volume of quenching buffer. Filter inlets were washed with 100 µL quenching buffer and centrifugation for 3 min at 1000 x g and the filter inlet were placed into a new tube.
Prior to initiation of the proteolysis, beads were centrifuged at 1000 x g for 3 min at 0 °C and the supernatant was discarded.

7.2.4 HDX Data Analysis

Generation of the peptide list and HDX analysis

The principles of the used data analysis already is published in [46, 110]. Using the MSMS experiments (see 7.2.2.2) a peptic peptide list containing peptide sequence, retention time, and charge state was generated. Peptide identification was conducted using Proteome Discoverer with SEQUEST HT search engine. Peptides were identified by mass of precursor ions (tolerance 6 ppm) and their fragment ion spectrum (tolerance 0.05 Da) using protein database contained at least the sequence of the protein of interest and porcine pepsin. No enzyme selectivity was applied and the identified peptides were manually evaluated. Peptides originated through cleavage after arginine, histidine, lysine, proline were excluded [79]. Percolator was used to estimate a FDR calculate and only peptides with high-confident identification (cut-off q-value ≤ 0.01) were kept in the HDX peptide list. Auto proteolytic pepsin peptides interfering with the antigen peptides in mass, retention time and charge were removed manually. Unique peptides deriving from the proteolysis antibody were examined by another LC-MSMS experiment with digestion of the antibody alone and under the same conditions used for the HDX proteolysis. Interfering peptides were removed on the same criteria as described above. The HDX data was recorded in MS1 mode only and were analysed with HDExaminer. HDX was calculated based on the centroid mass shift, which was compared to a non-deuterated control. The relative exchange of a peptide was calculated by dividing the obtained deuterium uptake (Da) by the maximum of exchangeable deuterium. The latter is the number of amino acids of a certain peptide except proline and the first two N-terminal amino acids since they showed a rapid back exchange [66]. The assignment and the spectra quality was checked manually and only peptides that could be analysed at least within two of three samples were included. Unless stated otherwise statistical analysis using the HDExaminer were based on α=0.05 and no back exchange correction was applied. The $\Delta\overline{HX}$ threshold was calculated by HDExaminer with the equations published by Hageman *et al.* [138] using the variance of the replicates. Depicting of H/D exchange data on X-ray crystallographic structures were conducted using PyMOL. [46, 110].

7.2.5 Examination of Peptide Carry Over

Carry over was monitored for each molecule by another LC-MSMS elution gradient with after (see 7.2.2.2) performed after the washing gradient. Potential eluting peptides were identified by Proteome Discoverer using MSMS analysis (see 7.2.4 and 7.3.3.1 for ANXA1). Additionally, HDExaminer was used to detect peptide carry over using EICs to determine intensities. Peptides were excluded from the HDX peptide list if they were identified by

ProteomeDiscoverer or showed >10% of the initially intensity of the previous injection by HDExaminer.

7.3 Project Specific

7.3.1 HDX-LC-MS Setup and Validation

7.3.1.1 Semi-Automated Interface for H/D exchange (SAIDE)

The cooling device (SAIDE) was tailor-made from MéCour Temperature Control according to Villar *et al.* [136]. The chamber (17x23x23 cm, HxWxL) was temperature-controlled by constant flow of propylene glycol (40%) chilled to -4 °C through tubes inside the wall of the chamber using a MiniChiller 280 pump. A 2-way-6-port valve (7725i, Rheodyne) and a 2-way-4-port valve were mounted through the bottom of the device. The eluents were pumped through the cooling loop (stainless steel capillary; 0.1 x 150 mm) that was connected to the 6-port valve equipped with a 20 µL stainless steel sample loop. The 6-port valve was connected with the column by a MarvelXact stainless steel capillary.

7.3.1.2 Peptic Proteolysis

ANXA1 (see 7.3.3.1, 41.1 µM) was diluted 1:1 (v/v) with HEPES equilibration buffer (pH 7.4) and incubated for 10 min at 20 °C. The pre-incubated ANXA1 was diluted 1:10 (v/v) in HEPES HDX buffer (1X, H_2O, pH 7.4) and after incubation for 30 sec at 20 °C aliquots of 20 µL were taken and quenched by adding 1:1 (v/v) ice-cold quenching solution (0.4 M TCEP and 0.8 M guanidine HCl dissolved quenching buffer, pH 2.2) resulting in a final pH of 2.5. Samples immediately were snap-frozen in liquid nitrogen and stored until analysis at -80 °C. Prior to injection, aliquots were thawed and 0.45 µL pepsin stock (pH 4.4) was added to the quenched samples. The digest was performed for 5 and 10 min in a water-ice bath (0 °C) or for 2 min at 20 °C using a thermo shaker. Samples were prepared and analysed in single measurements. The preparation and comparison of the bead-based and in-solution digest and HDX results were described within the case study analysis of ANXA1 in 7.3.3.1.

7.3.1.3 Verification of the Deuteration Back Exchange

Parts of this method are published in [110]. A mixture of 14 synthetic peptides (Intavis, Tübingen, Germany) was generated (Table 2). A stock solution was prepared containing 1 mg/mL of each peptide. Aliquots of 1 µL of the stock solution were diluted 1:10 (v/v) in PBS HDX buffer (1X, H_2O; pH 7.4), snap frozen (liq. nitrogen), freeze-dried (Figure 47) and stored at -20 °C. Deuteration was initiated adding 10 µL, 99.9% D_2O to an aliquot. After incubation overnight at 20 °C, deuteration was quenched by adding 10 µL ice cold quenching solution

(200 mM TCEP with 1.5% (v/v) FA and 4 M guanidine HCl dissolved in quenching buffer, pH 2.2) and samples immediately were snap frozen (liq. nitrogen) and stored at -80 °C until injection. For analysis samples were thawed and either injected immediately (0 min), incubated in a water-ice bath (~0 °C) for 2, 5, 10 or 20 min or at 20 °C for 2 or 10 min. After incubation, samples were injected into the SAIDE and analysed in MS mode as shown in 7.2.2.2 samples were prepared in triplicate. [110]

Fully deuterated samples of ANXA1 were generated as described in 7.3.3.1. Only peptides with identical sequence were used to compare the back exchange of the in-solution- and bead-based digest. Samples were prepared in triplicate and analysed using HDExaminer. Deuterium uptake was normalized to the theoretical exchangeable backbone amides. Since the ANXA1 peptide contain only 90% D_2O during labelling, these 90% of the theoretically exchangeable backbone protons were considered as fully deuterated. Every loss of deuterium from the theoretical calculated maximum was defined as back exchange.

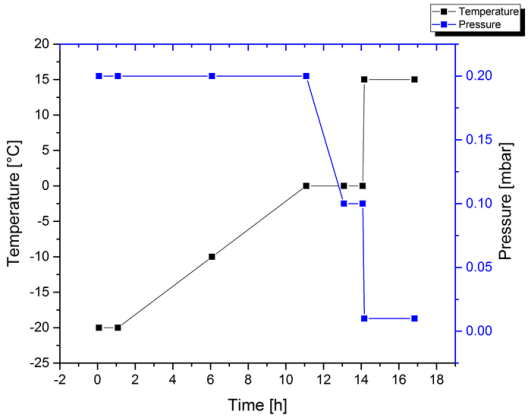

Figure 47: Freeze-drying method. *Aliquots were snap frozen (liq. nitrogen) and placed on a chilled shelve. Method duration = 17 h.*

7.3.1.4 Intraday and Interday Variability

HDX of SIRPα was measured as shown in 7.3.3.3. Here, the intraday variability corresponds to the variability between the samples of one analysis campaign. The interday variability, corresponding to the variability between two analysis campaigns. It was assessed by repeating the labelling and analysis of the same protein (SIRPα) after nine weeks. In between these campaigns, the SAIDE was removed and its temperature control was released. Labelling was performed for 5 min and 30 min. The analysis was performed using the deglycosylation workflow (see 7.3.3.3). However, to avoid additional HDX variance, peptides containing an N-glycosylation were excluded from the analysis. Differences between both campaigns were identified using a hybrid approach at α=0.05 including the $\Delta\overline{HX}$ threshold and p-values (Student's t-test).

7.3.2 Enzymatic Deglycosylation with a Novel Acidic PNGase

Parts of this section are published in [139].

7.3.2.1 Expression of the PNGase Rc

Expression and purification of PNGase Rc was performed by Dr. Philipp D. Kaiser (Recombinant Antibody Technology Group, NMI, Germany). Nucleic acid coding for amino acids 17-581 of peptide-N(4)-(N-acetyl-β-glucosaminyl)asparagine amidase from *Rudaea cellulosilytica* (Rc; UniParc ID UPI00146EBC6F) was synthesised with termination codon using *E. coli* codon usage and ligated into KpnI and NotI sites of pET30a(+) (Genscript Ltd. Nanjing, China) *E.coli* expression vector. *E.coli* strain BL21 (DE3) (New England Biolabs, Ipswich MA, USA) was transformed by the expression plasmid containing an open reading frame for PNGase Rc fused to N-terminal His_6-Tag. Three individual colonies were picked from a selection agar plate containing 50 µg/mL Kanamycin to inoculate 240 mL terrific broth medium. After overnight cultivation at 37 °C and 125 rpm, bacteria were centrifuged using 20000 x g at 4 °C, resuspended in 1 L fresh cultivation medium and grown until an optical density of 0,8 at 600 nm was reached. Protein expression was induced by adding 0.1 mM isopropyl-β-D-thiogalactopyranoside (IPTG) to the medium. The culture was further incubated overnight at room temperature under constant stirring. Bacterial mass was centrifuged at 6000 x g and 4 °C and resupended in 30 mL 1 X PBS (Life technologies, Paisley UK) supplemented with 363 mM NaCl, 50 mM imidazole and 1 mM PMSF. After one freeze and thaw cycle, bacterial cells were disrupted by pulsed sonication for 12 min (cycle 50%) in the presence of Protease-Inhibitor Mix B, 60000 units Lysozyme and 6000 Kunitz units DNAseI in a cooled stainless steel cup under constant mixing. The suspension was incubated by end-over-end rotation at 4 °C for 90 min before sonication was repeated. After centrifugation at 20000 x g and 4 °C the soluble extract was loaded onto a 1 mL HisTrap to purify PNGase Rc by immobilised metal affinity chromatography using ÄKTA pure 25 purification system. To dealt and increase protein purity subsequent size exclusion chromatography of the eluted protein peak fractions was performed on a HiLoad 26/600 Superdex 75 pg column using PBS as buffer. The protein peak was concentrated using an Amicon Ultra-15 10 K centrifugal device. Quality of the purification process was assessed by SDS-PAGE using a 12% gel stained by Coomassie as well as by western blotting (Table 18). For western blot analysis, proteins separated by 12% SDS-PAGE were transferred onto a Amersham Protran 0.45 µm nitrolcellulose blotting membrane using a PerfectBlue semi-dry electro blotter at 200 mA for 90 min. The blotted membrane was blocked with TBST substituted with 5% milk powder (M-TBST) and incubated with a penta His antibody (QIAGEN, Hilden, Germany) at 1/1000 dilution in M-TBST overnight at 4 °C. The membrane was washed 3 times for 5 min with TBST before a secondary anti-mouse antibody

labelled with alexa 647 (Thermo Fisher Scientific, Waltham, USA) was added for detection. After 1 h incubation at RT, the membrane was washed as described above and dried before the signals were detected with a 633 nm laser and 670 BP emission filter using a Typhoon TRIO. Aliquots of 50 µL of the PNGase were taken and snap frozen in liquid nitrogen and stored at -80 °C. [139]

Table 18: Composition of the 12% SDS gel.

2 x SDS	4% Stacking gel	12% Separation gel
H_2O [mL]	1.4	3.3
30 % Acrylamide mix [mL]	0.33	4.0
1.5 M Tris pH 8.8 [mL]	-	2.5
1.0 M Tris pH 6.8 [mL]	0.25	-
10% SDS [mL]	0.02	0.1
10% APS [mL]	0.02	0.1
TEMED [mL]	0.002	0.004

7.3.2.2 Examination of the PNGase Activity and Optimal Reaction pH and Temperature

PNGase activity

5 mg/mL trastuzumab in 20 mM histidine buffer (150 mM NaCl; pH 6.0) was kindly provided by MABDiscovery (Neuried, Germany).

The deglycosylation activity of the novel recombinant PNGase Rc and recombinant PNGase F from *F. meningosepticum* were compared. A typical sample of 50 µL consisted of 5 µL trastuzumab (5 mg/mL) and 40 µL, PNGase Rc deglycosylation buffer (pH 2.5) or PNGase F deglycosylation buffer (pH 7.5). Deglycosylation was initiated by adding 5 µL, 0.78 µM of each enzyme diluted in the corresponding buffer achieving a molar enzyme to substrate ratio (E:S) of 1:44. Samples were incubated in a thermo shaker for 2.5, 5, 10, 20 and 40 min at 37 °C. Aliquots of 10 µL were quenched by 5 min heat-denaturation at 95 °C or acidification by adding 10 µL, 1% (v/v) formic acid (FA, resulting pH = 2.3) for PNGase Rc or PNGase F, respectively. Samples were immediately snap frozen in liquid nitrogen and stored at -80 °C until injection into the HPLC-MS system. [139]

Temperature and pH-optimum

Temperature- and pH-optimum of PNGase Rc were tested using the same method as described above. Temperature optimum was determined by incubation for 10 min in a thermo shaker at 20, 30, 37, 50, 60 and 70 °C and pH 2.5 (PNGase Rc deglycosylation buffer). Additionally, one sample were incubated on-ice (4 °C). For determination of the pH-optimum samples of trastuzumab were diluted in 100 mM Glycine HCl buffer pH 2.0 or PNGase Rc deglycosylation buffer with pH 2.5; 3; 3.5; 4; 4.5 or 5. Samples were incubated for 10 min at 37 °C.

After incubation, deglycosylation of 10 µL aliquots were quenched by incubation at 95 °C for 5 min. Samples were immediately snap frozen in liquid nitrogen and stored at -80 °C until injection into the HPLC-MS system. [139]

Data analysis

For analysis samples were thawed and HPLC-MS analysis was conducted as described in 7.2.2.1 with an injection volume of 3 µL (1.5 µg antibody). Spectra of the eluting antibody peak were summed and resulting m/z spectra were charge-deconvoluted using the MaxEnt software. Parameter: 100.000 – 155.000 Da, data point spacing auto, instrument resolving power 10.000.

7.3.2.3 Native Protein Deglycosylation and N-glycan Specificity

Native protein deglycosylation of 20 µL (2 mg/mL) protein stock solutions of HRP (45.5 µM), RNase B (117.7 µM) or fetuin (41.3 µM) were carried out by adding 70 µL, PNGase Rc deglycosylation buffer 02 (pH 3.5) or PNGase F deglycosylation buffer (pH 7.5), for PNGase Rc or PNGase F, respectively. By adding 10 µL diluted PNGase deglycosylation was initiated using a molar E:S of 1:48. Samples were incubated for 0.5, 1, 3, 6 and 23 h at 37 °C and aliquots of 19.5 µL were quenched by adding 3 µL 10X sample reducing agent and 7.5 µL 4 X LDS sample buffer. Aliquots were immediately heat-denatured for 5 min at 95 °C. The acidic pH of the samples prepared with PNGase Rc was neutralized using 10% ammonia prior analysis. SDS-PAGE analysis was performed using the commercial NuPAGE system with a 4–12%, 12 Well, Bis-Tris gel according to the manufacturer's protocol. Thus, 15 µL of each sample was and 5 µL molecular marker (SeeBlue Plus2 pre-stained standard) was loaded onto the gel. A negative control was prepared according to the protocol for the PNGase Rc and the enzyme was replaced by the same volume of water. Blue BANDit dye was added and incubated for 60 min to visualise the protein bands followed by overnight destaining in doubled distilled water. [139]

7.3.2.4 PNGase Rc Deglycosylation within the HDX-Workflow

Preparation of the tryptic antibody digest

A protein preparation for the tryptic digest was performed as published in [176]. Thus, 50 µL (250 µg) trastuzumab was denatured and reduced by adding 190 µL denaturation buffer (400 mM Tris HCl, 8 M GdmCl, pH 8) and 20 µL 0.24 M dithiothreitol (DTT) diluted in denaturation buffer. After incubation at 37 °C for 60 min, 20 µL 0.6 M iodacetamid (IAA) was added for alkylation of the cysteine residues. After incubation for 15 min at RT, 20 µL 0.24 M DTT was added and the buffer was exchanged using NAP-5 columns. The column was equilibrated with digestion buffer (50 mM Tris HCl buffer pH 7.5) and subsequently the sample was loaded onto the columns, washed with 350 µL digestion buffer. The flow through was discarded and the sample was eluted with 482 µL digestion buffer. Proteolysis was initiated by adding 20 µL of 0.25 µg/µL trypsin gold and incubated overnight at 37 °C. Proteolysis was quenched by adding 20 µL 10% FA (v/v) resulting in a pH of 2.5.

Deglycosylation under HDX conditions at peptide level

Peptide deglycosylation was performed in a 40 µL sample volume. This consisted of 10 µL of the tryptic antibody digest, 5 µl of PNGase Rc of various concentrations (1-4 µM) diluted in PNGase Rc deglycosylation buffer, 4 µL PNGase Rc deglycosylation buffer stock, 1 µL H_2O and additional 20 µL PNGase Rc deglycosylation buffer. To assess the PNGase Rc tolerance against denaturing and reducing agents 5 µL 4 µM PNGase Rc was used. Furthermore, the 20 µL of PNGase Rc deglycosylation buffer was replaced by a mixture of the same buffer with varying concentration of TCEP, urea or GdmCl stock solutions to achieve final concentrations of 100-400 mM, 1-4 M and 1-4 M, respectively. Denaturants (GdmCl, urea) were prepared as 8 M stock solutions dissolved in quenching buffer. TCEP was prepared as 1 M stock solution dissolved in H_2O and the pH was adjusted to pH 2.5 using ammonia. Deglycosylation was performed for 2 min in a water-ice bath (~0 °C) and samples were subsequently snap frozen (liq. nitrogen) and stored at -80 °C until analysis by HPLC-MS.

HPLC-MS analysis

Samples were thawed and immediately 1 µL of each sample was analysed by an UltiMate 3000 RSLCnano system coupled to an Orbitrap Eclipse Tribrid Instrument. Injected samples were trapped on an Acclaim PepMap trapping column (C18, 5 x 0.3 mm, 5 µm particle size, 100 Å pore size) for 0.25 min at a flow rate of 120 µL/min with 2% (v/v) MeCN and 0.05% (v/v) trifluoroacetic acid (TFA) as solvent. The valve was switched to the analytical column and peptides were separated using an Acquity BEH M-Class C18 column (150 x 0.075 mm, 1.7 µm particle size, 130 Å pore size). Peptides were separated by a nano HPLC gradient shown in

Figure 48a followed by a column wash gradient (Figure 48b). MS and MSMS analysis were performed with 120,000 and 30,000 resolution using the orbitrap of the Orbitrap Eclipse Tribrid Instrument, respectively. Instrument configurations were used as follows: m/z: 200-2000; positive ion spray voltage of 2.1 kV and an ion transfer tube temperature of 275 °C. [139]

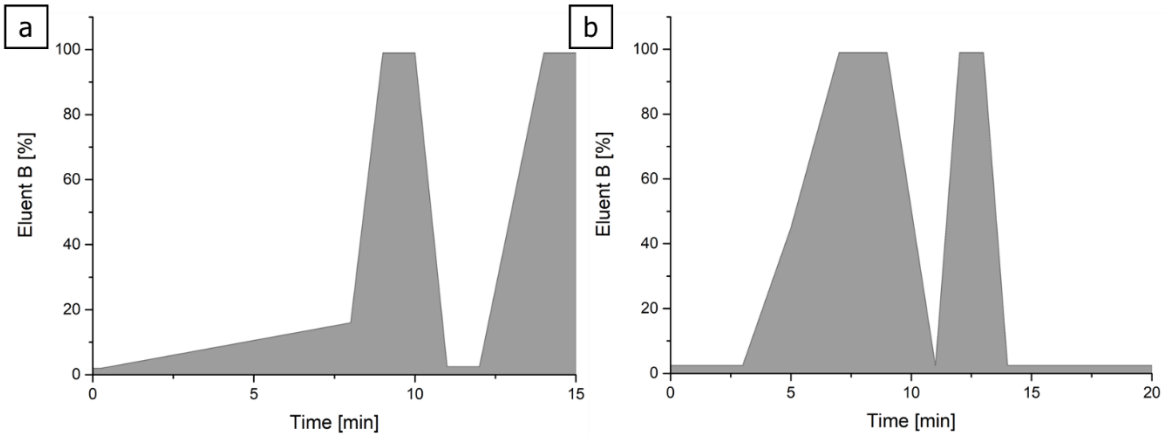

Figure 48: Nano HPLC gradient for the PNGase activity test under HDX-MS conditions (a) and a column-wash method (b). *Eluent A (EA): 0.1% (v/v) FA, eluent B (EB): 80% (v/v) MeCN and 0.1% (v/v) FA. Column oven temperature: 50 °C. Flow rate: 0.6 µL/min. (a). HPLC gradient: min 0-0.25, 2% EB; min 0.25-8, 2-16% EB, min 8-9, 16-99% EB; min 10-11, 99-2.5% EB, min 12-14, 2.5-99% EB. (b) Method was run after each separation gradient. HPLC gradient: min 0-3, 2.5% EB; min 3-5, 2.5-45% EB, min 5-7, 45-99% EB; min 9-11, 99-2.5% EB, min 11-12, 2.5-99% EB, min 13-14, 99-2.5% EB.*

Table 19: Included N-Glycosylated and deglycosylated masses of trastuzumab peptide species EICs (EEQYNSTYR) monitoring the deglycosylation efficiency. According to [139]

N-Glycosylation	Charge	m/z
A2G0F	3	878.64 - 880.40
A2G1F	3	932.66 - 934.43
A2G2F	3	986.67 - 988.45
A2G0F	2	1317.48 - 1320.09
A2G1F	2	1398.52 - 1401.12
A2G2F	2	1479.53 - 1482.14
Deglycosylated	2	595.70 - 597.31
Deglycosylated	1	1190.45 - 1193.55

7.3.3 Case Studies

7.3.3.1 Annexin-A1: A Calcium-Binding Antigen

ANXA1 expression and purification

ANXA1 was produced and purified by Dr. Philipp D. Kaiser (Recombinant Antibody Technology Group, NMI, Germany) [110].

ANXA1 cDNA was cloned into pGEX-6P-1 expression vector and was expressed in *E. coli* BL21 (DE3) as GST-ANXA1 fusion protein. Purification from soluble *E.coli* extract was conducted by GSTrap FF affinity chromatography according to the manufacturer's instructions. Buffer was exchanged to PreScission protease cleavage buffer via HiTrap desalting column, and subsequently PreScission protease was used to release the GST tag. The tag was removed by a combination of affinity capture using Glutathione Sepharose 4B and incubation with GST Trap resin. The buffer was exchanged to 20 mM HEPES pH 6.0, 150 mM NaCl by dialysis using D-Tube Dialyzer and purified ANXA1 (1.6 mg/mL) was stored at -80 °C. Purity and integrity of the recombinant ANXA1 were determined by SDS PAGE via Coomassie staining and mass spectrometry. [110]

Antibody expression and preparation

The anti-ANXA1 antibody was provided by MedAnnex (Edinburgh, Scotland) as published [110]. As described in the patent [120] the human monoclonal IgG1 was humanized from a murine IgG2b antibody generated by genetic immunisation with human ANXA1. Potential sequence instabilities within the CDR regions [121] were removed due to sequence optimisation and the presented antibody was produced in a Chinese hamster ovary (CHO) cell line based transient expression system. The formulation buffer of PBS was exchanged to 20 mM HEPES buffer containing 150 mM NaCl and 2 mM $CaCl_2$ using Centri-Sep desalting columns as the manufacturer's protocol described. A final concentration of 5.4 µg/µL (36.6 µM) was achieved.

Binding affinity determined by surface plasmon resonance (SPR)

SPR interaction analysis was performed on a Biacore 3000 system. A purified goat anti-human IgG Fc capturing antibody (Jackson ImmunoResearch Laboratories, Cambridgeshire, UK) was immobilised on a CM5 chip using amino coupling chemistry at a level of 13000 response units (RU). Binding experiments were conducted at 25 °C in HEPES-buffered saline (10 mM HEPES, 150 mM NaCl, 3.4 mM EDTA or 1 mM $CaCl_2$, and 0.05% (v/v) P20 surfactant). First, the anti-ANXA1 IgG was captured by the anti-human IgG to achieve a binding level of 300 (±50) RU at a concentration of 7 nM with a pulse of 60 sec at a flow rate of 10 µL/min. The binding kinetic

was collected at five individual ANXA1 concentrations of 25, 12.5, 6.25, 3.125 and 1.563 nM, in presence (1 mM $CaCl_2$) or absence (3.4 mM EDTA) of calcium through all flow cells (association). Analyte association was performed for 5 min followed by a dissociation phase in buffer for 10 minutes at 30 µL/min flow rate. The sensor surface was regenerated by 8 min injections of 10 mM glycine HCl, pH 2.0 at a flow rate of 10 µL/min followed by 5 sec injections of 50 mM NaOH at a flow rate of 60 µL/min. Data was fitted to a 1:1 binding with drifting baseline by BIAevaluation 4.1 software. [110]

Hydrogen-deuterium exchange

5 µl, 41.1 µM ANXA1 was either incubated with 5 µl, 36.6 µM anti-ANXA1 antibody or HEPES equilibration buffer (pH 7.4) for 10 min at 20 °C. Deuterium exchange of the complex was initiated by a 1:10 dilution (v/v) with HEPES HDX buffer (1X, D_2O pH 7.4). Ag:Ab (antigen:antibody) ratio was calculated according to Kochert *et al.* [72] using the equilibrium dissociation constant (K_D) of 2.66 nM ensuring a minimum of 89% complex formation. After incubation for 0.5, 5, 50, 500 min and 24 h at 20 °C, aliquots were quenched by adding 1:1 (v/v) ice-cold quenching solution (0.4 M TCEP and 0.8 M guanidine HCl dissolved in quenching buffer, pH 2.2) resulting in a final pH of 2.5. Samples were immediately snap-frozen in liquid nitrogen and stored until analysis at -80 °C. Samples for the proteolysis protocol using immobilized pepsin were deuterated for 5 and 500 min and prepared as described above. Prior to injection, aliquots were thawed and either 0.45 µL pepsin stock (pH 4.4) was added to the quenched samples (in-solution digest) or the samples were added to 20 µL settled pepsin gel (bead-based digest). Proteolysis in-solution and bead-based were performed in a water-ice bath for 10 or 1 min, respectively (Figure 49). Samples of the in-solution digest were injected immediately into the LC-MS system. Samples digested with immobilized pepsin were separated from the bead prior to injection via 0.22 µm filter inlet and centrifugation at 1000 x g for 30 s at 0 °C. Non-deuterated samples of ANXA1 and ANXA1:Ab complexes were prepared under the same conditions using buffers prepared with H_2O instead of D_2O. All experiments were performed in independent triplicates. [110]

Full deuteration labelling was attempted using a 50 mM HEPES buffer at pH 7.4 containing 150 mM NaCl, 1 mM $CaCl_2$ and 6 M urea-d4 prepared with in D_2O. Samples were incubated for 24 h at 20 °C and quenched by adding 1:1 (v/v) ice-cold quenching solution (0.2 M TCEP dissolved in quenching buffer, pH 2.6) to pH 3.0. Digestion and analysis were performed as described above. [110]

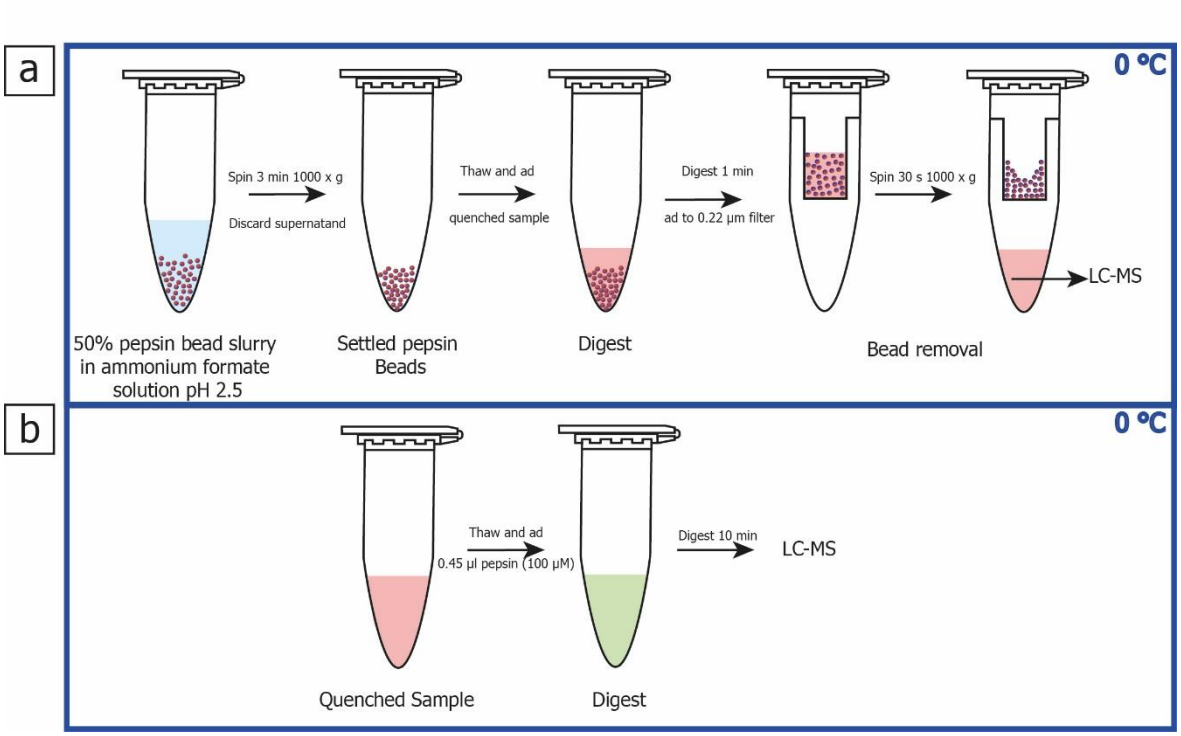

Figure 49: Schematic workflow of peptic digest using (a) immobilized pepsin or (b) pepsin in-solution. **HDX Data Analysis**

LC-MS data acquisition and analysis of HDX samples was performed as described above (see 7.2.2.2). Database search of the peptides was performed using Proteome Discoverer with Mascot search engine. The database contained the sequence of ANXA1, the anti-ANXA1 antibody and porcine pepsin. ANXA1 peptides overlapping with antibody peptides were removed according to criteria reported above (see 7.2.2.2). Samples were analysed using HDExaminer. The significant differences of the peptide deuterium uptake plots were calculated by Student's t-test ($p \leq 0.05$). The global $\Delta\overline{HX}$ threshold ($\alpha=0.05$) as calculated by HDExaminer was 0.64 Da or 0.25 Da for the in-solution and bead-based HDX analysis, respectively. The residual plot significance line was calculated with the determined $\Delta\overline{HX}$ threshold multiplied by the time points used. Normalized to the average peptide length. For the heat map calculation via HDExaminer, peptides were considered on the basis of residual plot significance criteria. [110]

7.3.3.2 SARS-CoV-2 - Receptor-Binding Domain (RBD): Method Throughput with Seven Nanobodies

Antigen characterization

10 µL RBD (38.4 µM) was mixed with the 5X rapid PNGase reducing buffer and incubated for 5 min at 80 °C. Deglycosylation was initiated adding 0.3 µL rapid PNGase F and the sample was incubated for 10 min at 50 °C, diluted 1:5 (v/v) with water and analysed subsequently using the intact protein analysis described in (see 7.2.2.1) with an injection volume of 4 µL (0.64 µg RBD).

Generation of the RBD specific peptide list and deuteration kinetics

The receptor-binding domain (RBD, UniProtKB, PODTC2, Spike SARS-CoV-2, aa 319-541) was expressed and purified by the group of Recombinant Antibody Technology (NMI, Germany) as published in [46].

To improve the peptide list of RBD the proteolysis was performed with different protocols (Table 20) and the identified peptides were combined to one list. Thus, different concentrations of the RBD were mixed 1:1 (v/v) with PBS pH 7.4 and incubated for 10 min at 25 °C. Samples were diluted 1:10 (v/v) in PBS HDX buffer (1X, pH 7.4) prepared with water and incubated for 30 sec at 25 °C. After incubation 15 µL aliquots were taken and quenched by adding 15 µL ice-cold quenching solution. Quenching solution was either 200 mM TCEP with 1.5% formic acid and 4 M guanidine HCl dissolved in quenching solution, pH 2.2, resulting in an final pH of 2.5 (low TCEP quench) or 400 mM TCEP and 4 M guanidine HCl dissolved in quenching solution, pH 2.1, leading to an final pH of 2.3 (high TCEP quench). Quenched samples were snap-frozen in liquid nitrogen and stored at -80 °C until injection. Different volumes of settled pepsin beads were prepared as described above (see 7.2.3). Aliquots were thawed and added either directly to the beads or were incubated in a thermo shaker at 20 °C for 60 sec in order to improve the disulphide bond reduction. Proteolysis was performed for additional 2 min and beads were removed by centrifugation at 1,000 x g for 30 sec at 0 °C via a 0.22 µm filter inlet. Samples were injected immediately into the HPLC-MS. Higher injection volume (full loop injection, 3X sample loop volume) was achieved by taking incubated aliquots of 30 µL that were quenched by 30 µL ice-cold quenching (Low quenching solution) solution and the same protocol using 20 µL settled pepsin gel was applied. All samples were analysed and identified using the method described in 7.2.2.2 and 7.2.4, respectively.

Table 20: Digestion and quench condition for high sequence coverage peptide identification of the RBD.

Concentration RBD	Quenching conditions 1:1 (v/v)	Additional reduction/ digest conditions	Amount of beads	Replicates
38.4 µM	Low TCEP Quench#	1 min 20 °C/ 2 min 0 °C;	20 µL	2
38.4 µM	High TCEP Quench#	1 min 20 °C/ 2 min 0 °C;	20 µL	1
73.0 µM	Low TCEP Quench*	- /2 min 0 °C;	20 µL	2
73.0 µM (Full loop injection)	Low TCEP Quench*	- /2 min 0 °C;	20 µL	1
73.0 µM	Low TCEP Quench*	- /2 min 0 °C;	30 µL	1

*200 mM TCEP, 1.5% formic acid; 4 M GdmCl dissolved in quenching buffer, pH 2.2

#400 mM TCEP; 4 M GdmCl in 100 mM dissolved in quenching buffer, pH 2.1

Uptake kinetic

The above described protocol using 38.4 µM RBD and the included 60 sec reduction step at 20 °C was used to determine the deuteration uptake kinetic of RBD. Deuteration was conducted for 0.5; 5; 10 and 500 min and 24 h at 25 °C and were performed in duplicate. HDX was extracted for 112 peptic peptides.

Nb affinity determination via biolayer interferometry (BLI)

Analysis of the binding affinity of purified Nbs (K_D) targeting RBD was determined via BLItz by Teresa Wagner (Recombinant Antibody Technology Group, NMI, Germany) as per manufacturer's protocols and published in Wagner *et al.* [46]. In brief, biotinylated RBDs were immobilized on high precision streptavidin SAX biosensors and the affinity for each Nb was examined with four sequentially diluted concentrations ranging from 15.625 to 500 nM. The chosen concentrations were adapted to the binding strength of the individual Nbs. A reference with PBS instead of Nb was conducted and a negative control with 500 nM non-binding GFP-Nb was measured. Data was analysed using the of BLItzPro software. [46]

Epitope analysis of seven Nbs targeting RBD

This method is published in [46]. Nanobodies were provided by the group of Recombinant Antibody Technology (NMI, Germany) and were produced and purified as published in [46]. HDX samples were prepared using 5 µL RBD (73 µM) that was either incubated with 2.5 µL PBS HDX buffer (1X, H_2O, pH 7.4) or a RBD-specific Nb (~2.5 mg/mL in PBS) at 25 °C for 10 min.

HDX of the pre-incubated complex was initiated by a 1:10 (v/v) dilution with PBS HDX buffer (1X, D_2O, pH 7.4). On basis of the pre-determined affinity constant of the seven Nbs (1.37 nM (NM1228), 3.66 nM (NM1226), 3.82 nM (NM1223), 22.70 nM (NM1221), 17.96 nM (NM1222); 8.23 nM (NM1230), and 8.34 nM (NM1224)) [46] a minimum complex formation of 90% was calculated according to Kochert *et al.* [72]. On the basis of the kinetic experiment deuteration for 5 and 50 min were chosen for epitope mapping. Experiments were performed in independent triplicates. Deuterium exchange was performed at 25 °C with a final D_2O concentration of 90%. After incubation 15 µL aliquots were quenched by adding 15 µL ice-cold quenching solution (200 mM TCEP with 1.5% formic acid and 4 M guanidine HCl dissolved in quenching solution, pH 2.2), immediately snap frozen (liq. nitrogen) and stored at -80 °C until measurement. The resulting pH of the quenched samples was 2.5. Immobilized pepsin was prepared as shown in 7.2.3. Prior to MS analysis aliquots were thawed and added to 30 µL settled pepsin gel. Proteolysis was performed for 2 min in a water ice bath and beads were removed by centrifugation at 1,000 x g for 30 sec at 0 °C using a 0.22 µm filter inlet. Samples were injected immediately into a LC-MS system (see 7.2.2.2). Buffers for the non-deuterated control samples were prepared using H_2O. A separate peptide list was generated for each Nb, respectively. Thus, the same proteolysis protocol was applied for the Nbs without addition of RBD. This list was screened for peptides overlapping in charge, sequence and retention time with peptides of the RBD. Similar peptides were removed from both lists. Samples were analysed using the LC-MS method described in 7.2.2.2.

Data analysis

General aspects of the data analysis were already described in 7.2.4. HDX analysis for a minimum of 79% of the RBD amino acid sequence was achieved. The deuterium uptake (Da) of each peptide was normalized to the exchangeable backbone protons and compared between RBD alone and in complex. To detect meaningful differences in HDX the average $\Delta\overline{HX}$ threshold in combination the average length of the peptides was used to calculate a global minimal detectable difference (%D). Peptides HDX differences below the defined threshold of 3% (α=0.05)), are defined as non-protected upon Nb binding. If the difference crossed the higher threshold of 5% (α=0.01)), a peptide was considered as protected.

7.3.3.3 Signal-Regulatory Protein Alpha (SIRPα): Integration of Post-HDX De-Glycosylation in Analysis

Parts of this section is already published in [139].

SIRPα preparation

To remove cryoprotectants from human SIRPα a buffer exchange into PBS was performed by Teresa Wagner (Recombinant Antibody Technology Group, NMI, Germany) using Zeba Spin Desalting Columns 7K MWCO according to the manufacturer's protocol. Columns were equilibrated with PBS followed by sample loading and centrifugation at 1500 x g for 2 min. From the flow through, the desalted human SIRPα was then collected. [139]

Intact antigen deglycosylation

2 µL SIRPα (40.2 µM) was diluted 1:10 (v/v) either with PBS pH 7.4 (PNGase F) or 100 mM citrate-NaOH buffer pH 2.5 (PNGase Rc). Deglycosylation was initiated by adding 0.5 µl, 3.6 µM PNGase to achieve a E:S ratio of 1:45 (M:M). Samples were incubated overnight at 37 °C and analysed subsequently using the intact protein analysis described in (7.2.2.1) with an injection volume of 8 µL (1.2 µg SIRPα). [139]

Determination of the micro- and macroheterogeneity of SIRPα

15 µL SIRPα (1.5 mg/mL) was denatured and reduced by adding 56 µL denaturation buffer (400 mM Tris HCl, pH 8; 8 M GdmCl) and 5 µL 0.24 M dithiothreitol and incubation for 1 h at 37 °C. Afterwards, cysteines were alkylated adding 5 µL 0.6 M iodoacetamide (incubated for 15 min at room temperature). The buffer was exchanged using Bio-Spin P-6 gel Tris-buffer columns as per the manufacturer's protocol.

SIRPα was proteolysed by adding 2 µL trypsin (0.25 µg/µL, E:S 1:50) and overnight incubation at 37 °C. Samples were analysed using the setup described in 7.3.2.4. Peptides were separated by a nano HPLC gradient shown in Figure 50a followed by a column wash gradient (Figure 50b). Using the orbitrap mass analyser of the Orbitrap Eclipse Tribrid instrument, samples were analysed by MS and MS/MS at 120,000 and 30,000 resolution, respectively. Determination of the N-glycans was performed using the software BioPharma Finder (mass tolerances, MS = 6 ppm, MS/MS = 0.05 Da). [139]

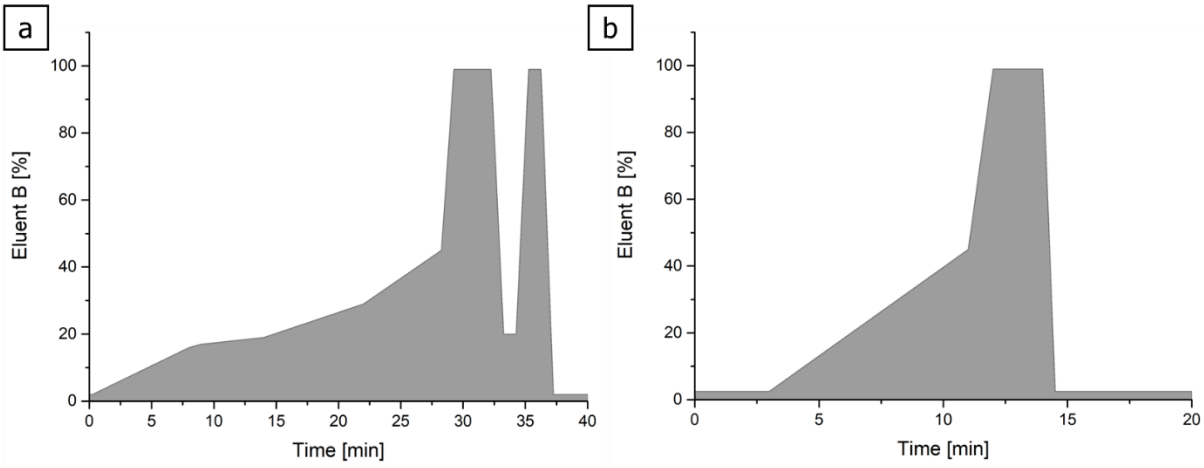

Figure 50: Nano HPLC gradient for the determination of SIRPα N-glycosylation micro- and macroheterogeneity (a) and a column-wash method (b). *Eluent A (EA): 0.1% (v/v) FA, eluent B (EB): 80% (v/v) MeCN and 0.1% (v/v) FA. Column oven temperature: 50 °C. Flow rate: 0.6 µL/min. (a). HPLC gradient: min 0-0.25, 2% EB; min 0.25-8, 2-16% EB, min 8-9, 16-17% EB; min 9-14, 17-19% EB, min 14-22, 19-29% EB, min 22-28.25, 29-45% EB, min 28.25-29.25, 45-99% EB, min 32.25-33.25, 99-20% EB, min 34.25-35.25, 20-99% EB, min 36.25-37.25, 99-2% EB. (b) Method was run after each separation gradient. HPLC gradient: min 0-3, 2.5% EB; min 3-11, 2.5-45% EB, min 11-12, 45-99% EB; min 14-14.5, 99-2.5% EB..*

Biophysical biolayer interferometry (BLI)

Analysis of the binding affinity of purified Nbs (K_D) targeting SIRPα was determined via Octet RED96e by Teresa Wagner (Recombinant Antibody Technology Group, NMI, Germany). Analysis was performed as per the manufacturer's protocol. In brief, SIRPα was biotinylated and immobilized on streptavidin coated biosensor tips (SA). The Nb concentrations were adapted according to their binding affinity ranging from 0.625 – 160 nM diluted in Octet buffer (PBS, 0.1% BSA, 0.02% Tween20) and a global fit was performed using four different Nb concentrations. For each run a reference sample was analysed using Octet buffer instead of the Nb within the association step. For affinity determination, the 1:1 global fit of Data Analysis HT 12.0 Software was used to examine k_{on}; k_{off} and subsequently the K_D of the different nanobodies. To identify shared epitopes of the different Nbs, epitope binning was performed by Teresa Wagner (Recombinant Antibody Technology Group, NMI, Germany) using the BLItz system. After immobilization of biotinylated SIRPα via streptavidin binding the different Nbs were subsequently loaded on the tip. Therefore, first 500 nM of Nb 04 were associated, followed by a short washing step and loading of the second Nb 02 (500 nM).

Generation of the SIRPα specific peptide list and deuteration kinetics

SIRPα was handled in a similar manner to the established workflow used for RBD for higher method throughput (Figure 51). In brief, 5 µL SIRPα (42 µM) was mixed with 2.5 µL PBS HDX buffer (1X, H_2O, pH 7.4) and incubated for 10 min at 25 °C. Samples were diluted 1:10 (v/v) in

PBS HDX buffer (1X, H_2O, pH 7.4) and incubated for 30 sec at 25 °C. After incubation 15 µL aliquots were taken and quenched by adding 15 µL ice-cold quenching solution (200 mM TCEP with 1.5% formic acid and 4 M guanidine HCl dissolved in quenching buffer, pH 2.2), immediately snap frozen in liquid nitrogen and stored at -80 °C. Prior to analysis aliquots were thawed, added to 30 µL settled pepsin gel (see 7.2.3) and digested for 2 min in a water-ice bath. Beads of the non-deglycosylated aliquots were removed by centrifugation at 1,000 x g for 30 sec at 0 °C using a 0.65 µm filter inlet and injected immediately into the LC-MS system. For additional deglycosylation 5 µL (4 µM) PNGase Rc in quenching buffer was placed in a tube underneath a 0.65 µm filter inlet and deglycosylation initiated by centrifugation (1,000 x g, 30 sec, 0 °C). Deglycosylation was performed for additional 2 min at 0 °C. Samples were analysed using LC-MSMS as described above (see 7.2.2.2 and 7.2.4). Deamidation at asparagine residues was included as dynamic modification for peptide identification. Experiments were performed in independent triplicate and a combined peptide list was generated. In order to increase the resulting peptide pool alternative preparation approaches were applied (Table 21) according to the experiments on the RBD and additional 20 peptic peptides were included to the list for HDX. [139]

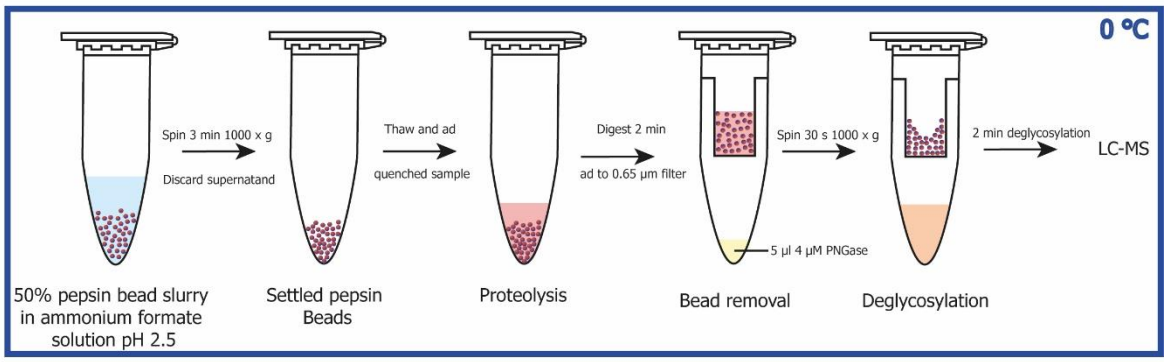

Figure 51: Scheme of the workflow for SIRPα bead-based digest with integrated deglycosylation as published in [139]. *Quenched samples were added to 30 µL settled pepsin beads and digested for 2 min at 0 °C. Beads were removed by centrifugation using a 0.65 µm filter inlet and deglycosylation subsequently was started. Samples were injected and analysed by LC-MS after 2 min of deglycosylation at 0 °C with 5 µL, 4 µM PNGase Rc.*

Table 21: Digestion, quenching and deglycosylation conditions for SIRPα.

Quenching conditions 1:1 (v/v)	Digest conditions 30 µL settled pepsin gel	Deglycosylation 4 µM PNGase Rc
Low TCEP Quench*	2 min 0 °C	No Deglycosylation
Low TCEP Quench*	5 min 0 °C	No Deglycosylation
Low TCEP Quench*	5 min 0 °C	2 min 0°C
High TCEP Quench#	5 min 0 °C	No Deglycosylation
High TCEP Quench#	2 min 0 °C	2 min 0°C

*200 mM TCEP, 1.5% formic acid ;4 M GdmCl dissolved in quenching buffer, pH 2.2

#400 mM TCEP; 4 M GdmCl dissolved in quenching buffer, pH 2.1

Epitope analysis of four Nbs targeting SIRPα

Epitope mapping was performed for four Nbs (01-04) provided by the group of Recombinant Antibody Technology (NMI, Germany) with concentrations of 90 µM (Nb 01), 103 µM (Nb 02), 99 µM (Nb 03) and 78 µM (Nb 04) (Wagner *et al.* manuscript in preparation). HDX samples were prepared using 5 µL SIRPα (42 µM) that was either incubated with 2.5 µL PBS HDX buffer (1X, H_2O, pH 7.4) or a SIRPα-specific Nb in PBS at 25 °C for 10 min. HDX of the pre-incubated complex was initiated by 1:10 (v/v) dilution with PBS HDX buffer (1X, D_2O, pH 7.4). After incubation for 5 and 30 min aliquots of 15 µL and quenched by adding 15 µL ice cold quenching solution (200 mM TCEP, 1.5% formic acid and 4 M guanidine HCl dissolved in quenching buffer, pH 2.2) leading to an final pH of 2.5. Samples immediately were snap frozen in liquid nitrogen and stored at -80 °C until injection. SIRPα:Nb03 complexes were incubated for 0.5 and 5 min and quenched as described above. Deuteration of the unbound SIRPα alone was performed for 0.5; 5 and 30 min in independent triplicates.

Digest and deglycosylation of the quenched samples were performed as described above for acquisition of the deuteration kinetic (Figure 51) and the sample were analysed as described in 7.2.3 and 7.2.4 the column was equipped with a VanGuard column (2.1 x 5 mm, particle: 1.7 µm; 130 Å). Epitope criteria of 7.3.3.2 were adapted to SIRPα. [139]

Data analysis

The principle of the data analysis already was described in 7.2.4. HDX analysis for a minimum of 83% of the SIRPα amino acid sequence was achieved. The deuterium uptake (Da) of each peptide was normalized to the exchangeable backbone protons and compared between SIRPα alone and in complex. To detect meaningful differences in HDX the average $\Delta\overline{HX}$ threshold in combination the average length of the peptides was used to calculate a global minimal detectable difference (%D). Summed peptide HDX differences below the defined threshold of

3% ($p \leq 0.05$) are defined as non-protected upon Nb binding. If the difference was ≥5% ($p \leq 0.01$), a peptide was considered as protected.

8 Outlook

This work successfully addressed the development of a generic HDX-MS setup and workflow for the elucidation of various protein-protein interactions. Furthermore, the deglycosylation workflow using the novel PNGase Rc facilitated the analysis of highly N-glycosylated and disulphide bonded proteins via HDX-MS. While this work was focussing on the elucidation of protein-protein interactions, the workflow might be expanded for other applications such as the detection of conformational changes and protein-ligand interactions. Moreover, the present workflow might be adapted to address other challenging analysis such as the elucidation of interfaces within multi-protein complexes or the HDX-MS analysis of membrane proteins.

For further improvements of the herein presented HDX-MS analysis one can address the following points:

- Towards a higher automation an online peptic proteolysis using a pepsin column might be implemented to the SAIDE. It is expected that this would further decreases the digestion time and thus the back exchange.
- In order to further improve the sensitivity of HDX analysis, the chromatographic separation time might be reduced resulting in lower back exchange.
- Regarding the commercialisation of the PNGase, the storage conditions can be further characterized. This includes:
    - Testing the possibility of freeze drying.
    - Long term storage and batch to batch variability of the enzyme.
- To further improve the deglycosylation efficiency, achieve a higher automation of the HDX-workflow and prevent the HPLC-MS system from undigested PNGase Rc, immobilization would be favourable.
    - Typically used HPLC solvents are acidified to ~pH 2.5 with formic acid. Provided that immobilization is possible, a cartridge can be packed for online peptide and protein HPLC-MS deglycosylation prior to the analytical column.

9 References

[1] S. G. HEDIN: *Trypsin and Antitrypsin*, Biochem. J., **1**, (1906) 474-483.

[2] H. LU, Q. ZHOU, J. HE, Z. JIANG, C. PENG, R. TONG, AND J. SHI: *Recent advances in the development of protein-protein interactions modulators: mechanisms and clinical trials*, Signal Transduct. Target Ther., **5**, (2020)

[3] O. KESKIN, A. GURSOY, B. MA, AND R. NUSSINOV: *Principles of protein-protein interactions: what are the preferred ways for proteins to interact?*, Chem. Rev., **108**, (2008) 1225-1244.

[4] K. VENKATESAN, J. F. RUAL, A. VAZQUEZ, U. STELZL, I. LEMMENS, T. HIROZANE-KISHIKAWA, T. HAO, M. ZENKNER, X. XIN, K. I. GOH, M. A. YILDIRIM, N. SIMONIS, K. HEINZMANN, F. GEBREAB, J. M. SAHALIE, S. CEVIK, C. SIMON, A. S. DE SMET, E. DANN, A. SMOLYAR, A. VINAYAGAM, H. YU, D. SZETO, H. BORICK, A. DRICOT, N. KLITGORD, R. R. MURRAY, C. LIN, M. LALOWSKI, J. TIMM, K. RAU, C. BOONE, P. BRAUN, M. E. CUSICK, F. P. ROTH, D. E. HILL, J. TAVERNIER, E. E. WANKER, A. L. BARABASI, AND M. VIDAL: *An empirical framework for binary interactome mapping*, Nat. Methods, **6**, (2009) 83-90.

[5] M. C. SMITH AND J. E. GESTWICKI: *Features of protein-protein interactions that translate into potent inhibitors: topology, surface area and affinity*, Expert Rev. Mol. Med., **14**, (2012) 16.

[6] G. SCHREIBER: *CHAPTER 1 Protein–Protein Interaction Interfaces and their Functional Implications*, in *Protein–Protein Interaction Regulators*, RSC, (2021) 1-24.

[7] K. M. POLURI, K. GULATI, AND S. SARKAR: (2021, 01.08.2022). *Protein-Protein Interactions*. *1*.

[8] Y. PHILLIP, M. HAREL, R. KHAIT, S. QIN, H. X. ZHOU, AND G. SCHREIBER: *Contrasting factors on the kinetic path to protein complex formation diminish the effects of crowding agents*, Biophys. J., **103**, (2012) 1011-1019.

[9] G. SOWMYA AND S. RANGANATHAN: *Protein-protein interactions and prediction: a comprehensive overview*, Protein Pept. Lett., **21**, (2014) 779-789.

[10] X. PENG, J. WANG, W. PENG, F. X. WU, AND Y. PAN: *Protein-protein interactions: detection, reliability assessment and applications*, Brief Bioinform., **18**, (2017) 798-819.

[11] T. CLACKSON AND J. A. WELLS: *A hot spot of binding energy in a hormone-receptor interface*, Science, **267**, (1995) 383-386.

[12] B. C. CUNNINGHAM AND J. A. WELLS: *High-resolution epitope mapping of hGH-receptor interactions by alanine-scanning mutagenesis*, Science, **244**, (1989) 1081-1085.

[13] H. M. KALCKAR: *Kaj Ulrik Linderstrom-Lang, scientist, man, artist*, Science, **131**, (1960) 1420-1425.

[14] V. SALMASO AND S. MORO: *Bridging Molecular Docking to Molecular Dynamics in Exploring Ligand-Protein Recognition Process: An Overview*, Front. Pharmacol., **9**, (2018) 923.

[15] T. L. NERO, C. J. MORTON, J. K. HOLIEN, J. WIELENS, AND M. W. PARKER: *Oncogenic protein interfaces: small molecules, big challenges*, Nat. Rev. Cancer, **14**, (2014) 248-262.

[16] H. C. JUBB, A. P. PANDURANGAN, M. A. TURNER, B. OCHOA-MONTANO, T. L. BLUNDELL, AND D. B. ASCHER: *Mutations at protein-protein interfaces: Small changes over big surfaces have large impacts on human health*, Prog. Biophys. Mo.l Biol., **128**, (2017) 3-13.

[17] L. L. BLAZER AND R. R. NEUBIG: *Small molecule protein-protein interaction inhibitors as CNS therapeutic agents: current progress and future hurdles*, Neuropsychopharmacology, **34**, (2009) 126-141.

[18] J. A. WELLS AND C. L. MCCLENDON: *Reaching for high-hanging fruit in drug discovery at protein-protein interfaces*, Nature, **450**, (2007) 1001-1009.

[19] H. KAPLON, M. MURALIDHARAN, Z. SCHNEIDER, AND J. M. REICHERT: *Antibodies to watch in 2020*, MAbs, **12**, (2020)

[20] R. M. LU, Y. C. HWANG, I. J. LIU, C. C. LEE, H. Z. TSAI, H. J. LI, AND H. C. WU: *Development of therapeutic antibodies for the treatment of diseases*, J. Biomed. Sci., **27**, (2020)

[21] E. O. SAPHIRE, R. L. STANFIELD, M. D. MAX CRISPIN, P. W. H. I. PARREN, P. M. RUDD, R. A. DWEK, D. R. BURTON, AND I. A. WILSON: *Contrasting IgG Structures Reveal Extreme Asymmetry and Flexibility*, J. Mol. Biol., **319**, (2002) 9-18.

[22] M. L. CHIU, D. R. GOULET, A. TEPLYAKOV, AND G. L. GILLILAND: *Antibody Structure and Function: The Basis for Engineering Therapeutics*, Antibodies, **8**, (2019)

[23] C. HAMERS-CASTERMAN, T. ATARHOUCH, S. MUYLDERMANS, G. ROBINSON, C. HAMERS, E. B. SONGA, N. BENDAHMAN, AND R. HAMERS: *Naturally occurring antibodies devoid of light chains*, Nature, **363**, (1993) 446-448.

[24] S. MUYLDERMANS: *Nanobodies: natural single-domain antibodies*, Annu. Rev. Biochem., **82**, (2013) 775-797.

[25] S. MUYLDERMANS: *A guide to: generation and design of nanobodies*, FEBS J., **288**, (2020) 2084-2102.

[26] J. R. INGRAM, F. I. SCHMIDT, AND H. L. PLOEGH: *Exploiting Nanobodies' Singular Traits*, Annu. Rev. Immunol., **36**, (2018) 695-715.

[27] D. J. BARLOW, M. S. EDWARDS, AND J. M. THORNTON: *Continuous and discontinuous protein antigenic determinants*, Nature, **322**, (1986) 747-748.

[28] P. HASTE ANDERSEN, M. NIELSEN, AND O. LUND: *Prediction of residues in discontinuous B-cell epitopes using protein 3D structures*, Protein Sci., **15**, (2006) 2558-2567.

[29] X. DENG, U. STORZ, AND B. J. DORANZ: *Enhancing antibody patent protection using epitope mapping information*, MAbs, **10**, (2018) 204-209.

[30] R. Y. HUANG, A. A. TYMIAK, AND G. CHEN: *Utility of Hydrogen Exchange Mass Spectrometry in Epitope Mapping*, in *Hydrogen Exchange Mass Spectrometry of Proteins*, D. D. Weis, (2016) 247-263.

[31] W. M. ABBOTT, M. M. DAMSCHRODER, AND D. C. LOWE: *Current approaches to fine mapping of antigen-antibody interactions*, Immunology, **142**, (2014) 526-535.

[32] L. G. MILROY, T. N. GROSSMANN, S. HENNIG, L. BRUNSVELD, AND C. OTTMANN: *Modulators of protein-protein interactions*, Chem. Rev., **114**, (2014) 4695-4748.

[33] K. MIURA: *An Overview of Current Methods to Confirm Protein-Protein Interactions*, Protein Pept. Lett., **25**, (2018) 728-733.

[34] E. T. BODER AND K. D. WITTRUP: *Yeast surface display for screening combinatorial polypeptide libraries*, Nat. Biotechnol., **15**, (1997) 553-557.

[35] E. ENGVALL AND P. PERLMANN: *Enzyme-linked immunosorbent assay (ELISA) quantitative assay of immunoglobulin G*, Immunochemistry, **8**, (1971) 871-874.

[36] E. STENBERG, B. PERSSON, H. ROOS, AND C. URBANICZKY: *Quantitative determination of surface concentration of protein with surface plasmon resonance using radiolabeled proteins*, J. Colloid Interface Sci., **143**, (1991) 513-526.

[37] J. CONCEPCION, K. WITTE, C. WARTCHOW, S. CHOO, D. YAO, H. PERSSON, J. WEI, P. LI, B. HEIDECKER, W. MA, R. VARMA, L. S. ZHAO, D. PERILLAT, G. CARRICATO, M. RECKNOR, K. DU, H. HO, T. ELLIS, J. GAMEZ, M. HOWES, J. PHI-WILSON, S. LOCKARD, R. ZUK, AND H. TAN: *Label-free detection of biomolecular interactions using BioLayer interferometry for kinetic characterization*, Comb. Chem. High Throughput Screen, **12**, (2009) 791-800.

[38] S. A. GAI AND K. D. WITTRUP: *Yeast surface display for protein engineering and characterization*, Curr. Opin. Struct. Biol., **17**, (2007) 467-473.

[39] J. R. COCHRAN, Y. S. KIM, M. J. OLSEN, R. BHANDARI, AND K. D. WITTRUP: *Domain-level antibody epitope mapping through yeast surface display of epidermal growth factor receptor fragments*, J. Immunol. Methods, **287**, (2004) 147-158.

[40] T. A. NAJAR, S. KHARE, R. PANDEY, S. K. GUPTA, AND R. VARADARAJAN: *Mapping Protein Binding Sites and Conformational Epitopes Using Cysteine Labeling and Yeast Surface Display*, Structure, **25**, (2017) 395-406.

[41] W. S. AHN, T. S. KIM, Y. J. PARK, Y. K. PARK, H. D. KIM, AND J. KIM: *Production, characterization, and epitope mapping of monoclonal antibodies of ribosomal protein S3 (rpS3)*, Anim. Cells Syst. (Seoul), **25**, (2021) 323-336.

[42] M. KANG, S. Y. KIM, S. S. AN, AND Y. R. JU: *Characterizing affinity epitopes between prion protein and beta-amyloid using an epitope mapping immunoassay*, Exp. Mol. Med., **45**, (2013)

[43] P. ESTEP, F. REID, C. NAUMAN, Y. LIU, T. SUN, J. SUN, AND Y. XU: *High throughput solution-based measurement of antibody-antigen affinity and epitope binning*, MAbs, **5**, (2013) 270-278.

[44] D. YANG, A. SINGH, H. WU, AND R. KROE-BARRETT: *Comparison of biosensor platforms in the evaluation of high affinity antibody-antigen binding kinetics*, Anal. Biochem., **508**, (2016) 78-96.

[45] G. HAO, J. S. WESOLOWSKI, X. JIANG, S. LAUDER, AND V. D. SOOD: *Epitope characterization of an anti-PD-L1 antibody using orthogonal approaches*, J. Mol. Recognit., **28**, (2015) 269-276.

[46] T. R. WAGNER, E. OSTERTAG, P. D. KAISER, M. GRAMLICH, N. RUETALO, D. JUNKER, J. HAERING, B. TRAENKLE, M. BECKER, A. DULOVIC, H. SCHWEIZER, S. NUESKE, A. SCHOLZ, A. ZECK, K. SCHENKE-LAYLAND, A. NELDE, M. STRENGERT, J. S. WALZ, G. ZOCHER, T. STEHLE, M. SCHINDLER, N. SCHNEIDERHAN-MARRA, AND U. ROTHBAUER: *NeutrobodyPlex-monitoring SARS-CoV-2 neutralizing immune responses using nanobodies*, EMBO Rep., **22**, (2021)

[47] J. LI, H. WEI, S. R. KRYSTEK, JR., D. BOND, T. M. BRENDER, D. COHEN, J. FEINER, N. HAMACHER, J. HARSHMAN, R. Y. HUANG, S. H. JULIEN, Z. LIN, K. MOORE, L. MUELLER, C. NORIEGA, P. SEJWAL, P. SHEPPARD, B. STEVENS, G. CHEN, A. A. TYMIAK, M. L. GROSS, AND L. A. SCHNEEWEIS: *Mapping the Energetic Epitope of an Antibody/Interleukin-23 Interaction with Hydrogen/Deuterium Exchange, Fast Photochemical Oxidation of Proteins Mass Spectrometry, and Alanine Shave Mutagenesis*, Anal. Chem., **89**, (2017) 2250-2258.

[48] D. R. DAVIES AND G. H. COHEN: *Interactions of protein antigens with antibodies*, Proc. Natl. Acad. Sci. USA, **93**, (1996) 7-12.

[49] W. BECKER, K. C. BHATTIPROLU, N. GUBENSAK, AND K. ZANGGER: *Investigating Protein-Ligand Interactions by Solution Nuclear Magnetic Resonance Spectroscopy*, Chem. Phys. Chem., **19**, (2018) 895-906.

[50] J. P. RENAUD, A. CHARI, C. CIFERRI, W. T. LIU, H. W. REMIGY, H. STARK, AND C. WIESMANN: *Cryo-EM in drug discovery: achievements, limitations and prospects*, Nat. Rev. Drug Discov., **17**, (2018) 471-492.

[51] E. NOGALES: *The development of cryo-EM into a mainstream structural biology technique*, Nat. Methods, **13**, (2016) 24-27.

[52] C. YU AND L. HUANG: *Cross-Linking Mass Spectrometry: An Emerging Technology for Interactomics and Structural Biology*, Anal. Chem., **90**, (2018) 144-165.

[53] M. M. ZHANG, R. Y. HUANG, B. R. BENO, E. G. DEYANOVA, J. LI, G. CHEN, AND M. L. GROSS: *Epitope and Paratope Mapping of PD-1/Nivolumab by Mass Spectrometry-Based Hydrogen-Deuterium Exchange, Cross-linking, and Molecular Docking*, Anal. Chem., **92**, (2020) 9086-9094.

[54] T. PIMENOVA, A. NAZABAL, B. ROSCHITZKI, J. SEEBACHER, O. RINNER, AND R. ZENOBI: *Epitope mapping on bovine prion protein using chemical cross-linking and mass spectrometry*, J. Mass. Spectrom., **43**, (2008) 185-195.

[55] M. ZHOU, Q. LI, AND R. WANG: *Current Experimental Methods for Characterizing Protein-Protein Interactions*, Chem. Med. Chem., **11**, (2016) 738-756.

[56] D. M. HAMBLY AND M. L. GROSS: *Laser flash photolysis of hydrogen peroxide to oxidize protein solvent-accessible residues on the microsecond timescale*, J. Am. Soc. Mass. Spectrom., **16**, (2005) 2057-2063.

[57] X. R. LIU, M. M. ZHANG, AND M. L. GROSS: *Mass Spectrometry-Based Protein Footprinting for Higher-Order Structure Analysis: Fundamentals and Applications*, Chem. Rev., **120**, (2020) 4355-4454.

[58] A. HVIDT AND K. LINDERSTRØM-LANG: *Exchange of hydrogen atoms in insulin with deuterium atoms in aqueous solutions*, Biochim. Biophys. Acta, **14**, (1954) 574-575.

[59] S. W. ENGLANDER: *A Hydrogen Exchange Method Using Tritium and Sephadex: Its Application to Ribonuclease*, Biochemistry, **2**, (1963) 798-807.

[60] S. W. ENGLANDER: *Hydrogen exchange and mass spectrometry: A historical perspective*, J. Am. Soc. Mass Spectrom., **17**, (2006) 1481-1489.

[61] J. J. ROSA AND F. M. RICHARDS: *An experimental procedure for increasing the structural resolution of chemical hydrogen-exchange measurements on proteins: Application to ribonuclease S peptide*, J. Mol. Biol., **133**, (1979) 399-416.

[62] J. J. ENGLANDER, J. R. ROGERO, AND S. W. ENGLANDER: *Protein hydrogen exchange studied by the fragment separation method*, Anal. Biochem., **147**, (1985) 234-244.

[63] Z. ZHANG AND D. L. SMITH: *Determination of amide hydrogen exchange by mass spectrometry: a new tool for protein structure elucidation*, Protein Sci., **2**, (1993) 522-531.

[64] P. F. JENSEN AND K. D. RAND: *Hydrogen Exchange: A Sensitive Analytical Window into Protein Conformation and Dynamics*, in *Hydrogen Exchange Mass Spectrometry of Proteins*, D. D. Weis, Wiley, (2016) 1-17.

[65] P. F. JENSEN, G. COMAMALA, M. B. TRELLE, J. B. MADSEN, T. J. JORGENSEN, AND K. D. RAND: *Removal of N-Linked Glycosylations at Acidic pH by PNGase A Facilitates Hydrogen/Deuterium Exchange Mass Spectrometry Analysis of N-Linked Glycoproteins*, Anal. Chem., **88**, (2016) 12479-12488.

[66] Y. BAI, J. S. MILNE, L. MAYNE, AND S. W. ENGLANDER: *Primary structure effects on peptide group hydrogen exchange*, Proteins, **17**, (1993) 75-86.

[67] E. S. GALLAGHER AND J. W. HUDGENS: *Mapping Protein-Ligand Interactions with Proteolytic Fragmentation, Hydrogen/Deuterium Exchange-Mass Spectrometry*, Methods Enzymol., **566**, (2016) 357-404.

[68] L. MAYNE: *Hydrogen Exchange Mass Spectrometry*, Methods Enzymol., **566**, (2016) 335-356.

[69] T. E. WALES AND J. R. ENGEN: *Hydrogen exchange mass spectrometry for the analysis of protein dynamics*, Mass Spectrom. Rev., **25**, (2006) 158-170.

[70] M. M. KRISHNA, L. HOANG, Y. LIN, AND S. W. ENGLANDER: *Hydrogen exchange methods to study protein folding*, Methods, **34**, (2004) 51-64.

[71] J. J. ENGLANDER, C. DEL MAR, W. LI, S. W. ENGLANDER, J. S. KIM, D. D. STRANZ, Y. HAMURO, AND V. L. WOODS, JR.: *Protein structure change studied by hydrogen-deuterium exchange, functional labeling, and mass spectrometry*, Proc. Natl. Acad. Sci. USA, **100**, (2003) 7057-7062.

[72] B. A. KOCHERT, R. E. IACOB, T. E. WALES, A. MAKRIYANNIS, AND J. R. ENGEN: *Hydrogen-Deuterium Exchange Mass Spectrometry to Study Protein Complexes*, Methods Mol. Biol., **1764**, (2018) 153-171.

[73] C. R. MORGAN AND J. R. ENGEN: *Investigating solution-phase protein structure and dynamics by hydrogen exchange mass spectrometry*, Curr. Protoc. Protein Sci., **Chapter 17**, (2009)

[74] G. R. MASSON, J. E. BURKE, N. G. AHN, G. S. ANAND, C. BORCHERS, S. BRIER, G. M. BOU-ASSAF, J. R. ENGEN, S. W. ENGLANDER, J. FABER, R. GARLISH, P. R. GRIFFIN, M. L. GROSS, M. GUTTMAN, Y. HAMURO, A. J. R. HECK, D. HOUDE, R. E. IACOB, T. J. D. JORGENSEN, I. A. KALTASHOV, J. P. KLINMAN, L. KONERMANN, P. MAN, L. MAYNE, B. D. PASCAL, D. REICHMANN, M. SKEHEL, J. SNIJDER, T. S. STRUTZENBERG, E. S. UNDERBAKKE, C. WAGNER, T. E. WALES, B. T. WALTERS, D. D. WEIS, D. J. WILSON, P. L. WINTRODE, Z. ZHANG, J. ZHENG, D. C. SCHRIEMER, AND K. D. RAND: *Recommendations for performing, interpreting and reporting hydrogen deuterium exchange mass spectrometry (HDX-MS) experiments*, Nat. Methods, **16**, (2019) 595-602.

[75] J. PAN, S. ZHANG, C. E. PARKER, AND C. H. BORCHERS: *Subzero temperature chromatography and top-down mass spectrometry for protein higher-order structure characterization: method validation and application to therapeutic antibodies*, J. Am. Chem. Soc., **136**, (2014) 13065-13071.

[76] M. FANG, Z. WANG, K. A. CUPP-SUTTON, T. WELBORN, K. SMITH, AND S. WU: *High-throughput hydrogen deuterium exchange mass spectrometry (HDX-MS) coupled with subzero-temperature ultrahigh pressure liquid chromatography (UPLC) separation for complex sample analysis*, Anal. Chim. Acta., **1143**, (2021) 65-72.

[77] L. CRAVELLO, D. LASCOUX, AND E. FOREST: *Use of different proteases working in acidic conditions to improve sequence coverage and resolution in hydrogen/deuterium exchange of large proteins*, Rapid Commun. Mass Spectrom., **17**, (2003) 2387-2393.

[78] M. REY, M. YANG, K. M. BURNS, Y. YU, S. P. LEES-MILLER, AND D. C. SCHRIEMER: *Nepenthesin from monkey cups for hydrogen/deuterium exchange mass spectrometry*, Mol. Cell Proteomics, **12**, (2013) 464-472.

[79] Y. HAMURO, S. J. COALES, K. S. MOLNAR, S. J. TUSKE, AND J. A. MORROW: *Specificity of immobilized porcine pepsin in H/D exchange compatible conditions*, Rapid Commun. Mass Spectrom., **22**, (2008) 1041-1046.

[80] K. D. RAND, C. M. ADAMS, R. A. ZUBAREV, AND T. J. JORGENSEN: *Electron capture dissociation proceeds with a low degree of intramolecular migration of peptide amide hydrogens*, J. Am. Chem. Soc., **130**, (2008) 1341-1349.

[81] E. TRABJERG, Z. E. NAZARI, AND K. D. RAND: *Conformational analysis of complex protein states by hydrogen/deuterium exchange mass spectrometry (HDX-MS): Challenges and emerging solutions*, Trends Anal. Chem., **106**, (2018) 125-138.

[82] P. J. HOGG: *Disulfide bonds as switches for protein function*, Trends Biochem. Sci., **28**, (2003) 210-214.

[83] P. STANLEY, H. SCHACHTER, AND N. TANIGUCHI: *N-Glycans*, in *Essentials of Glycobiology, 2nd edition*, A. Varki, R. Cummings, J. Esko, H. Freeze, P. Stanley, C. Bertozzi, *et al.*, Cold Spring Harbor (NY), (2009).

[84] R. J. SOLA AND K. GRIEBENOW: *Glycosylation of therapeutic proteins: an effective strategy to optimize efficacy*, BioDrugs, **24**, (2010) 9-21.

[85] A. VARKI: *Biological roles of glycans*, Glycobiology, **27**, (2017) 3-49.

[86] C. REILY, T. J. STEWART, M. B. RENFROW, AND J. NOVAK: *Glycosylation in health and disease*, Nat. Rev. Nephrol., **15**, (2019) 346-366.

[87] K. OHTSUBO AND J. D. MARTH: *Glycosylation in cellular mechanisms of health and disease*, Cell, **126**, (2006) 855-867.

[88] E. WEERAPANA AND B. IMPERIALI: *Asparagine-linked protein glycosylation: from eukaryotic to prokaryotic systems*, Glycobiology, **16**, (2006) 91R-101R.

[89] A. PLANINC, J. BONES, B. DEJAEGHER, P. VAN ANTWERPEN, AND C. DELPORTE: *Glycan characterization of biopharmaceuticals: Updates and perspectives*, Anal. Chim. Acta, **921**, (2016) 13-27.

[90] D. HOUDE, Y. PENG, S. A. BERKOWITZ, AND J. R. ENGEN: *Post-translational modifications differentially affect IgG1 conformation and receptor binding*, Mol. Cell. Proteomics, **9**, (2010) 1716-1728.

[91] R. Y. HUANG AND J. W. HUDGENS: *Effects of desialylation on human alpha1-acid glycoprotein-ligand interactions*, Biochemistry, **52**, (2013) 7127-7136.

[92] C. PUCHADES, B. KUKRER, O. DIEFENBACH, E. SNEEKES-VRIESE, J. JURASZEK, W. KOUDSTAAL, AND A. APETRI: *Epitope mapping of diverse influenza Hemagglutinin drug candidates using HDX-MS*, Sci. Rep., **9**, (2019)

[93] Y. LIANG, M. GUTTMAN, T. M. DAVENPORT, S. L. HU, AND K. K. LEE: *Probing the Impact of Local Structural Dynamics of Conformational Epitopes on Antibody Recognition*, Biochemistry, **55**, (2016) 2197-2213.

[94] Z. DARULA AND K. F. MEDZIHRADSZKY: *Glycan side reaction may compromise ETD-based glycopeptide identification*, J. Am. Soc. Mass Spectrom., **25**, (2014) 977-987.

[95] M. GUTTMAN, M. SCIAN, AND K. K. LEE: *Tracking hydrogen/deuterium exchange at glycan sites in glycoproteins by mass spectrometry*, Anal. Chem., **83**, (2011) 7492-7499.

[96] G. R. MASSON, M. L. JENKINS, AND J. E. BURKE: *An overview of hydrogen deuterium exchange mass spectrometry (HDX-MS) in drug discovery*, Expert Opin. Drug Discovery, **12**, (2017) 981-994.

[97] J. PAN, S. ZHANG, A. CHOU, AND C. H. BORCHERS: *Higher-order structural interrogation of antibodies using middle-down hydrogen/deuterium exchange mass spectrometry*, Chem. Sci., **7**, (2016) 1480-1486.

[98] T. WANG AND J. VOGLMEIR: *PNGases as valuable tools in glycoprotein analysis*, Protein Pept. Lett., **21**, (2014) 976-985.

[99] T. H. PLUMMER, J. H. ELDER, S. ALEXANDER, A. W. PHELAN, AND A. L. TARENTINO: *Demonstration of peptide:N-glycosidase F activity in endo-beta-N-acetylglucosaminidase F preparations*, J. Biol. Chem., **259**, (1984) 10700-10704.

[100] N. TAKAHASHI AND H. NISHIBE: *Some characteristics of a new glycopeptidase acting on aspartylglycosylamine linkages*, J. Biochem., **84**, (1978) 1467-1473.

[101] F. ALTMANN, S. SCHWEISZER, AND C. WEBER: *Kinetic comparison of peptide: N-glycosidases F and A reveals several differences in substrate specificity*, Glycoconjugate J., **12**, (1995) 84-93.

[102] R. R. GUO, G. COMAMALA, H. H. YANG, M. GRAMLICH, Y. M. DU, T. WANG, A. ZECK, K. D. RAND, L. LIU, AND J. VOGLMEIR: *Discovery of Highly Active Recombinant PNGase H(+) Variants Through the Rational Exploration of Unstudied Acidobacterial Genomes*, Front. Bioeng. Biotechnol., **8**, (2020)

[103] T. WANG, Z. P. CAI, X. Q. GU, H. Y. MA, Y. M. DU, K. HUANG, J. VOGLMEIR, AND L. LIU: *Discovery and characterization of a novel extremely acidic bacterial N-glycanase with combined advantages of PNGase F and A*, Biosci. Rep., **34**, (2014)

[104] J. M. HAYES, A. FROSTELL, E. F. COSGRAVE, W. B. STRUWE, O. POTTER, G. P. DAVEY, R. KARLSSON, C. ANNEREN, AND P. M. RUDD: *Fc gamma receptor glycosylation modulates the binding of IgG glycoforms: a requirement for stable antibody interactions*, J. Proteome. Res., **13**, (2014) 5471-5485.

[105] N. D. WAGNER, Y. HUANG, T. LIU, AND M. L. GROSS: *Post-HDX Deglycosylation of Fc Gamma Receptor IIIa Glycoprotein Enables HDX Characterization of Its Binding Interface with IgG*, J. Am. Soc. Mass Spectrom., **32**, (2021) 1638-1643.

[106] G. COMAMALA, C. C. KROGH, V. S. NIELSEN, J. P. KUTTER, J. VOGLMEIR, AND K. D. RAND: *Hydrogen/Deuterium Exchange Mass Spectrometry with Integrated Electrochemical Reduction and Microchip-Enabled Deglycosylation for Epitope Mapping of Heavily Glycosylated and Disulfide-Bonded Proteins*, Anal. Chem., **93**, (2021) 16330-16340.

[107] Y. HAMURO AND S. J. COALES: *Optimization of Feasibility Stage for Hydrogen/Deuterium Exchange Mass Spectrometry*, J. Am. Soc. Mass Spectrom., **29**, (2018) 623-629.

[108] X. YAN, H. ZHANG, J. WATSON, M. I. SCHIMERLIK, AND M. L. DEINZER: *Hydrogen/deuterium exchange and mass spectrometric analysis of a protein containing multiple disulfide bonds: Solution structure of recombinant macrophage colony stimulating factor-beta (rhM-CSFbeta)*, Protein Sci., **11**, (2002) 2113-2124.

[109] H. M. ZHANG, S. M. MCLOUGHLIN, S. D. FRAUSTO, H. TANG, M. R. EMMETT, AND A. G. MARSHALL: *Simultaneous reduction and digestion of proteins with disulfide bonds for hydrogen/deuterium exchange monitored by mass spectrometry*, Anal. Chem., **82**, (2010) 1450-1454.

[110] M. GRAMLICH, H. C. W. HAYS, S. CRICHTON, P. D. KAISER, A. HEINE, N. SCHNEIDERHAN-MARRA, U. ROTHBAUER, D. STOLL, S. MAIER, AND A. ZECK: *HDX-MS for Epitope Characterization of a Therapeutic ANTIBODY Candidate on the Calcium-Binding Protein Annexin-A1*, Antibodies, **10**, (2021)

[111] A. ROSENGARTH, V. GERKE, AND H. LUECKE: *X-ray structure of full-length annexin 1 and implications for membrane aggregation*, J. Mol. Biol., **306**, (2001) 489-498.

[112] M. A. LIZARBE, J. I. BARRASA, N. OLMO, F. GAVILANES, AND J. TURNAY: *Annexin-phospholipid interactions. Functional implications*, Int. J. Mol. Sci., **14**, (2013) 2652-2683.

[113] S. LIEMANN AND R. HUBER: *Three-dimensional structure of annexins*, Cell Mol. Life Sci., **53**, (1997) 516-521.

[114] M. H. SHEIKH AND E. SOLITO: *Annexin A1: Uncovering the Many Talents of an Old Protein*, Int. J. Mol. Sci., **19**, (2018)

[115] G. S. D. PURVIS, E. SOLITO, AND C. THIEMERMANN: *Annexin-A1: Therapeutic Potential in Microvascular Disease*, Front. Immunol., **10**, (2019)

[116] G. SHAO, H. ZHOU, Q. ZHANG, Y. JIN, AND C. FU: *Advancements of Annexin A1 in inflammation and tumorigenesis*, OncoTargets and Therapy, **12**, (2019) 3245-3254.

[117] F. D'Acquisto, M. Perretti, and R. J. Flower: *Annexin-A1: a pivotal regulator of the innate and adaptive immune systems*, Br. J. Pharmacol., **155**, (2008) 152-169.
[118] F. D'Acquisto, N. Paschalidis, A. L. Sampaio, A. Merghani, R. J. Flower, and M. Perretti: *Impaired T cell activation and increased Th2 lineage commitment in Annexin-1-deficient T cells*, Eur. J. Immunol., **37**, (2007) 3131-3142.
[119] F. D'Acquisto, A. Merghani, E. Lecona, G. Rosignoli, K. Raza, C. D. Buckley, R. J. Flower, and M. Perretti: *Annexin-1 modulates T-cell activation and differentiation*, Blood, **109**, (2007) 1095-1102.
[120] F. D'Acquisto and M. Perretti, *ANNEXIN 1 ANTIBODY*, WO 2011/154705 A1(2011), Available: https://patentscope.wipo.int/search/en/detail.jsf?docId=WO2011154705, (last accessd on 23.09.2021).
[121] H. C. W. Hays, C. B. Wood, and T. C. Flatau, *ANTI HUMAN ANNEXIN A1 ANTIBODY*, United States Patent, US 2020/0031911 A1(2020), Available: https://www.freepatentsonline.com/y2020/0031911.html, (last accessd on 23.09.2021).
[122] H. Ge, X. Wang, X. Yuan, G. Xiao, C. Wang, T. Deng, Q. Yuan, and X. Xiao: *The epidemiology and clinical information about COVID-19*, Eur. J. Clin. Microbiol. Infect. Dis., **39**, (2020) 1011-1019.
[123] M. Mofijur, I. M. R. Fattah, M. A. Alam, A. Islam, H. C. Ong, S. M. A. Rahman, G. Najafi, S. F. Ahmed, M. A. Uddin, and T. M. I. Mahlia: *Impact of COVID-19 on the social, economic, environmental and energy domains: Lessons learnt from a global pandemic*, Sustain. Prod. Consum., **26**, (2021) 343-359.
[124] D. Wrapp, N. Wang, K. S. Corbett, J. A. Goldsmith, C. L. Hsieh, O. Abiona, B. S. Graham, and J. S. McLellan: *Cryo-EM structure of the 2019-nCoV spike in the prefusion conformation*, Science, **367**, (2020) 1260-1263.
[125] T. Zhou, Y. Tsybovsky, J. Gorman, M. Rapp, G. Cerutti, G. Y. Chuang, P. S. Katsamba, J. M. Sampson, A. Schon, J. Bimela, J. C. Boyington, A. Nazzari, A. S. Olia, W. Shi, M. Sastry, T. Stephens, J. Stuckey, I. T. Teng, P. Wang, S. Wang, B. Zhang, R. A. Friesner, D. D. Ho, J. R. Mascola, L. Shapiro, and P. D. Kwong: *Cryo-EM Structures of SARS-CoV-2 Spike without and with ACE2 Reveal a pH-Dependent Switch to Mediate Endosomal Positioning of Receptor-Binding Domains*, Cell Host Microbe, **28**, (2020) 867-879.
[126] J. Kreye, S. M. Reincke, H. C. Kornau, E. Sanchez-Sendin, V. M. Corman, H. Liu, M. Yuan, N. C. Wu, X. Zhu, C. D. Lee, J. Trimpert, M. Holtje, K. Dietert, L. Stoffler, N. von Wardenburg, S. van Hoof, M. A. Homeyer, J. Hoffmann, A. Abdelgawad, A. D. Gruber, L. D. Bertzbach, D. Vladimirova, L. Y. Li, P. C. Barthel, K. Skriner, A. C. Hocke, S. Hippenstiel, M. Witzenrath, N. Suttorp, F. Kurth, C. Franke, M. Endres, D. Schmitz, L. M. Jeworowski, A. Richter, M. L. Schmidt, T. Schwarz, M. A. Muller, C. Drosten, D. Wendisch, L. E. Sander, N. Osterrieder, I. A. Wilson, and H. Pruss: *A Therapeutic Non-self-reactive SARS-CoV-2 Antibody Protects from Lung Pathology in a COVID-19 Hamster Model*, Cell, **183**, (2020) 1058-1069.
[127] J. Hansen, A. Baum, K. E. Pascal, V. Russo, S. Giordano, E. Wloga, B. O. Fulton, Y. Yan, K. Koon, K. Patel, K. M. Chung, A. Hermann, E. Ullman, J. Cruz, A. Rafique, T. Huang, J. Fairhurst, C. Libertiny, M. Malbec, W. Y. Lee, R. Welsh, G. Farr, S. Pennington, D. Deshpande, J. Cheng, A. Watty, P. Bouffard, R. Babb, N. Levenkova, C. Chen, B. Zhang, A. Romero Hernandez, K. Saotome, Y. Zhou, M. Franklin, S. Sivapalasingam, D. C. Lye, S. Weston, J. Logue, R. Haupt, M. Frieman, G. Chen, W. Olson, A. J. Murphy, N. Stahl, G. D. Yancopoulos, and C. A. Kyratsous: *Studies in humanized mice and convalescent humans yield a SARS-CoV-2 antibody cocktail*, Science, **369**, (2020) 1010-1014.
[128] L. Hanke, L. Vidakovics Perez, D. J. Sheward, H. Das, T. Schulte, A. Moliner-Morro, M. Corcoran, A. Achour, G. B. Karlsson Hedestam, B. M. Hallberg, B. Murrell, and G. M. McInerney: *An alpaca nanobody neutralizes SARS-CoV-2 by blocking receptor interaction*, Nat. Commun., **11**, (2020) 4420.
[129] P. A. Koenig, H. Das, H. Liu, B. M. Kummerer, F. N. Gohr, L. M. Jenster, L. D. J. Schiffelers, Y. M. Tesfamariam, M. Uchima, J. D. Wuerth, K. Gatterdam, N. Ruetalo, M. H.

CHRISTENSEN, C. I. FANDREY, S. NORMANN, J. M. P. TODTMANN, S. PRITZL, L. HANKE, J. BOOS, M. YUAN, X. ZHU, J. L. SCHMID-BURGK, H. KATO, M. SCHINDLER, I. A. WILSON, M. GEYER, K. U. LUDWIG, B. M. HALLBERG, N. C. WU, AND F. I. SCHMIDT: *Structure-guided multivalent nanobodies block SARS-CoV-2 infection and suppress mutational escape*, Science, **371**, (2021)

[130] C. O. BARNES, C. A. JETTE, M. E. ABERNATHY, K. A. DAM, S. R. ESSWEIN, H. B. GRISTICK, A. G. MALYUTIN, N. G. SHARAF, K. E. HUEY-TUBMAN, Y. E. LEE, D. F. ROBBIANI, M. C. NUSSENZWEIG, A. P. WEST, JR., AND P. J. BJORKMAN: *SARS-CoV-2 neutralizing antibody structures inform therapeutic strategies*, Nature, **588**, (2020) 682-687.

[131] A. N. BARCLAY AND T. K. VAN DEN BERG: *The interaction between signal regulatory protein alpha (SIRPalpha) and CD47: structure, function, and therapeutic target*, Annu. Rev. Immunol., **32**, (2014) 25-50.

[132] W. ZHANG, Q. HUANG, W. XIAO, Y. ZHAO, J. PI, H. XU, H. ZHAO, J. XU, C. E. EVANS, AND H. JIN: *Advances in Anti-Tumor Treatments Targeting the CD47/SIRPalpha Axis*, Front. Immunol., **11**, (2020) 18.

[133] D. HATHERLEY, S. C. GRAHAM, K. HARLOS, D. I. STUART, AND A. N. BARCLAY: *Structure of signal-regulatory protein alpha: a link to antigen receptor evolution*, J. Biol. Chem., **284**, (2009) 26613-22619.

[134] D. HATHERLEY, S. M. LEA, S. JOHNSON, AND A. N. BARCLAY: *Polymorphisms in the human inhibitory signal-regulatory protein alpha do not affect binding to its ligand CD47*, J. Biol. Chem., **289**, (2014) 10024-10028.

[135] P. A. OLDENBORG: *CD47: A Cell Surface Glycoprotein Which Regulates Multiple Functions of Hematopoietic Cells in Health and Disease*, ISRN Hematol., **2013**, (2013)

[136] M. T. VILLAR, D. E. MILLER, A. W. FENTON, AND A. ARTIGUES: *SAIDE: A Semi-Automated Interface for Hydrogen/Deuterium Exchange Mass Spectrometry*, Proteomica, **6**, (2010) 63-69.

[137] J. FANG, K. D. RAND, P. J. BEUNING, AND J. R. ENGEN: *False EX1 signatures caused by sample carryover during HX MS analyses*, Int. J. Mass Spectrom., **302**, (2011) 19-25.

[138] T. S. HAGEMAN AND D. D. WEIS: *Reliable Identification of Significant Differences in Differential Hydrogen Exchange-Mass Spectrometry Measurements Using a Hybrid Significance Testing Approach*, Anal. Chem., **91**, (2019) 8008-8016.

[139] M. GRAMLICH, S. MAIER, P. D. KAISER, B. TRAENKLE, T. R. WAGNER, J. VOGLMEIR, D. STOLL, U. ROTHBAUER, AND A. ZECK: *A Novel PNGase Rc for Improved Protein N-Deglycosylation in Bioanalytics and Hydrogen-Deuterium Exchange Coupled With Mass Spectrometry Epitope Mapping under Challenging Conditions*, Anal. Chem., (2022)

[140] H. Y. WEON, S. H. YOO, Y. J. KIM, C. M. LEE, B. Y. KIM, Y. A. JEON, S. B. HONG, R. ANANDHAM, AND S. W. KWON: *Rudaea cellulosilytica gen. nov., sp. nov., isolated from soil*, Int. J. Syst. Evol. Microbiol., **59**, (2009) 2308-2312.

[141] J. M. WALKER: (2005)

[142] I. SANCHEZ-DE MELO, P. GRASSI, F. OCHOA, J. BOLIVAR, F. J. GARCIA-COZAR, AND M. C. DURAN-RUIZ: *N-glycosylation profile analysis of Trastuzumab biosimilar candidates by Normal Phase Liquid Chromatography and MALDI-TOF MS approaches*, J. Proteomics, **127**, (2015) 225-233.

[143] S. NEELAMEGHAM, K. AOKI-KINOSHITA, E. BOLTON, M. FRANK, F. LISACEK, T. LUTTEKE, N. O'BOYLE, N. H. PACKER, P. STANLEY, P. TOUKACH, A. VARKI, R. J. WOODS, AND S. D. GROUP: *Updates to the Symbol Nomenclature for Glycans guidelines*, Glycobiology, **29**, (2019) 620-624.

[144] T. WANG, S. L. ZHENG, L. LIU, AND J. VOGLMEIR: *Development of a colorimetric PNGase activity assay*, Carbohydr. Res., **472**, (2019) 58-64.

[145] J. Q. FAN AND Y. C. LEE: *Detailed studies on substrate structure requirements of glycoamidases A and F*, J. Biol. Chem., **272**, (1997) 27058-27064.

[146] H. C. JOAO AND R. A. DWEK: *Effects of glycosylation on protein structure and dynamics in ribonuclease B and some of its individual glycoforms*, Eur. J. Biochem., **218**, (1993) 239-244.

[147] M. WINDWARDER AND F. ALTMANN: *Site-specific analysis of the O-glycosylation of bovine fetuin by electron-transfer dissociation mass spectrometry*, J. Proteomics, **108**, (2014) 258-268.
[148] A. L. TARENTINO AND T. H. PLUMMER: *Oligosaccharide accessibility to peptide:N-glycosidase as promoted by protein-unfolding reagents*, J. Biol. Chem., **257**, (1982) 10776-10780.
[149] X. WENG, H. LUECKE, I. S. SONG, D. S. KANG, S. H. KIM, AND R. HUBER: *Crystal structure of human annexin I at 2.5 A resolution*, Protein Sci., **2**, (1993) 448-458.
[150] A. ROSENGARTH AND H. LUECKE: *A Calcium-driven Conformational Switch of the N-terminal and Core Domains of Annexin A1*, J. Mol. Biol., **326**, (2003) 1317-1325.
[151] S. MAIER, ed, (2020).
[152] R. YAN, Y. ZHANG, Y. LI, L. XIA, Y. GUO, AND Q. ZHOU: *Structural basis for the recognition of SARS-CoV-2 by full-length human ACE2*, Science, **367**, (2020) 1444-1448.
[153] J. LAN, J. GE, J. YU, S. SHAN, H. ZHOU, S. FAN, Q. ZHANG, X. SHI, Q. WANG, L. ZHANG, AND X. WANG: *Structure of the SARS-CoV-2 spike receptor-binding domain bound to the ACE2 receptor*, Nature, **581**, (2020) 215-220.
[154] P. S. MERKLE, E. TRABJERG, S. HONGJIAN, M. FERBER, M. A. CUENDET, T. J. D. JORGENSEN, I. LUESCHER, M. IRVING, V. ZOETE, O. MICHIELIN, AND K. D. RAND: *Probing the Conformational Dynamics of Affinity-Enhanced T Cell Receptor Variants upon Binding the Peptide-Bound Major Histocompatibility Complex by Hydrogen/Deuterium Exchange Mass Spectrometry*, Biochemistry, **60**, (2021) 859-872.
[155] M. J. CHALMERS, S. A. BUSBY, B. D. PASCAL, Y. HE, C. L. HENDRICKSON, A. G. MARSHALL, AND P. R. GRIFFIN: *Probing protein ligand interactions by automated hydrogen/deuterium exchange mass spectrometry*, Anal. Chem., **78**, (2006) 1005-1014.
[156] V. L. WOODS, JR. AND Y. HAMURO: *High resolution, high-throughput amide deuterium exchange-mass spectrometry (DXMS) determination of protein binding site structure and dynamics: utility in pharmaceutical design*, J. Cell. Biochem. Suppl., **37**, (2001) 89-98.
[157] D. J. CUMMINS, A. ESPADA, S. J. NOVICK, M. MOLINA-MARTIN, R. E. STITES, J. F. ESPINOSA, H. BROUGHTON, D. GOSWAMI, B. D. PASCAL, J. A. DODGE, M. J. CHALMERS, AND P. R. GRIFFIN: *Two-Site Evaluation of the Repeatability and Precision of an Automated Dual-Column Hydrogen/Deuterium Exchange Mass Spectrometry Platform*, Anal. Chem., **88**, (2016) 6607-6614.
[158] M. J. WATSON, R. HARKEWICZ, E. A. HODGE, C. VORAUER, J. PALMER, K. K. LEE, AND M. GUTTMAN: *Simple Platform for Automating Decoupled LC-MS Analysis of Hydrogen/Deuterium Exchange Samples*, J. Am. Soc. Mass Spectrom., **32**, (2021) 597-600.
[159] J. AHN, M. C. JUNG, K. WYNDHAM, Y. Q. YU, AND J. R. ENGEN: *Pepsin immobilized on high-strength hybrid particles for continuous flow online digestion at 10,000 psi*, Anal. Chem., **84**, (2012) 7256-7262.
[160] R. MAJUMDAR, P. MANIKWAR, J. M. HICKEY, J. ARORA, C. R. MIDDAUGH, D. B. VOLKIN, AND D. D. WEIS: *Minimizing carry-over in an online pepsin digestion system used for the H/D exchange mass spectrometric analysis of an IgG1 monoclonal antibody*, J. Am. Soc. Mass Spectrom., **23**, (2012) 2140-2148.
[161] B. T. WALTERS, A. RICCIUTI, L. MAYNE, AND S. W. ENGLANDER: *Minimizing back exchange in the hydrogen exchange-mass spectrometry experiment*, J. Am. Soc. Mass Spectrom., **23**, (2012) 2132-2139.
[162] G. COMAMALA, J. B. MADSEN, J. VOGLMEIR, Y. M. DU, P. F. JENSEN, E. C. OSTERLUND, M. B. TRELLE, T. J. D. JORGENSEN, AND K. D. RAND: *Deglycosylation by the Acidic Glycosidase PNGase H(+) Enables Analysis of N-Linked Glycoproteins by Hydrogen/Deuterium Exchange Mass Spectrometry*, J. Am. Soc. Mass Spectrom., **31**, (2020) 2305-2312.
[163] M. J. CHALMERS, S. A. BUSBY, B. D. PASCAL, G. M. WEST, AND P. R. GRIFFIN: *Differential hydrogen/deuterium exchange mass spectrometry analysis of protein-ligand interactions*, Expert Rev. Proteomics, **8**, (2011) 43-59.
[164] Y. YANG, G. WANG, T. SONG, C. B. LEBRILLA, AND A. J. R. HECK: *Resolving the micro-heterogeneity and structural integrity of monoclonal antibodies by hybrid mass spectrometric approaches*, MAbs, **9**, (2017) 638-645.

[165] V. DOTZ, R. HASELBERG, A. SHUBHAKAR, R. P. KOZAK, D. FALCK, Y. ROMBOUTS, D. REUSCH, G. W. SOMSEN, D. L. FERNANDES, AND M. WUHRER: *Mass spectrometry for glycosylation analysis of biopharmaceuticals*, Trends Anal. Chem., **73**, (2015) 1-9.

[166] T. OLIVEIRA, M. THAYSEN-ANDERSEN, N. H. PACKER, AND D. KOLARICH: *The Hitchhiker's guide to glycoproteomics*, Biochem. Soc. Trans., **49**, (2021) 1643-1662.

[167] E. STAUDACHER, F. ALTMANN, I. B. H. WILSON, AND L. MAERZ: *Fucose in N-glycans: from plant to man*, Biochim. Biophys. Acta, Gen. Subj., **1473**, (1999) 216-236.

[168] I. B. WILSON, R. ZELENY, D. KOLARICH, E. STAUDACHER, C. J. STROOP, J. P. KAMERLING, AND F. ALTMANN: *Analysis of Asn-linked glycans from vegetable foodstuffs: widespread occurrence of Lewis a, core alpha1,3-linked fucose and xylose substitutions*, Glycobiology, **11**, (2001) 261-274.

[169] V. BLANCHARD, M. FRANK, B. R. LEEFLANG, R. BOELENS, AND J. P. KAMERLING: *The structural basis of the difference in sensitivity for PNGase F in the de-N-glycosylation of the native bovine pancreatic ribonucleases B and BS*, Biochemistry, **47**, (2008) 3435-3446.

[170] S. ZHU, P. LIUNI, T. CHEN, C. HOUY, D. J. WILSON, AND D. A. JAMES: *Epitope screening using Hydrogen/Deuterium Exchange Mass Spectrometry (HDX-MS): An accelerated workflow for evaluation of lead monoclonal antibodies*, Biotechnol. J., **17**, (2022)

[171] M. YUAN, N. C. WU, X. ZHU, C.-C. D. LEE, R. T. Y. SO, H. LV, C. K. P. MOK, AND I. A. WILSON: *A highly conserved cryptic epitope in the receptor binding domains of SARS-CoV-2 and SARS-CoV*, Science, **368**, (2020) 630-633.

[172] T. J. JORGENSEN, H. GARDSVOLL, K. DANO, P. ROEPSTORFF, AND M. PLOUG: *Dynamics of urokinase receptor interaction with Peptide antagonists studied by amide hydrogen exchange and mass spectrometry*, Biochemistry, **43**, (2004) 15044-15057.

[173] J. GOVAERT, M. PELLIS, N. DESCHACHT, C. VINCKE, K. CONRATH, S. MUYLDERMANS, AND D. SAERENS: *Dual beneficial effect of interloop disulfide bond for single domain antibody fragments*, J. Biol. Chem., **287**, (2012) 1970-1979.

[174] B. TRAENKLE, P. D. KAISER, S. PEZZANA, J. RICHARDSON, M. GRAMLICH, T. R. WAGNER, D. SEYFRIED, M. WELDLE, S. HOLZ, Y. PARFYONOVA, S. NUESKE, A. M. SCHOLZ, A. ZECK, M. JAKOBI, N. SCHNEIDERHAN-MARRA, M. SCHALLER, A. MAURER, C. GOUTTEFANGEAS, M. KNEILLING, B. J. PICHLER, D. SONANINI, AND U. ROTHBAUER: *Single-Domain Antibodies for Targeting, Detection, and In Vivo Imaging of Human CD4+ Cells*, Front. Immunol., **12**, (2021)

[175] P. K. GLASOE AND F. A. LONG: *Use of Glass Electrodes to Measure Acidities in Deuterium Oxide*, J. Phys. Chem., **64**, (1960) 188-190.

[176] A. ZECK, J. T. REGULA, V. LARRAILLET, B. MAUTZ, O. POPP, U. GOPFERT, F. WIEGESHOFF, U. E. VOLLERTSEN, I. H. GORR, H. KOLL, AND A. PAPADIMITRIOU: *Low level sequence variant analysis of recombinant proteins: an optimized approach*, PLoS ONE, **7**, (2012)

10 Appendix

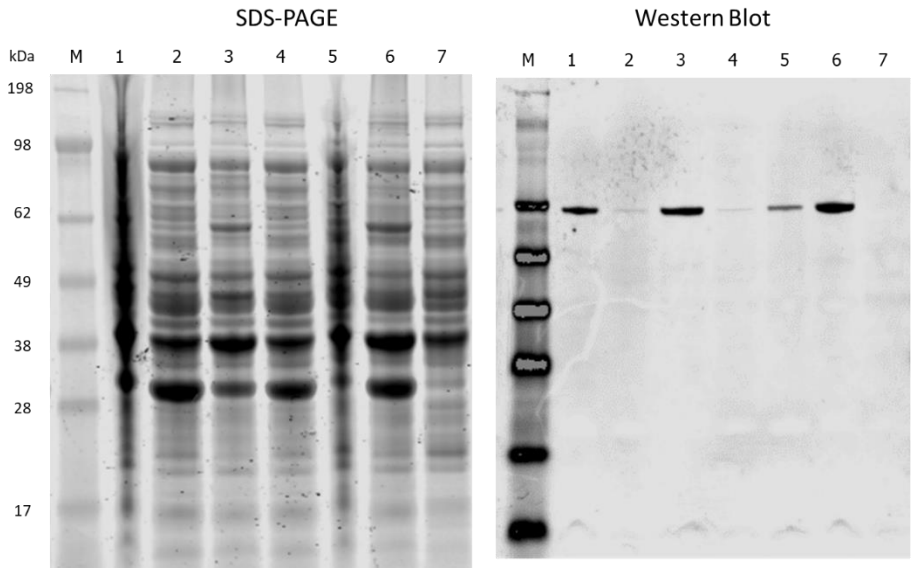

Figure A1: Feasibility of the recombinant expression of the acidic PNGases using PNGase Dj. *The expression was conducted in E. coli BL21 (DE3) and induced with 1 mM IPTG at a bacterial, optical density of 0.8 (OD600). The expression of the PNGase was conducted at room temperature, 30 °C or 37 °C. After incubation overnight, cells were ruptured and centrifuged. The supernatant and the pellet were separated and analysed via SDS-PAGE and Western Blot. Lane 1: Pellet of expression at T= RT; Lane 2: Supernatant of expression at T= RT. Lane 3: Pellet of expression at T= 30 °C; Lane 4: Supernatant of expression at T = 30 °C. Lane 5: Pellet after incubation without addition of IPTG. Lane 6: Pellet of expression at T= 37 °C; Lane 7: Supernatant of expression at T = 37 °C. PNGase Dj detected by a primary anti-His-tag Ab (mouse) and secondary Ab anti-Mouse labelled with alexa 647.*

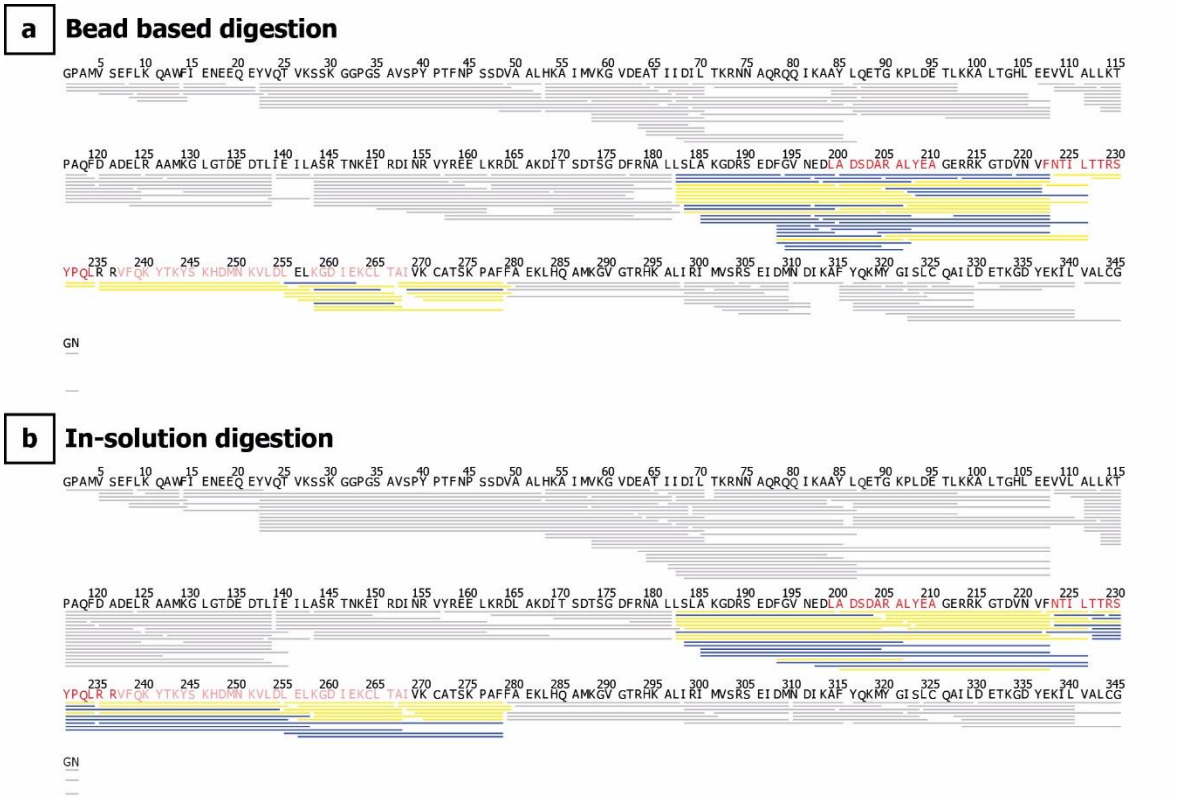

Figure A2: Sequence coverage (100%) and redundancy of ANXA1 using the bead-based digestion (a) and the in-solution digestion (b) as published in [110]. *Peptides that were identical in their sequence within repeat III in protected region upon antibody-ANXA1 interaction are depicted in in yellow, peptides obtained in one of the two approaches only are shown in blue. Amino acids marked highlighted in red show the refined interaction region with significant deuteration differences of the covering peptides.*

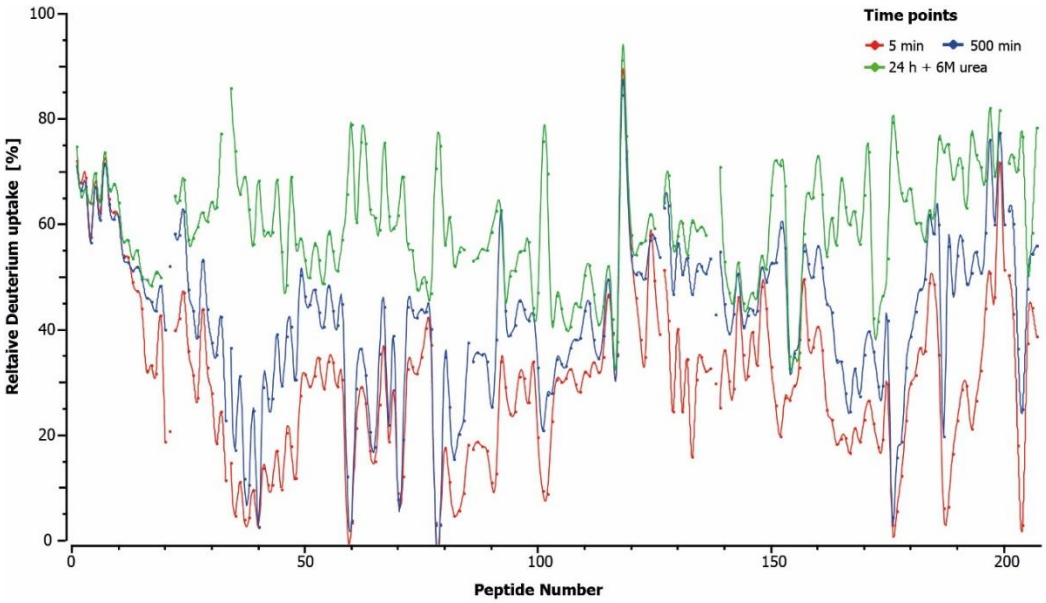

Figure A3: Deuterium uptake kinetic of ANXA1 deriving peptides using the bead-based digest as published in [110]. *The butterfly plot revealed a high and low deuteration pattern in an alternating manner. Peptides are numbered based on their first N terminal amino acid from N- to C-terminus. Peptides with the same N-terminal aa were numbered on basis of the length from shorter to longer peptides. N-terminal high accessible peptides showed a high overall deuteration with a flattened increase in deuterium uptake over time with no increase under denaturing conditions. The core region of ANXA1 (repeats I – IV) except repeat III (~105-171) show slower deuteration with high increase in deuteration upon denaturation.*

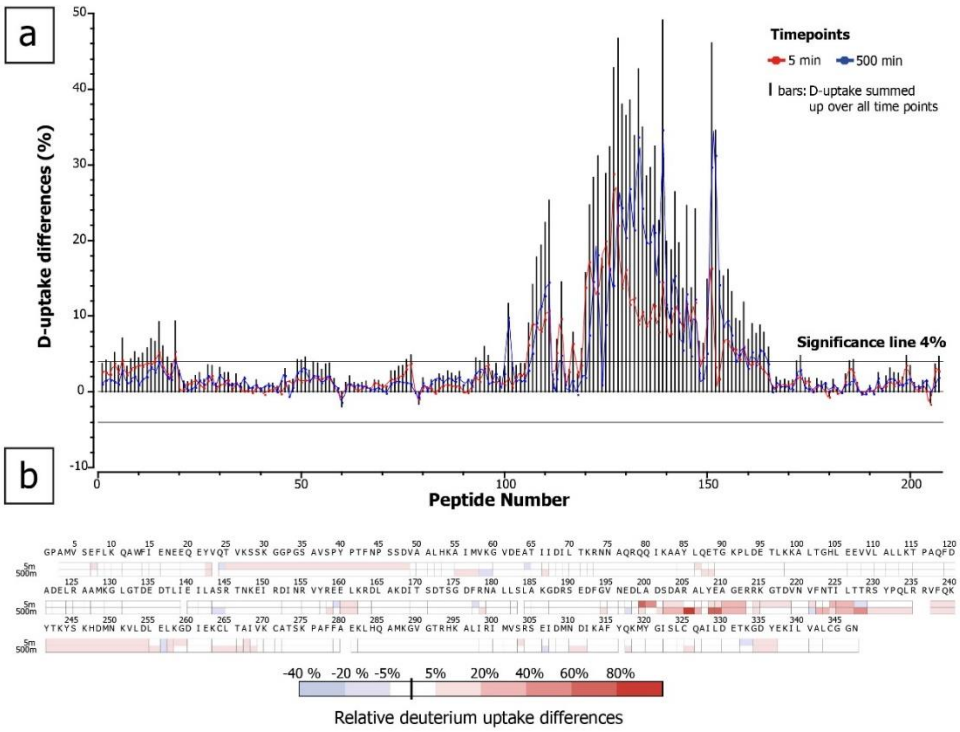

Figure A4: Results of the epitope mapping using the bead-based digest revealed deuteration differences within three regions of repeat III as published within the supplementary material [110]. *(a) Differential deuterium uptake of ANXA1 deriving peptides complexed by an anti-ANXA1 antibody and alone. ANXA1 was labelled for 5 and 500 min digested with immobilized at 0 °C for 1 min. Partially overlapping peptides are numbered based on the N-terminal aa from the N- to the C-terminus. Peptides with the same N-terminal aa were numbered on basis of the length from shorter to longer peptides. (c) Computed heat map of anti-ANXA1 antibody epitope regions taking into account the data from all overlapping peptides for the different time points.*

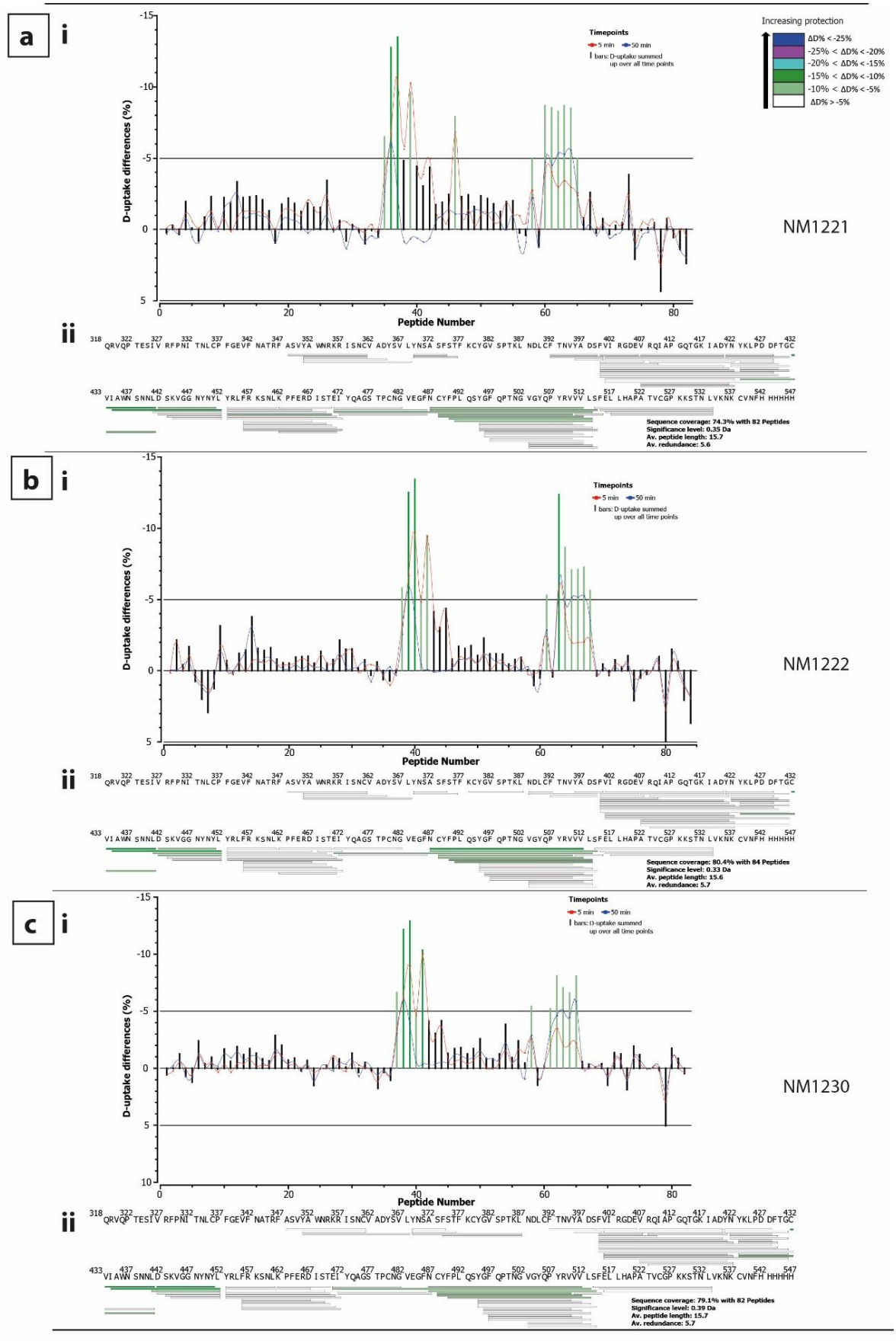
a
i
Timepoints
5 min
50 min
bars: D-uptake summed up over all time points
Increasing protection
ΔD% < -25%
-25% < ΔD% < -20%
-20% < ΔD% < -15%
-15% < ΔD% < -10%
-10% < ΔD% < -5%
ΔD% > -5%
D-uptake differences (%)
Peptide Number
NM1221
ii
QRVQP TESIV RFPNI TNLCP FGEVF NATRF ASVYA WNRKR ISNCV ADYSV LYNSA SFSTF KCYGV SPTKL NDLCF TNVYA DSFVI RGDEV RQIAP GQTGK IADYN YKLPD DFTGC
VIAWN SNNLD SKVGG NYNYL YRLFR KSNLK PFERD ISTEI YQAGS TPCNG VEGFN CYFPL QSYGF QPTNG VGYQP YRVVV LSFEL LHAPA TVCGP KKSTN LVKNK CVNFH HHHHH
Sequence coverage: 74.3% with 82 Peptides
Significance level: 0.35 Da
Av. peptide length: 15.7
Av. redundance: 5.6
b
i
Timepoints
5 min
50 min
bars: D-uptake summed up over all time points
D-uptake differences (%)
Peptide Number
NM1222
ii
QRVQP TESIV RFPNI TNLCP FGEVF NATRF ASVYA WNRKR ISNCV ADYSV LYNSA SFSTF KCYGV SPTKL NDLCF TNVYA DSFVI RGDEV RQIAP GQTGK IADYN YKLPD DFTGC
VIAWN SNNLD SKVGG NYNYL YRLFR KSNLK PFERD ISTEI YQAGS TPCNG VEGFN CYFPL QSYGF QPTNG VGYQP YRVVV LSFEL LHAPA TVCGP KKSTN LVKNK CVNFH HHHHH
Sequence coverage: 80.4% with 84 Peptides
Significance level: 0.33 Da
Av. peptide length: 15.6
Av. redundance: 5.7
c
i
Timepoints
5 min
50 min
bars: D-uptake summed up over all time points
D-uptake differences (%)
Peptide Number
NM1230
ii
QRVQP TESIV RFPNI TNLCP FGEVF NATRF ASVYA WNRKR ISNCV ADYSV LYNSA SFSTF KCYGV SPTKL NDLCF TNVYA DSFVI RGDEV RQIAP GQTGK IADYN YKLPD DFTGC
VIAWN SNNLD SKVGG NYNYL YRLFR KSNLK PFERD ISTEI YQAGS TPCNG VEGFN CYFPL QSYGF QPTNG VGYQP YRVVV LSFEL LHAPA TVCGP KKSTN LVKNK CVNFH HHHHH
Sequence coverage: 79.1% with 82 Peptides
Significance level: 0.39 Da
Av. peptide length: 15.7
Av. redundance: 5.7

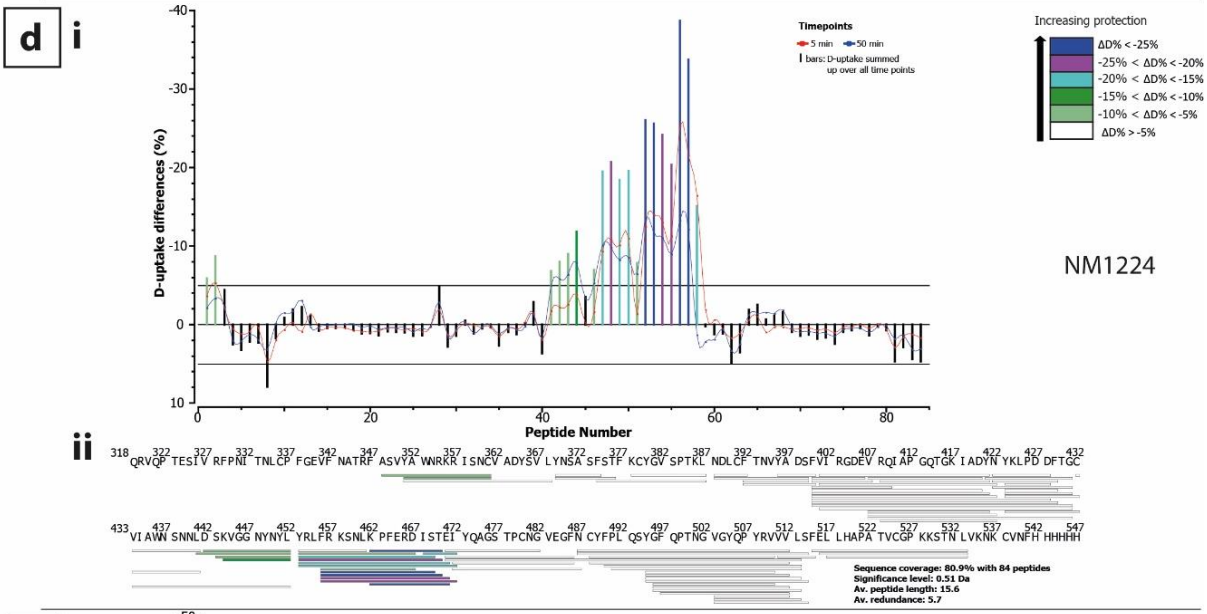
d
i
Timepoints
5 min
50 min
bars: D-uptake summed
up over all time points
Increasing protection
ΔD% < -25%
-25% < ΔD% < -20%
-20% < ΔD% < -15%
-15% < ΔD% < -10%
-10% < ΔD% < -5%
ΔD% > -5%
D-uptake differences (%)
Peptide Number
NM1224
ii
Sequence coverage: 80.9% with 84 peptides
Significance level: 0.51 Da
Av. peptide length: 15.6
Av. redundance: 5.7

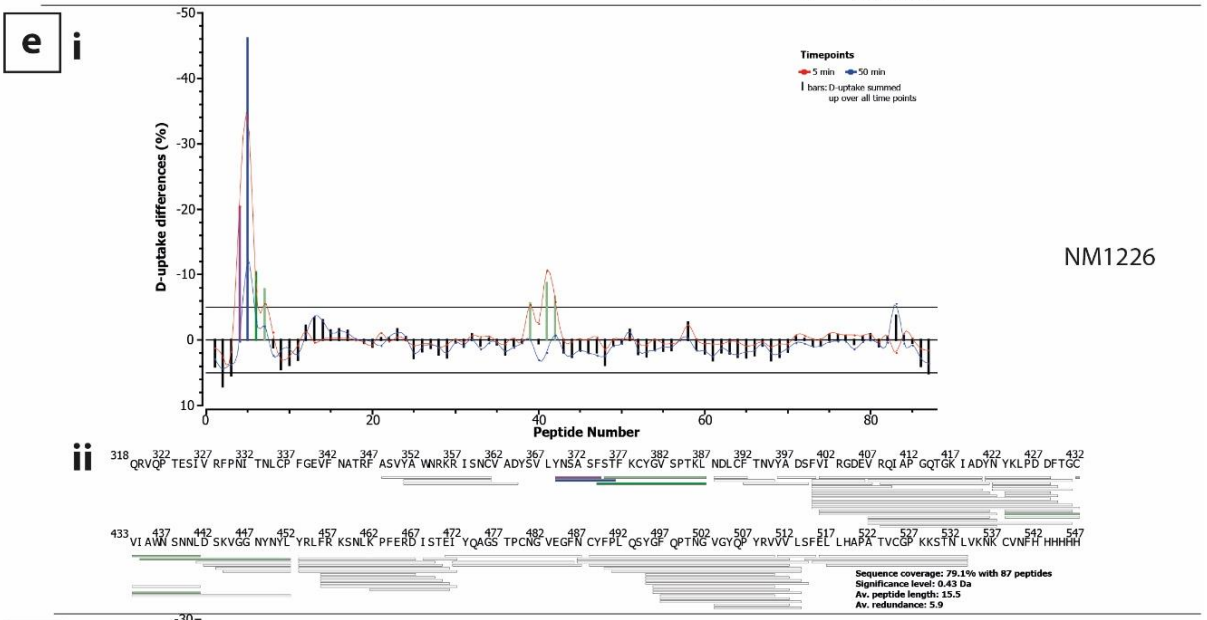
e
i
Timepoints
5 min
50 min
bars: D-uptake summed
up over all time points
D-uptake differences (%)
Peptide Number
NM1226
ii
Sequence coverage: 79.1% with 87 peptides
Significance level: 0.43 Da
Av. peptide length: 15.5
Av. redundance: 5.9

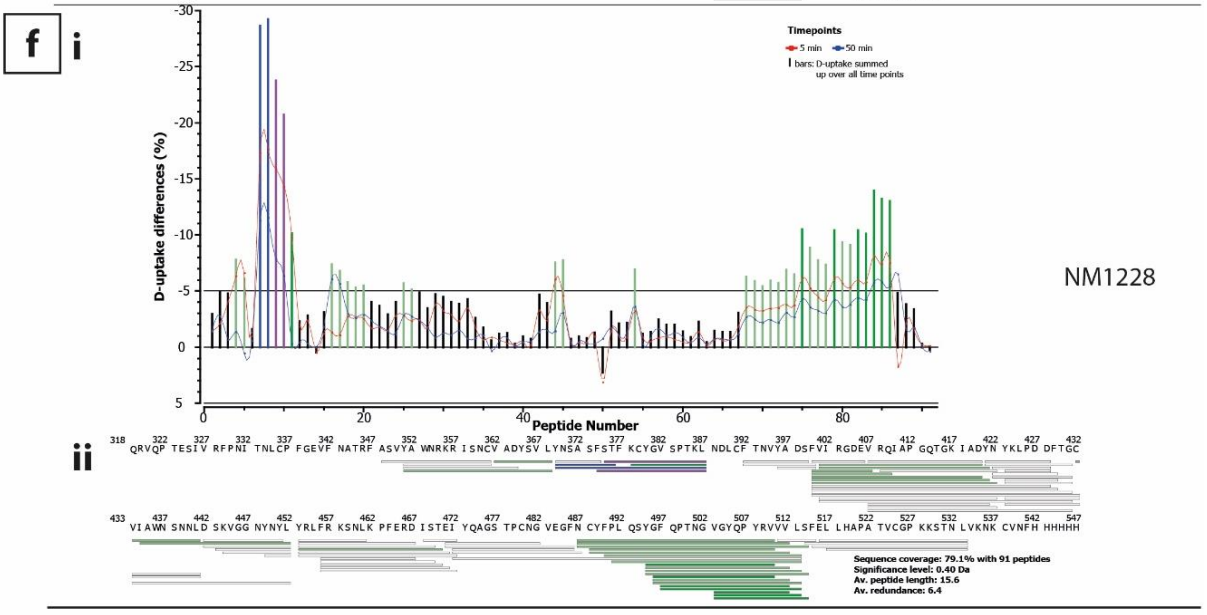
f
i
Timepoints
5 min
50 min
bars: D-uptake summed
up over all time points
D-uptake differences (%)
Peptide Number
NM1228
ii
Sequence coverage: 79.1% with 91 peptides
Significance level: 0.40 Da
Av. peptide length: 15.6
Av. redundance: 6.4

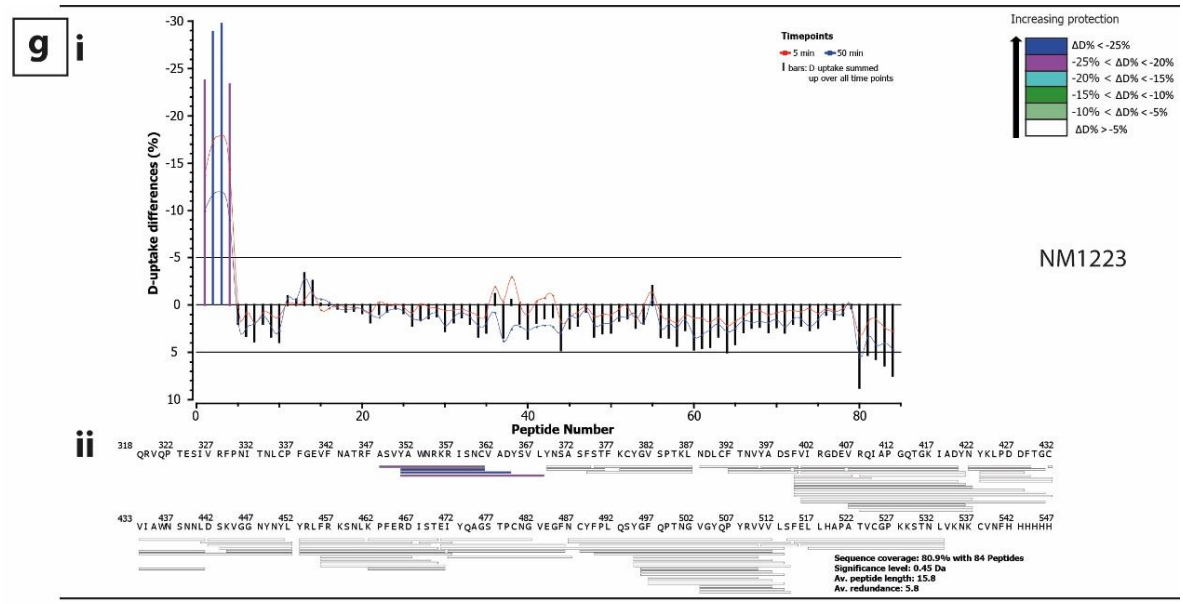

Figure A5: Results of the epitope mapping of seven Nbs (NM1221 (A); NM1222 (B); NM1230 (C); NM1224 (D); NM1226 (E); NM1228 (F) and NM 1223 (G) targeting the RBD as published in [46]. *The residual differences of HDX of partially overlapping peptic peptides were numbered form the N- to the C-terminus and on a second basis from short to long peptides (I). Bars showed the summed differences (ΔD; %) of both examined continuous labelling time points (5 and 50 min). The minimum significant deuterium uptake difference (significance level;* $\Delta\overline{HX}$ *threshold x* 2 (*number of time points) was calculated from the variance of triplicate runs. A peptide was considered as protected, if the peptides showed a 5% HDX difference as calculated by the* $\Delta\overline{HX}$ *threshold (p≤0.01) and the peptide average length. In contrast, peptides HDX were considered as unaffected by the Nb binding, if they showed <3% difference as calculated by the* $\Delta\overline{HX}$ *threshold (p≤0.05) and the peptide average length. The corresponding peptide bars (I) as well as the peptides depicted on the sequence of the RBD (II) were color-coded according to the legend shown in A. Sequence coverage map of peptides used for HDX data analysis for each nanobody RBD pair.*

Figure A6: Epitope regions of seven nanobodies mapped qualitatively on the primary sequence of the RBD. *Elucidated regions showing HDX reduction are coloured according to the Nb-sets. Amino acids involved in the RBD:ACE2 interaction interface [152, 153] are highlighted with bold letters. Lacking sequence coverage of HDX is shown with grey letters. Regions with low intrinsic HDX are shown with italic type letters.*

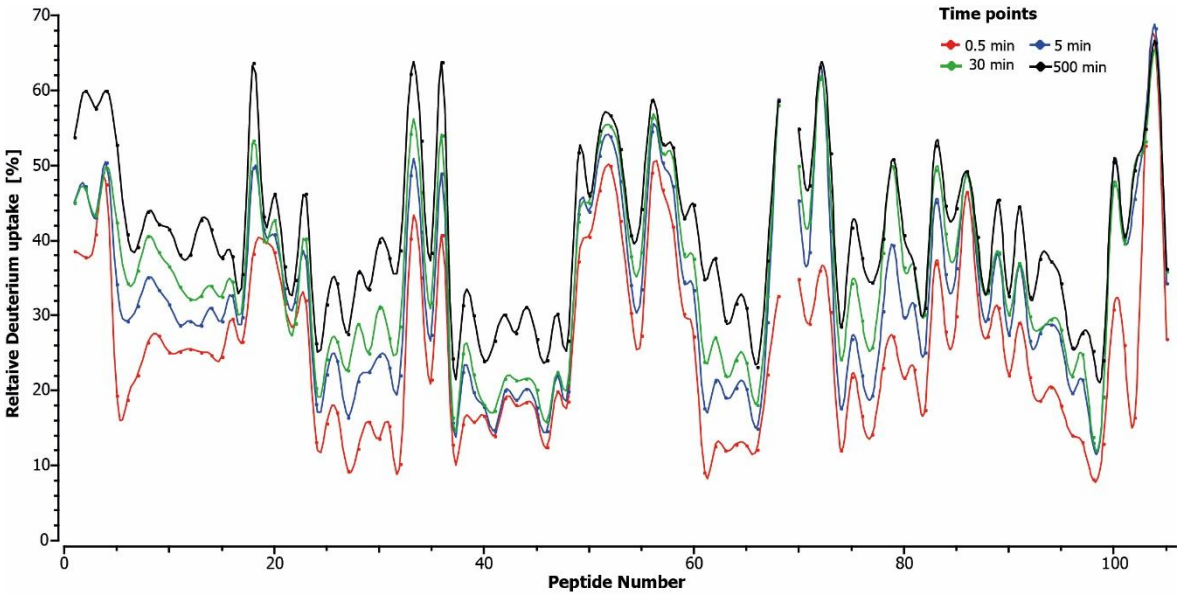

Figure A7: Deuterium uptake kinetic of 105 SIRPα deriving peptides leading to a sequence coverage of 86%. *Peptides are numbered based on their first N terminal amino acid from N- to C-terminus. Peptides with the same N-terminal aa were numbered on basis of the length from shorter to longer peptide. HDX was performed in independent replicates (n=2). One regions covered by peptides 37-48 (residues ~140-155) showed a resistance against deuteration (≤20% deuteration after 30 min). As per consensus guidelines [74], HDX uptake plots as well as a summary table can be found in Figure A19 and Table A4.*

Based on the data volume additional appendix figures and tables can be found on the corresponding CD (printed format) or PDF file (online format), attached to the work.

This includes figures:

- Figure A8: FigureA8_UptakePlots_Intraday&Interday_Variability.pdf
- Figure A9: FigureA9_ UptakePlots_ANXA1_In-Solution.pdf
- Figure A10: FigureA10_UptakePlots_ANXA1_Bead-Based.pdf
- Figure A11: FigureA11_UptakePlots_RBD_Kinetic.pdf
- Figure A12: FigureA12_UptakePlots_RBD_NM1221.pdf
- Figure A13: FigureA13_UptakePlots_RBD_NM1222.pdf
- Figure A14: FigureA14_UptakePlots_RBD_NM1223.pdf
- Figure A15: FigureA15_UptakePlots_RBD_NM1224.pdf
- Figure A16: FigureA16_UptakePlots_RBD_NM1226.pdf
- Figure A17: FigureA17_UptakePlots_RBD_NM1228.pdf
- Figure A18: FigureA18_UptakePlots_RBD_NM1230.pdf
- Figure A19: FigureA19_UptakePlots_SIRPa_Kinetic.pdf
- Figure A20: FigureA20_UptakePlots_SIRPa_Nb01.pdf
- Figure A21: FigureA21_UptakePlots_SIRPa_Nb02.pdf

- Figure A22: FigureA22_UptakePlots_SIRPa_Nb03.pdf
- Figure A23: FigureA23_UptakePlots_SIRPa_Nb04.pdf

And tables:

- Table A1: TableA1_Intra&Interday_Variability_Summary_Table.xlsx
- Table A2: TableA2_ANXA1_In-Solution_Bead-Based_HDX_Summary_Table.xslx
- Table A3: TableA3_RBD_Nb_HDX_Summary_Table.xslx
- Table A4: TableA4_SIRPa_Nb_HDX_Summary_Table.xslx